Proceedings of the

2nd GLOREAM/ EURASAP Workshop

Copenhagen
September 6-8, 2004

Modern developments in modelling and chemical data analysis

Jørgen Brandt and Lise M. Frohn (Eds.)

National Environmental Research Institute
Ministry of the Environment · Denmark

Proceedings of the

2nd GLOREAM/ EURASAP Workshop

Copenhagen
September 6-8, 2004

Modern developments in modelling and chemical data analysis

Jørgen Brandt and Lise M. Frohn (Eds.)

National Environmental Research Institute
Ministry of the Environment · Denmark

Data sheet

Title: Proceedings of the 2nd GLOREAM/EURASAP Workshop
Copenhagen, September 6-8, 2004

Subtitle: Modern developments in modelling and chemical data analysis

Editors Jørgen Brandt, Lise M. Frohn

Department: Department of Atmospheric Research

Publisher: National Environmental Research Institute ©
Ministry of the Environment
URL: http://www.dmu.dk

Date of publication: September 2005

Please cite as: Brandt, J. & Frohn, L.M. (eds.) 2005: Proceedings of the 2nd GLOREAM/EURASAP Workshop, Copenhagen, September 6-8, 2004**.** Modern developments in modelling and chemical data analysis. National Environmental Research Institute, Denmark. 130pp.

Abstract: These proceedings contain some of the papers presented at the 2nd GLOREAM/EURASAP Workshop, which was held at Miljøkontrollen (Copenhagen EPA), Copenhagen, September 6-8, 2004. The general aim of this open workshop, chaired by Prof. Peter Builtjes, TNO, was to present and discuss results concerning recent developments in tropospheric chemical transport modelling. The workshop was organised in five sessions; 1) Model developments, 2) Model applications/model systems, 3) Computational aspects, 4) Assessment and regulation, and 5) Aerosol modelling. A total of 21 papers were presented at the workshop.

Keywords: Air Pollution, Modelling, Applications, Assessment, GLOREAM, EURASAP

Layout: Majbritt Ulrich

ISBN: 87-7772-886-6

Number of pages: 130

Internet-version: The report is available only as a PDF-file from NERI's homepage http://www2.dmu.dk/1_viden/2_Publikationer/3_Ovrige/rapporter/2gloreameurasapproceedings.pdf

Contents

Preface

These proceedings contain some of the papers presented at the 2^{nd} GLOREAM/EURASAP Workshop, which was held at Miljøkontrollen (Copenhagen EPA), Copenhagen, September 6-8, 2004. The local organisers of the workshop were Jørgen Brandt, Lise M. Frohn and Maria Pedersen, National Environmental Research Institute, Department of Atmospheric Environment.

The general aim of this open workshop, chaired by Prof. Peter Builtjes, TNO, was to present and discuss results concerning recent developments in tropospheric chemical transport modelling. The workshop was organised in five sessions; 1) Model developments, 2) Model applications/model systems, 3) Computational aspects, 4) Assessment and regulation, and 5) Aerosol modelling. A total of 21 papers were presented at the workshop.

The GLOREAM/EURASAP Workshop is a combination of the previously existing research programme GLOREAM (GLObal and REgional Air pollution Modelling) and EURASAP (EURopean Association for the Science of Air Pollution). The first GLOREAM/EURASAP Workshop took place in Cologne in 2003.

Jørgen Brandt and Lise M. Frohn (editors)

The Incorporation of Aerosol Processes in Polair3D

K. Fahey, E. Debry, H. Foudhil, and B. Sportisse

CEREA, Research and Teaching Center in Atmospheric Environment, Joint Laboratory École Nationale des Ponts et Chaussées/ Électricité de France R&D. Cité Descartes, Champs sur Marne, F-77455 Marne la Vallée Cedex, France

Abstract

The treatment of aerosol processes has recently been added to the three-dimensional chemical transport model, Polair3D. Along with transport, the processes of condensation, evaporation, coagulation, nucleation, and aqueous phase processing are considered. In this paper, the formulation of the size resolved aerosol model (SIREAM) and its incorporation into Polair3D are outlined. Preliminary results in the three dimensional domain are reasonable. These results are discussed along with the future direction of aerosol treatment in Polair3D.

Introduction

Atmospheric aerosol has been implicated in the development of adverse health effects, visibility reduction, and the formation of acid rain and fogs and also has a strong influence on the earth's energy balance. This atmospheric particulate matter is a complex mixture of inorganic and organic components, with composition varying over the aerosol size range of a few nanometers to several micrometers. Particles can be emitted directly from various anthropogenic and biogenic sources or can be formed in the atmosphere from inorganic or organic precursor gases. Secondary aerosol can comprise a significant fraction of atmospheric PM, and as $PM_{2.5}$ can have a lifetime on the order of a couple days, significant transport may occur before particles are ultimately removed from the atmosphere (Seinfeld and Pandis, 1998; Seigneur, 2001).

Three dimensional chemical transport models provide the necessary tools to develop not only a better understanding of the formation and distribution of atmospheric pollutants but also sound strategies to control them. In order to develop appropriate strategies to control particulate mass, the important physical and chemical processes affecting the transformation of the aerosol size and composition distribution need be considered in these models.

Here we present the incorporation of the treatment of aerosol processes in the three-dimensional chemical transport model, Polair3D. Recent improvements to the gas-phase only version of Polair include the addition of both a Modal Aerosol Model (MAM) and a size-resolved aerosol model (SIREAM) along with the Carnegie Mellon University Variable Size-Resolution aqueous phase chemistry Model (VSRM). This paper will focus primarily on the addition of SIREAM.

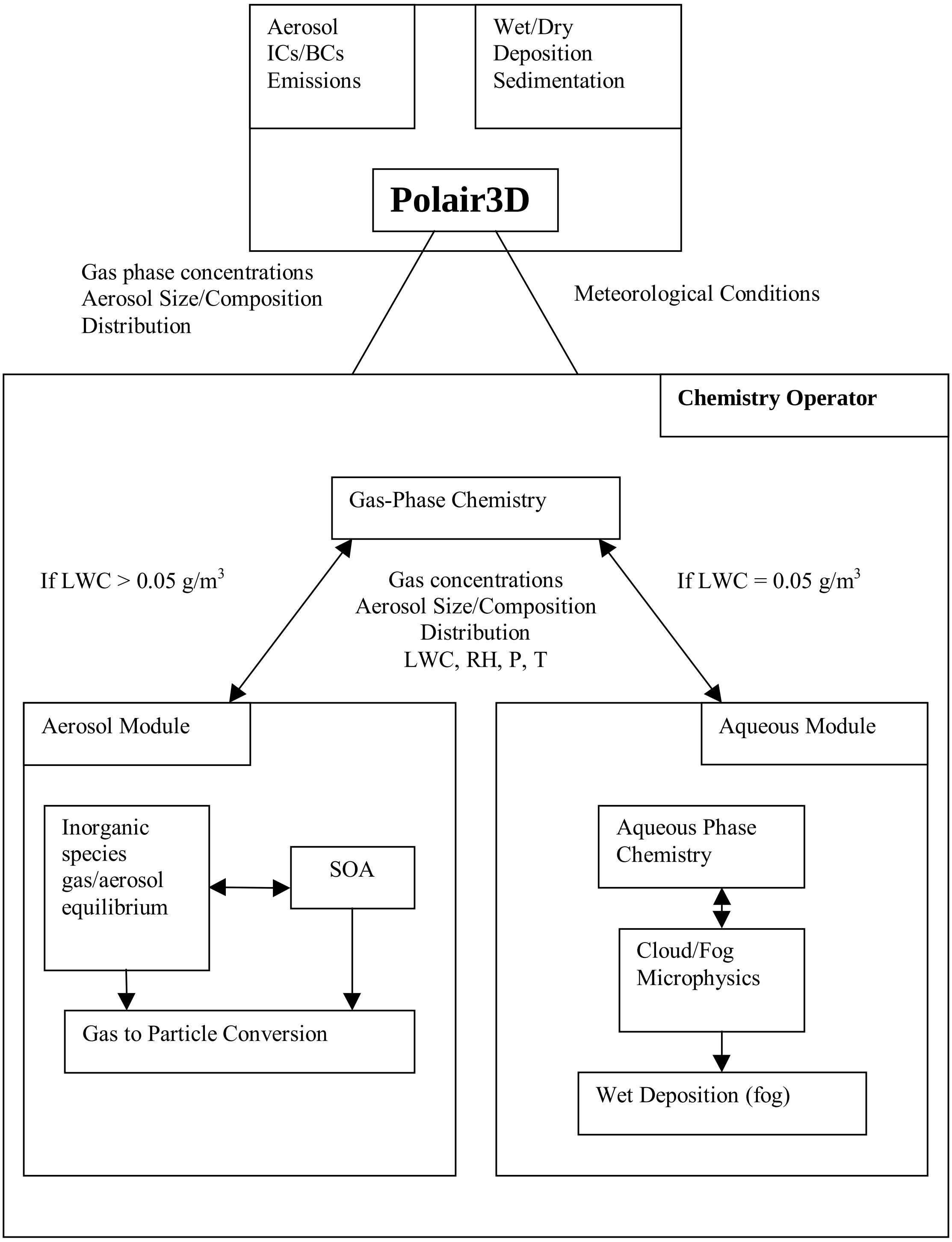

Figure 1. Schematic of the treatment of aerosol processes in Polair3D

Polair3D

Polair3D was developed at the Research and Teaching Center in Atmospheric Environment (CEREA), a joint laboratory of Ecole Nationale des Ponts et Chaussées and Electricité de France R&D, and is a three-dimensional Eulerian model that treats the chemical transformations and transport of major gas phase and particulate pollutants. Advection, diffusion, deposition, emission, and chemical production are treated so that the evolution of a three dimensional grid of pollutants can be generated over time. Validation studies have been performed in the past using earlier gas-phase-only versions of Polair. The effects of the recently added aerosol processes are currently being examined. See Figure 1 for a schematic of the aerosol module structure in Polair3D.

SIREAM

The Size Resolved Aerosol Model (SIREAM) treats the major processes that affect the aerosol size/composition distribution. The size range is approximated by a discrete user-specified number of size sections or “bins” and composition is assumed to be uniform within each of these bins. The following species are treated: sodium, sulfate, ammonium, nitrate, chloride, water, mineral dust, elemental carbon, primary organic aerosol, and 8 secondary organic species. The user can specify the range of diameters considered, number of size bins, which processes to simulate, and the invocation of certain simplifying assumptions (e.g., neglect of the Kelvin effect, instantaneous equilibrium) in order to choose the best combination of accuracy and efficiency for a given application.

SIREAM considers nucleation, condensation/evaporation, and coagulation. Nucleation is described by a binary or ternary scheme (Vehkamaki et al., 2002; Napari et al., 2002). Coagulation is given by the equations for Brownian coagulation. The driving force for condensation or evaporation is the difference between the bulk gas phase concentration and the concentration at the aerosol surface (given by a thermodynamics package). Due to this mass transfer, particles grow (condensation) or shrink (volatilization). SIREAM employs the moving sectional approach in order to account for these changes in particle size. The section boundaries evolve with time according to the growth law and then the sectional masses are projected back onto a fixed grid.

There are three approaches taken to describe mass transfer between gas and aerosols in a modeling framework (Debry and Sportisse, 2004; Capaldo et al., 2000; Zhang et al, 2004, Pilinis et al., 2000). These are the instantaneous equilibrium, dynamic, and hybrid methods. In SIREAM, the user can specify any of these methods for the calculation of gas to particle mass transfer. For all of these approaches, however, the aerosol thermodynamics problem needs to be solved. In the case of inorganics, ISORROPIA is used to calculate instantaneous equilibrium concentrations (forward mode) or the surface concentration used to determine the driving force of mass transfer between gas and aerosol phases in the case of dynamic mass transfer (reverse mode) (Nenes et al., 1998, 1999). For organic species, a pseudo-ideal solution is assumed and mass transfer is calculated based on an absorption model as described by Pankow (Pankow, 1994a,b; Schell et al, 2001).

For cells with a liquid water content exceeding a critical value (i.e., 0.05 g/m^3), the aqueous phase chemistry module is called instead of SIREAM. The aqueous module used here is the Carnegie Mellon University Variable Size Resolution aqueous phase chemistry Model (VSRM) (Fahey and Pandis, 2001). Droplets form instantaneously on particles that exceed the user specified critical diameter, while remaining particles serve as interstitial aerosol. After evaporation, the particle sections will have grown due to the increased aerosol mass resulting from the aqueous phase reactions. Following the aqueous phase chemistry calculations the aerosol distribution is mapped back onto the fixed grid.

Other processes treated in this three-dimensional framework include heterogeneous reactions, size resolved emissions and deposition, along with the advective and diffusive transport common to both gas and aerosol phase species (Jacob, 2000, 2004).

Preliminary Results

Some limited testing of Polair3D with the newly added aerosol processes has been performed. Simulations have been run over the Lille and European domains. Comparisons between modeled values and observations have only been made for the Lille simulation. Ongoing work includes the validation of the model with measurements for a European simulation during Spring 2001.

Lille

The objective of the 3D simulation over Lille was to assess the impact of different emission scenarios related to traffic from the years 1998 to 2015. A comprehensive study of gas phase chemistry has already been accomplished with the gas-phase-only version of Polair3D. Here we present some preliminary results for PM as obtained with SIREAM.

Over Lille, SIREAM was run in fully equilibrium mode with three size sections. Aqueous phase chemistry was not active. Figure 2 shows the comparison of simulated PM with sensor measurements. One can see that for the month of January 1998, the measurements and simulated results agree well, both in magnitude and temporal variation. Figures 3a and 3b show the model predictions for $PM_{2.5}$ and PM_{10} respectively for the surface level of the domain. Further studies on the impact of aerosols over Lille have yet to be performed.

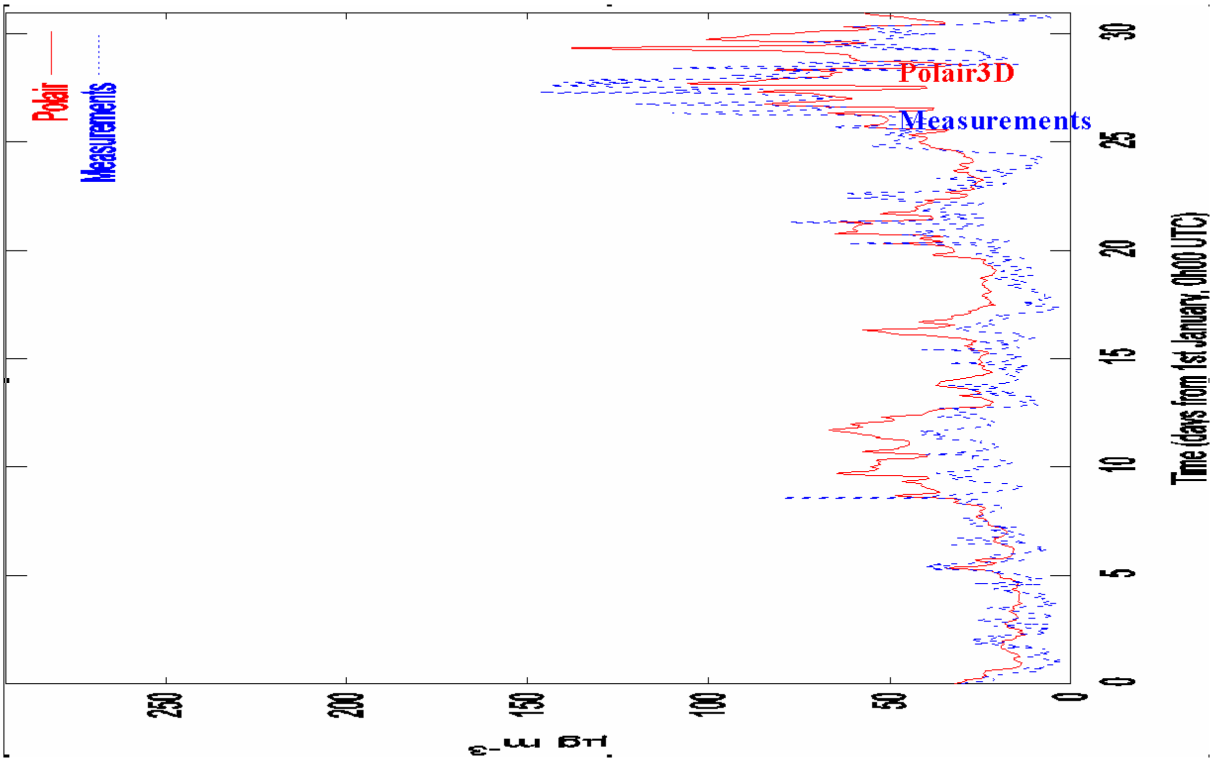

Figure 2. Comparison of PM_{10} measurements (blue) and modeled values (red). The initial time is January 1, 1998.

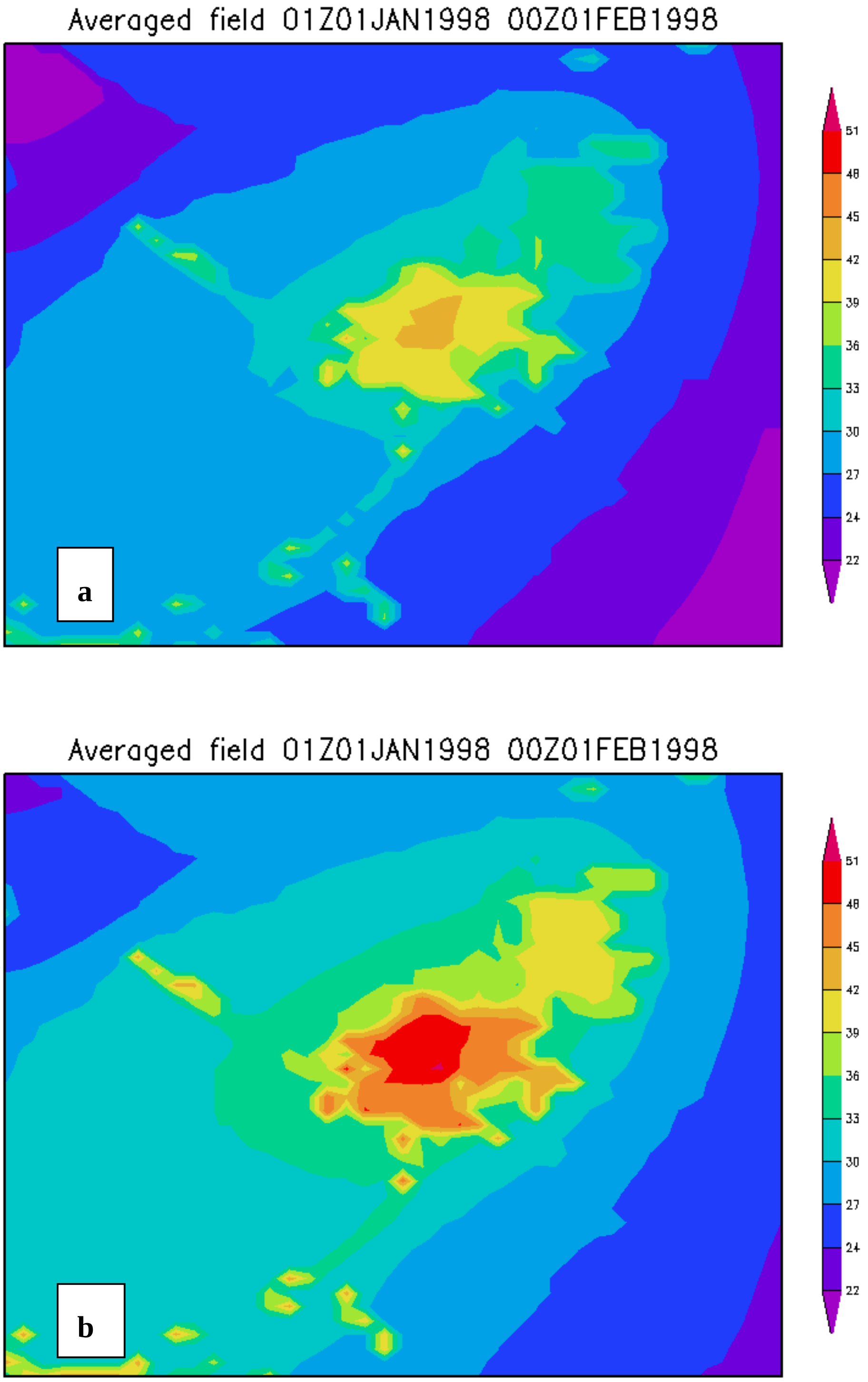

Figure 3. **(a)** Average $PM_{2.5}$ and **(b)** PM_{10} concentration over Lille for the month of January 1998

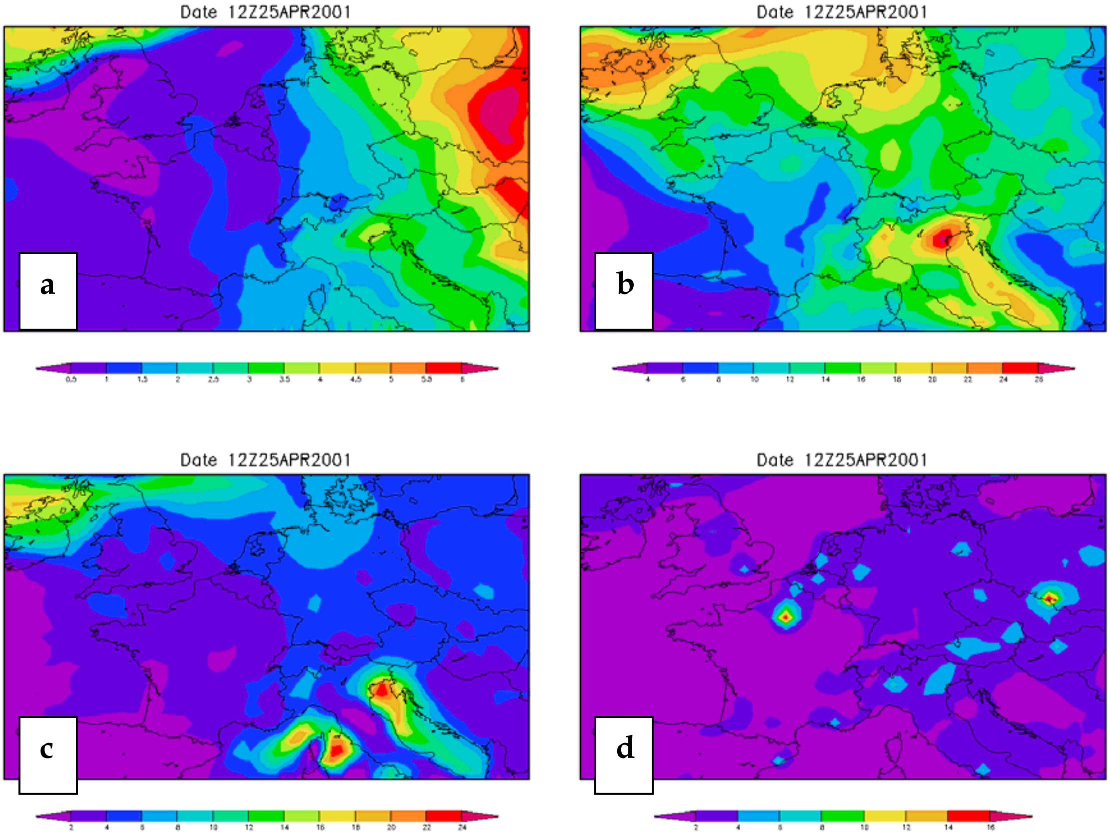

Figure 4. Modeled (instantaneous equilibrium – no cloud chemistry) PM_{10} surface concentrations over Europe for April 25, 2001, at noon for (a) sulfate, (b) nitrate, (c) ammonium, and (d) total organic aerosol

Europe

Three dimensional simulations have been run over Europe for the Spring of 2001. There have not as yet been comparisons with measurements, but in Figures 4 through 6, some preliminary results are shown for the model under different conditions. Each model run is performed with 10 size bins, and the figures show the predicted concentrations of major species for dynamic and equilibrium conditions, for active cloud chemistry and neglected cloud chemistry. The plots shown are for day 3 of the simulation, April 25th, at noon.

Figures 4a through 4d show PM_{10} sulfate, nitrate, ammonium, and total organic aerosol surface concentrations for the instantaneous equilibrium method. Cloud chemistry is neglected. Figures 5a through 5d show the same for dynamic mass transfer. The methods compare rather well for sulfate, as might be expected. Sulfuric acid has a very low vapor pressure and rapidly condenses onto the aerosol phase. However one can see significant differences between ammonium and nitrate concentrations, where the equilibrium method tends to predict higher values for the species than the dynamic simulation.

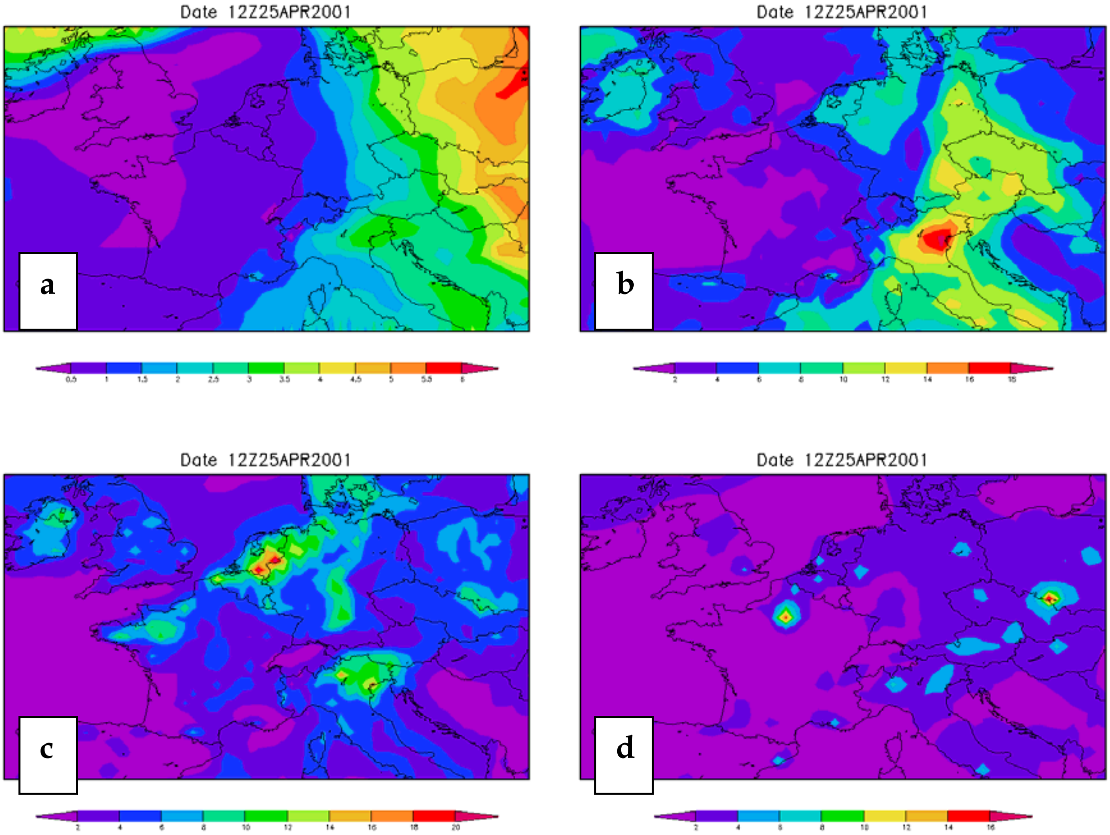

Figure 5. Modeled (dynamic mass transfer – no cloud chemistry) PM_{10} surface concentrations over Europe for April 25, 2001, at noon for (a) sulfate, (b) nitrate, (c) ammonium, and (d) total organic aerosol

Figure 6a shows PM_{10} sulfate concentrations (dynamic) for a simulation with active cloud chemistry. Comparing figures 6a and 5a, one can see that even by the third day of simulation, a difference between the sulfate values on the ground level is visible (and would be even greater in the upper layers), and this is due at least in part to the chemical production in clouds and fogs.

Values for total organic aerosol seem low in comparison with the other major components, thus indicating perhaps that the SOA module should be revisited. Possible future work may include the extension of the SOA module to include an option for a mechanistic description of SOA formation (Pun et al, 2002). Further work needs to be done to better link the combined effects of inorganic and organic species on mass transfer between the phases (Koo et al., 2003).

Conclusions and Future Work

Aerosol processes have recently been added to the three dimensional chemical transport model Polair3D. 17 aerosol species are considered and represent biogenic and anthropogenic compounds, organic and inorganic, primary and secondary. The processes treated by the size-resolved aerosol module (SIREAM) include nucleation, coagulation, and condensation/evaporation, and mass transfer can be treated using the dynamic, hybrid, or instantaneous equilibrium methods. Aqueous phase processing has also been added in the form of the VSRM aqueous phase chemistry model. Other aerosol processes treated in this three-dimensional framework include heterogeneous reactions, size resolved emissions and deposition, along with advective and diffusive transport.

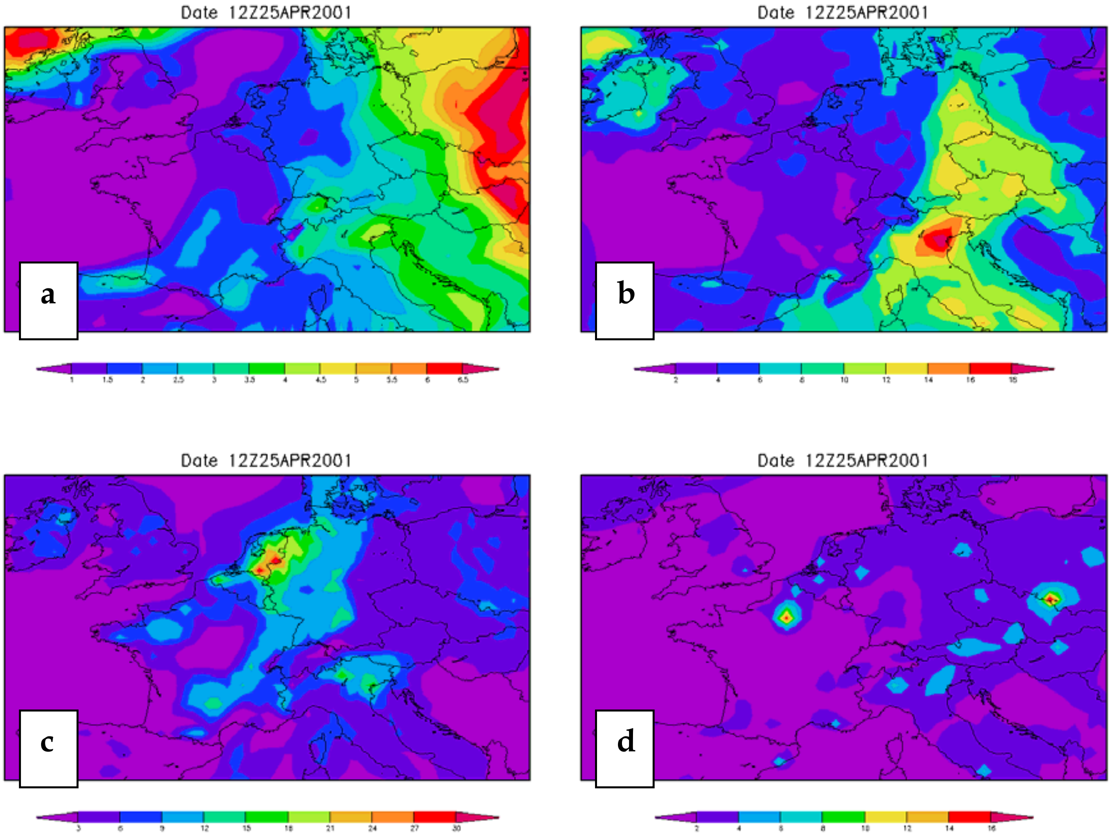

Figure 6. Modeled (dynamic mass transfer – active cloud chemistry) PM_{10} surface concentrations over Europe for April 25, 2001, at noon for (a) sulfate, (b) nitrate, (c) ammonium, and (d) total organic aerosol

Preliminary simulations have been run with the aerosol-inclusive version of Polair3D. The comparison with observations for the simulation over Lille looks promising, and Polair3D follows the absolute amounts and trends of observed particulate matter concentrations for January 1998. For the European simulations, comparisons between observations and modeled values have not yet been made. On a first look, however, the values for the major species look reasonable. Areas of improvement for the model might include a more rigorous SOA module or the development of a better link between the aqueous phase chemistry module and the wet deposition routine. Validating the aerosol model within the three-dimensional framework will require extensive comparison with observations. This work is currently underway.

References

Capaldo, K.P., Pilinis,C., Pandis, S.N. (2000) A computationally efficient hybrid approach for dynamic gas/aerosol transfer in air quality models. *Atmos. Environ.* 34, 3617-3627.

Debry, E., Sportisse, B. (2004) Reduction of the general dynamic equation for atmospheric aerosols: theoretical and numerical investigation. Submitted for publication.

Fahey, K.M., Pandis, S.N. (2001) Optimizing model performance: variable size-resolution in cloud chemistry modeling. *Atmos. Environ*. 35, 4471-4478.

Jacob, D.J. (2000) Heterogeneous chemistry and tropospheric ozone. Atmos. Environ. 34, 2131-2159.

Jacob, D.J. (2004) Personal communication to Bruno Sportisse.

Koo, B., Ansari, A.S., Pandis, S.N. (2003) Integrated approaches to modeling the organic and inorganic atmospheric aerosol components. *Atmos. Environ.* 37, 4757-4768.

Napari, I., Noppel, M., Vehkamaki, H., Kulmala, M. (2002) Parameterization of ternary nucleation rates for H_2SO_4-NH_3-H_2O vapor. *Journal of Geophysical Research.* 107, 4381.

Nenes, A., Pandis, S.N., Pilinis, C. (1998) ISORROPIA: a new thermodynamic model for inorganic multicomponent atmospheric aerosols. *Aquatic Geochemistry* 4, 123-152.

Nenes, A., Pandis, S.N., Pilinis, C. (1999) Continued development and testing of a new thermodynamic aerosol module for urban and regional air quality models. *Atmos. Environ.* 33, 1553-1560.

Pankow, J.F. (1994a) An absorption model of the gas/particle partitioning of organic compounds in the atmosphere. *Atmos. Environ*. 28, 185-188.

Pankow, J.F. (1994b) An absorption model of the gas/aerosol partitioning involved in the formation of secondary organic aerosol. *Atmos. Environ.* 28, 189-193.

Pilinis, C., Capaldo, K.P., Nenes, A., Pandis, S.N. (2000) MADM – A new multicomponent aerosol dynamics model. *Aerosol. Sci. Technol*. 32:482-502.

Pun, B.K., Griffin, R.J., Seigneur, C., Seinfeld, J.H. (2002) Secondary organic aerosol: 2. Thermodynamic model for gas/particle partitioning of molecular constituents. *Journal of Geophysical Research.* 107(D17), 4333.

Schell, B., Ackermann, I.J., Hass, H., Binkowski, F.S., Ebel, A. (2001) Modeling the formation of secondary organic aerosol within a comprehensive air quality model system. *Journal of Geophysical Research.* 106, 28275-28293.

Seigneur, C. (2001) Current status of air quality models for particulate matter. *J. Air & Waste Manage. Assoc.* 51, 1508-1521.

Seinfeld J. H. and Pandis S. N. (1998) Atmospheric Chemistry and Physics: From Air Pollution to Global Change. J. Wiley, New York.

Vehkamaki, H., Kulmala, M., Napari, I., Lehtinen, K.E.J., Timmreck, C., Noppel, M., Laaksonen, A. (2002) An improved parameterization for sulfuric acid-water nucleation rates for tropospheric and stratospheric conditions. *Journal of Geophysical Research.* 107, 4622.

Zhang, Y., Pun, B., Vijayaraghavan, K., Wu, S., Seigneur, C., Pandis, S.N., Jacobson, M.Z., Nenes, A., Seinfeld, J.H. (2004) Development and application of the Model of Aerosol Dynamics, Reaction, Ionization, and Dissolution (MADRID). *Journal of Geophysical Research.* 109.

Aerosol Modelling with CAMx and PMCAMx

Sebnem Andreani-Aksoyoglu, Johannes Keller and Andre S.H. Prévôt

Laboratory of Atmospheric Chemistry, Paul Scherrer Institut, Villigen PSI, 5232 Switzerland

Introduction

Recently there have been significant improvements with respect to aerosol modelling. Models with 1-atmosphere approach are able to simulate both gaseous and particulate pollutants and suitable for episodic and annual calculations (Ackermann et al., 1998; Schell et al., 2001). There are also more complete models including full-science algorithms for aerosol modelling (Griffin et al., 2003; Bessagnet et al.; 2004; Zhang et al., 2004). However, such models are more complex and demanding. A model intercomparison study showed that a more complex model approach to the aerosol problem does not automatically lead to better results in a 3-dimensional application (Hass et al., 2003). As long as speciated aerosol measurements with high time resolution are limited, necessity of using so called full-science aerosol models is questionable. In this study, two air quality models with different approaches were applied to two domains, northern Italy and Switzerland, to investigate the capabilities, strengths and weaknesses.

Modelling

Models

In this study, two CAMx models (The Comprehensive Air Quality Model with extensions) were used. CAMx is an Eulerian photochemical dispersion model that allows for integrated assessment of gaseous and particle air pollution over many scales (Environ, 2004a). The first model is the CAMx version 4.0. It has a 1-atmosphere approach for gaseous and particulate air pollution modelling. Aqueous sulfate and nitrate formation in cloud water is calculated using RADM aqueous chemistry algorithm (Chang et al., 1987). Partitioning of condensible organic gases to secondary organic aerosols (SOA) to form a condensed organic solution phase is performed by the semi-volatile equilibrium scheme called SOAP (Strader et al., 1998). There are four SOA classes depending on the gaseous precursors. The first three classes represent SOA formed from anthropogenic precursors and the aerosols in the fourth class are formed from the biogenic precursors. ISORROPIA thermodynamic model is used to calculate the partitioning of inorganic aerosol constituents between gas and particle phases (Nenes et al., 1998). Particle sizes are static. Primary particles are modelled as fine and/or coarse particles whereas secondary species are modelled as fine particles. In this study, the particle size range for these secondary aerosol species was chosen as 0.04 - 2.5 µm, as indicated by experimental results.

The second model used in this study is PMCAMx (version 3.01) which contains full science aerosol algorithms (Environ, 2003). It is a more complete aerosol model than CAMx (version 4.0), but it is more demanding as well. Aerosol dynamics and particle size distribution are treated with a sectional approach covering the range of 0.04 µm to 40 µm. PMCAMx contains a more complete aqueous chemistry mechanism (Variable Size Resolution Model) developed by the Carnegie Mellon University. The two models have similar gas phase mechanisms (CBMIV/SAPRC99), inorganic (ISORROPIA) and organic (SOAP) aerosol treatment. The main difference is in the particle size distribution, aerosol dynamics and aqueous chemistry mechanisms (Table 1).

Table 1. Comparison of CAMx and PMCAMx models

	CAMx (v4.0)	PMCAMx (v3.01)
Approach	1-atmosphere	full-science PM model
gas-phase mechanism	CBMIV/SAPRC99	CBMIV/SAPRC99
inorganic aerosols	ISORROPIA	ISORROPIA
organic aerosols	SOAP	SOAP
aqueous chemistry	RADM	VSRM
particle size	fine/coarse	10-sectional
relative cpu time	1	3

Applications

Northern Italy

The first application was carried out over a domain covering northern Italy, for the period 11-13 May 1998 (Figure 1). The model domain consists of 47x54 grid cells with a resolution of 3km x 3km. There are 8 layers in a terrain-following coordinate system, the first being 50m above ground. The model top was set at about 3000 m agl. The same input data from the modelling study using the previous CAMx version 3.10 were used for this application (Andreani-Aksoyoglu et al., 2004). Simulations started on May 11 at 1200 central European summer time (CEST) and ended on May 13 at 2400 CEST. The first 12 hours were used to initialize the model.

Switzerland

The second study was carried out in a domain covering Switzerland and some parts of the neighbouring countries (Figure 2) during an exceptionally hot period between 4 and 7 August 2003. The model domain encloses 650 km in the west-east and 450 km in the north-south direction with a horizontal resolution of 9 km. In the vertical direction 10 layers with varying heights were used, lowest being 30 m above ground. The model top is at about 4000 m above ground. For this application, meteorological data were calculated using MM5 meteorological model (PSU, NCAR, 2004). Initial and boundary trace gas conditions were extracted from the output of the European model REM3, provided by the Free University of Berlin. The emission inventory of gaseous species for Europe was based on an inventory provided by the Free University of Berlin. Emissions in Switzerland were compiled from various sources for the year 2000. No particle emissions were included yet. CAMx results refer to PM2.5 whereas PMCAMx calculates the aerosol concentrations for each of the 10 size bins between 0.04 and 40 μm. The sum of the first 6 sections which corresponds to PM2.5, was compared with CAMx results.

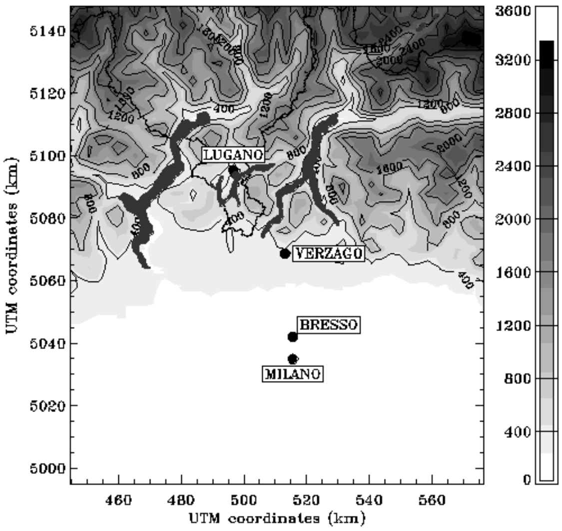

Figure 1. Topography of the model domain (masl) for northern Italy.

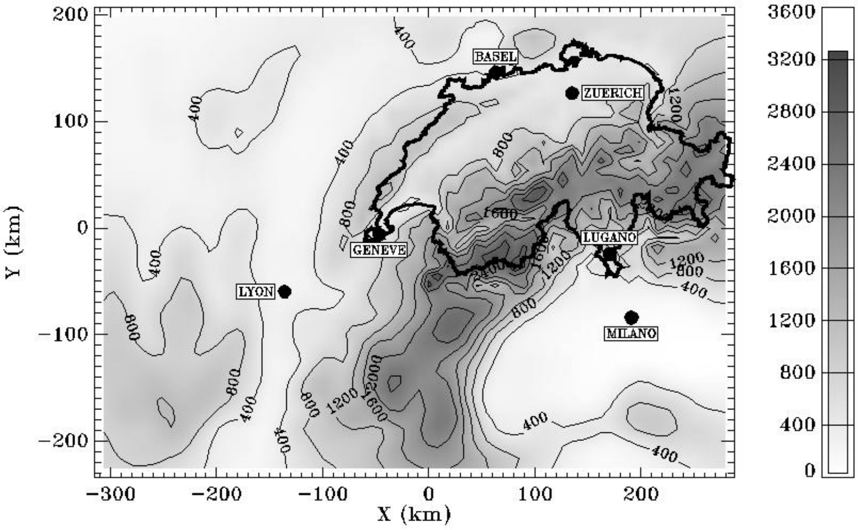

Figure 2. Topography of the model domain (masl) for Switzerland.

Results and discussion

Northern Italy

Comparison of model results with measurements of secondary inorganic aerosols performed in Verzago, 35 km north of Milan, shows that the particulate NO_3 and NH_4 levels are similar and close to the observations in the afternoon (Figure 3). At night, CAMx predicts higher nitrate concentrations than PMCAMx. In case of particulate SO_4, PMCAMx predicts slightly lower concentrations than CAMx and both model results are lower than measurements at night. Since both models use the same inorganic aerosol module and the same gas-phase mechanism, similar results are expected. However, it should be kept in mind that the gas-phase chemistry of PMCAMx is still based on an earlier version (CAMx 3.01). The updated

CBMIV mechanism in CAMx may lead to differences in results with respect to sulfate production and nighttime nitrate chemistry. Overestimation of nitrate at night by CAMx may also be due in part to assuming all nitrate is fine. The difference in the aqueous chemistry mechanism is not expected to be significant under the clear sky conditions used in this study. Boundary conditions for the particulate species in PMCAMx are not exactly the same as in CAMx because of various size sections. This may also lead to differences between the model results.

In general, PMCAMx predicts lower levels at night for all SOA classes (Figure 4). Afternoon levels of SOA1 and SOA3 are the same for both models. On the other hand, model results of SOA2, which is the aerosol product of toluene and xylene look quite different. Since the same aerosol parameters are used in both models, discrepancies are possibly due to differences in model versions. Biogenic SOA (SOA4) is about 20% of the total predicted SOA. It is difficult to validate the calculated secondary organic aerosol concentrations because there are no direct measurements. Estimations based on black carbon and total organic carbon measurements yielded an SOA range of 4 – 5 μg/m^3 for daily average (Andreani-Aksoyoglu et al., 2004). The average of calculated values in Verzago are in the same range (5.4 for CAMx and 4.4 for PMCAMx).

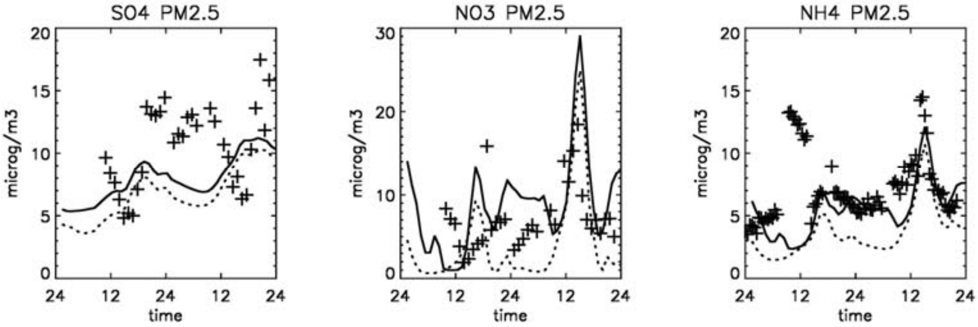

Figure 3. Diurnal variation of measured (+) and predicted concentrations. μg m^{-3}) by CAMx (solid line) and PMCAMx (dotted line) of particulate SO_4^{2-}, NO_3^- and NH_4^+ in Verzago.

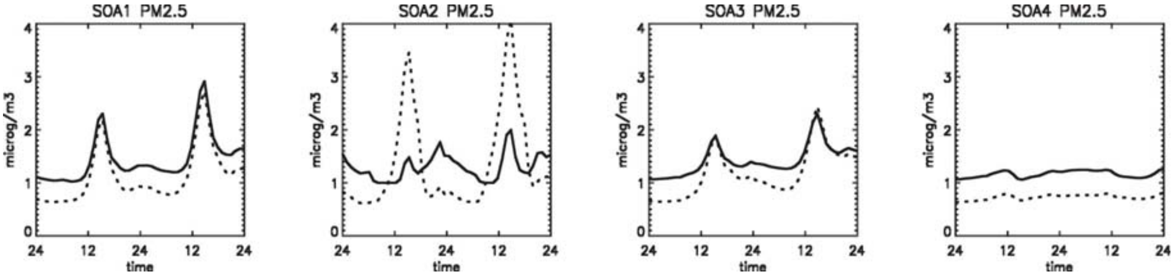

Figure 4. Diurnal variation of predicted concentrations. μg m^{-3}) of 4 SOA species by CAMx (solid line) and PMCAMx (dotted line) in Verzago.

Switzerland

The model results over the Swiss domain are compared only with each other due to lack of measurements of aerosol species (Figure 5). There are significant differences in sulfate concentrations calculated by the models. Nitrate concentrations are the same in the afternoon, but night values differ. CAMx predicts higher concentrations at night as in the first application.

Some emission sensitivity tests were performed to understand the significance of the difference between the CAMx and PMCAMx results. The highest uncertainties in anthropogenic emissions are believed to be in NH_3 and SO_2 emissions, around 20-30% (Hass et al., 2003). Therefore two more simulations with CAMx were carried out using 20% reduced SO_2 and NH_3 emissions, respectively. Reduction of SO_2 emissions by 20% did not effect sulfate particle concentrations (Figure 6). This means that the difference between CAMx and PMCAMx is larger than the uncertainties in SO_2 emissions. On the other hand, reduction in NH_3 emissions caused a significant decrease in particulate nitrate and ammonium, reducing the gap between the two model results. One can say therefore that the difference between the nitrate results of the two models is in the same range as uncertainties in NH_3 emissions.

On the other hand, SOA formation in both models is similar (Figure 7). Anthropogenic secondary aerosol concentrations (SOA1-SOA3) are much lower in northern Switzerland than in the south and in the region of Milan. The biogenic contribution to SOA which is more than 80% in the northern part of Switzerland is therefore much larger than in northern Italy.

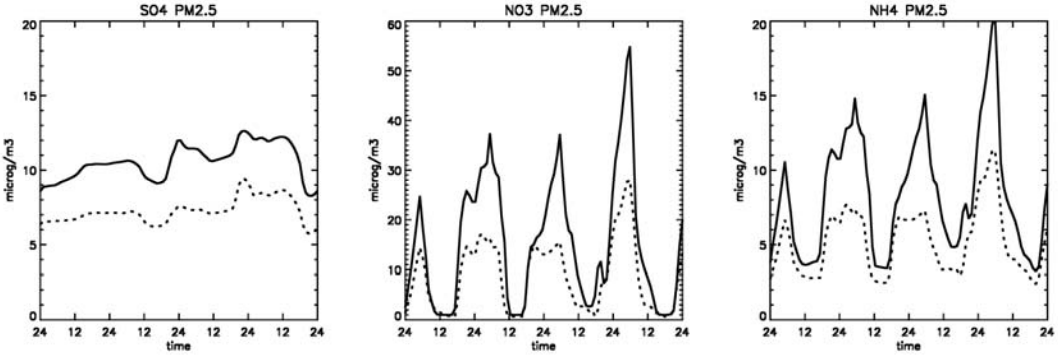

Figure 5. Diurnal variation of predicted concentrations. $\mu g\ m^{-3}$) by CAMx (solid line) and PMCAMx (dotted line) of particulate SO_4^{2-}, NO_3^- and NH_4^+ in Tänikon.

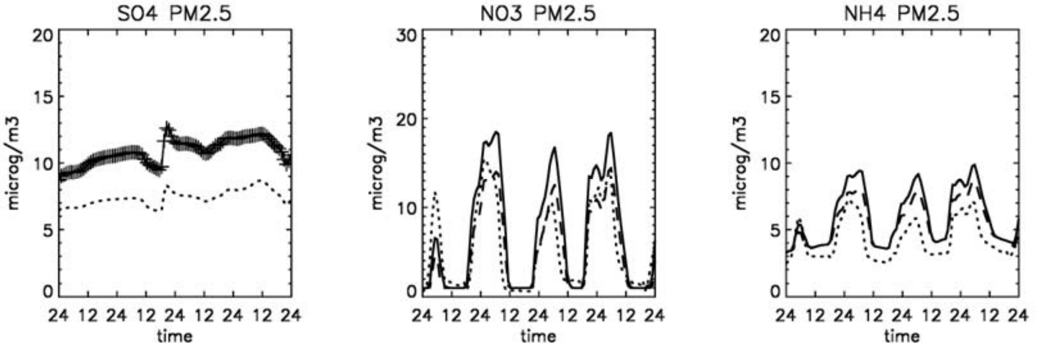

Figure 6. Diurnal variation of predicted concentrations. $\mu g\ m^{-3}$) of particulate SO_4^{2-}, NO_3^- and NH_4^+ by PMCAMx (dotted line) and by CAMx with 100% emissions (solid line), with 80% SO_2 emissions (+), with 80% NH_3 emissions (dashed line) during 4-7 August 2003 in Zürich.

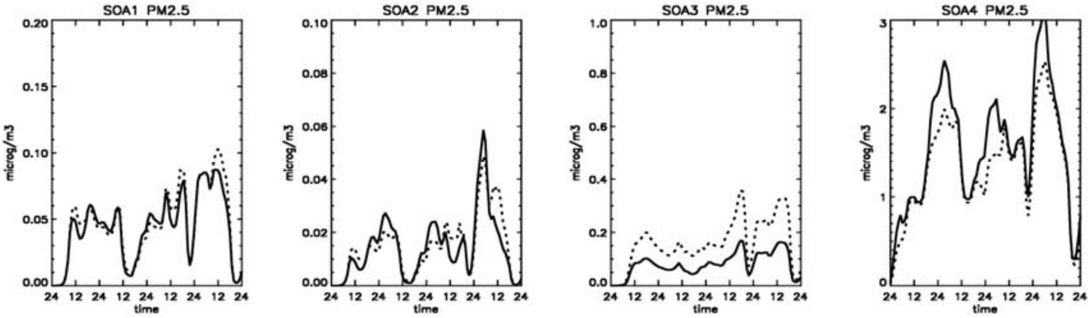

Figure 7. Diurnal variation of predicted concentrations, μg m^{-3}) of SOA by CAMx (solid line) and PMCAMx (dotted line) during 4-7 August 2003 in Tänikon.

Conclusions

On the basis of two applications, the results of two models with different complexity, CAMx and PMCAMx, are comparable. Model predictions of inorganic aerosols are rather close to observations for the study in northern Italy. Overestimation of nitrate at night by CAMx may be due in part to assuming nitrate only in the fine fraction or due to the different versions of gas-phase mechanisms (CBMIV). However, the difference between the model results for nitrate is in the same range as the uncertainties in NH_3 emissions. On the other hand, the difference in sulfate predictions between two models is larger than the uncertainties in SO_2 emissions. SOA predictions of the two models are almost the same. Both models indicated a lower biogenic contribution to SOA in northern Italy (about 20%) than in northern Switzerland (about 80%). Although SOA predictions cannot be validated by direct measurements, estimates from black carbon and total organic carbon measurements in northern Italy suggest that model results are in the same range.

Differences between the model results can be either due to the model versions which were not the same in this study (CAMx version 4.0, PMCAMx based on CAMx version 3.01) or to the different approach for particle size. Computer time required by PMCAMx is about 3 times higher than the time needed by CAMx. Although PMCAMx has the capability of calculating the aerosol species in various size sections, as long as there are limited measurements of speciated aerosols, it is difficult to evaluate the results. Most of the particle measurements in Europe consists of PM10 only. Using more complex models such as PMCAMx requires measurements of aerosol species with smaller size (not only PM10) with higher resolution in time and space. Finally, we should consider that the concept of equilibrium of the partitioning between gas phase and aerosol organics is not valid anymore considering studies of Jang et al. (2002) and Kalberer et al. (2004). Due to polymerization reactions in the aerosol, more organics can partition into the aerosols compared to prediction of equilibrium models. Some improvements in the aerosol models are therefore needed in the future. It is worth mentioning that a new version of CAMx (version 4.10s) was released in August 2004 and it offers the possibility to use multi-sectional aerosol size treatment in addition to the simpler fine/coarse approach (Environ, 2004b). Since the two different approaches for aerosol modelling are implemented in the same model, it will be easier to make comparison in future studies.

Acknowledgements

We would like to thank the LOOP community for providing us with various data from northern Italy. The output data of European Model REM3 was kindly provided by J. Flemming (FUB) to be used as boundary conditions. We are grateful to R.Stern (FUB), A.Graff (UBA) and M. van Loon (TNO) for European emissions, INFRAS and METEOTEST for the Swiss emission data. G. Yarwood from ENVIRON is gratefully acknowledged for providing the PMCAMx code.

References

Andreani-Aksoyoglu, S., Prevot, A.S.H., Baltensperger, U., Keller, J., Dommen, J., 2004, Modeling of formation and distribution of secondary aerosols in the Milan area (Italy), *J. Geophys. Res.,* **109:** D05306, doi:10.1029/2003JD004231.

Ackermann, I.J., Hass, H., Memmesheimer, M., Ebel, A., Binkowski, F.S., Shankar, U., 1998, Modal aerosol dynamics model for Europe: Development and first applications, *Atmos. Environ.*, **32**:2981.

Bessagnet, B., Hodzic A., Vautard R., Beekmann M., Cheinet S., Honore C., Liousse C., Rouil L., 2004, Aerosol modelling with CHIMERE-preliminary evaluation at the continental scale, *Atmos. Environ.*, **38**: 2803.

Chang, J.S., Brost., R.A., Isaksen, I.S.A., Madronich, S., Middleton, P., Stockwell, W.R., Walcek, C.J., 1987, A Three-dimensional Eulerian Acid Deposition Model: Physical Concepts and Formulation, *J. Geophys. Res*., **92**:14,681.

Environ, 2003, Final Report CRC project A-30, Development of an advanced photochemical model for particulate matter: PMCAMx, Environ.

Environ, 2004a, User's Guide, Comprehensive Air Quality Model with Extensions (CAMx), Version 4.00, Environ International Corporation, California, January 2004.

Environ, 2004b, User's Guide, Comprehensive Air Quality Model with Extensions (CAMx), Version 4.10s, Environ International Corporation, California, August 2004.

Griffin, R.J., Nguyen, K., Dabdub, D., Seinfeld, J.H., 2003, A coupled hydrophobic-hydrophilic model for predicting secondary organic aerosol formation, *J. Atmos. Chem*., **44**:171.

Jang, M., Czoschke, N.M., Lee, S., Kamens, R.M., 2002, Heterogeneous atmospheric aerosol production by acid-catalyzed particle-phase reactions, *Science*, **298**: 814.

Hass, H., van Loon, M., Kessler, C., Stern, R., Matthijsen, J., Sauter, F., Zlatev, Z., Langner, J., Foltescu, V., Schaap, M. , 2003, Aerosol Modeling: Results and Intercomparison from European Regional-scale Modeling Systems, EUROTRAC 2.

Kalberer M., D. Paulsen, M. Sax, M. Steinbacher, J. Dommen, A.S.H. Prevot, R. Fisseha, E. Weingartner, V. Frankevich, R. Zenobi, U. Baltensperger, 2004, Identification of polymers as major components of atmospheric organic aerosols, *Science*, **303:** 1659.

Nenes A., S.N. Pandis, C. Pilinis, 1998, ISORROPIA: A new thermodynamic equilibrium model for multiphase multicomponent inorganic aerosols, *Aquat. Geoch*., **4**:123.

PSU, NCAR, 2004, MM5 Version 3 Tutorial Presentations. http://www.mmm.ucar.edu/mm5/mm5v3/tutorial/presentations/tut-presentations.html.

Schell B., I.J. Ackermann, H. Hass, F.S. Binkowski, A. Ebel, 2001, Modeling the formation of secondary organic aerosol within a comprehensive air quality modeling system, *J. Geophys. Res.,* **106**:28275.

Strader R., C. Gurciullo, S.N. Pandis, N. Kumar, F.W. Lurmann, 1998, Development of gas-phase chemistry, secondary organic aerosol, and aqueous-phase chemistry modules for PM modeling. Final Report for CRC Project A21-1 prepared for the Coordinating research Council, Atlanta, GA by Sonoma technology, Inc., Petaluma, CA, STI-97510-1822-FR.

Zhang Y., B. Pun, K. Vijayaraghavan, S.-Y. Wu, C. Seigneur, S.N. Pandis, M. Jacobson, A. Nenes, J.H. Seinfeld, 2004, Development and application of the model of aerosol Dynamics, Reaction, Ionization, and Dissolution (MADRID), *J. Geophys. Res.,* **109**:D01202, doi:10.1029/2003JD003501.

Influence of Reducing the Highway Speed Limit to 80 km/h on Ozone in Switzerland

Johannes Keller, Sebnem Andreani-Aksoyoglu, Michel Tinguely and André Prévôt

Laboratory of Atmospheric Chemistry, Paul Scherrer Institut, CH-5232 Villigen PSI

Introduction

Summer 2003 was an extraordinarily hot and dry season with ozone levels frequently exceeding the legal thresholds. (BUWAL, 2003; BUWAL, 2004). The number of hours with ozone levels > 120 µg m^{-3} was 2 to 3 times the values recorded in previous years. The most frequent exceedances of the NABEL network were measured at the southern stations Lugano and Magadino and at the elevated locations Laegern, Chaumont and Rigi. As an emergency action to reduce ozone levels in southern Switzerland, a general speed limit of 80 km/h on the freeways A2 and A13 of canton Ticino was set from 12 to 17 August 2003. This measure, however, was not based on scientific findings.

In the view of a possibly increased frequency of hot summers, the following questions arose:

- Is a general speed limit for whole Switzerland during more than 1 week suitable for reducing peak ozone?
- What is the spatial pattern of ozone change?
- What is the maximum decrease if emissions are reduced in Switzerland only?
- What is the maximum decrease if emissions are reduced abroad as well?

To give answers to these questions, the air quality model CAMx (ENVIRON, 2003) together with the meteorological pre-processor MM5 (PSU/NCAR, 2004) was applied to 2 nested domains that include Switzerland. A new emission inventory for 2000 (reference year) taking into account changes of traffic emissions due to the speed reductions to 80 km/h was set up.

Meteorology

For the present study 2 nested domains in a Lambert Conformal projection were defined:

Coarse grid (domain 1):

centre longitude : 8 deg E
centre latitude : 47.5 deg N
grid cell size: 27 km x 27 km
number of cells: 35 x 29

Fine grid (domain 2):

grid cell size: 9 km x 9 km
number of cells: 72 x 54

The positions of these domains are shown in Figure 1 together with an example of the wind field.

The current version of MM5 uses 25 pressure levels. The thickness of a given layer varies with surface altitude. At the surface pressure of 950 hPa the bottom layer thickness is about 40 m.

Time period of the simulation was 4 - 7 August 2003. MM5 was initialized by data of the “alpine model” (aLMo) of MeteoSwiss. aLMo is a non-hydrostatic model operational at MeteoSwiss since April 2001. It is based on the Local Model (LM) developed in the frame of the COnsortium for Small scale MOdelling (COSMO, 2002). MM5 was nudged by both aLMo data and surface measurements provided by the Swiss ANETZ stations. Weather conditions during that period were characterized by low pressure gradients over Central Europe. Noon temperatures varied roughly between 30 and 35 deg C in the Swiss Plateau. Due to the small pressure gradients, aLMo wind fields were mostly very irregular, the wind speeds often being small. As examples, Figure 1 shows the surface wind fields on 5 August 2003 at 12:00 h UTC (13:00 h CET) for the coarse domain 1.

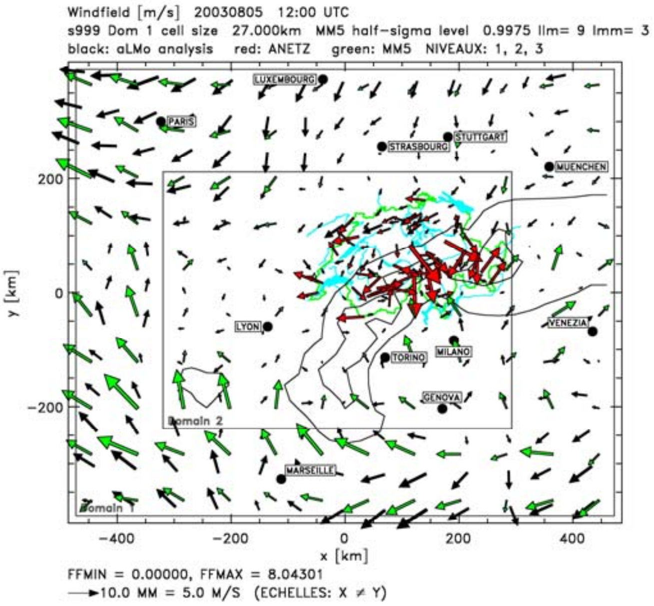

Figure 1: aLMo (black), ANETZ (red) and MM5 (green) wind fields of model domain 1 on 5 August 2003 at 12:00 h UTC (13:00 h CET). The boundaries of the CAMx domains 1 and 2 are depicted in grey. Only every 9th aLMo vector and every 3rd MM5 vector is shown.

Emissions

Gridded emission rates for regular time intervals (usually 1 h) are required as input for the air quality model CAMx. The organic compounds must be converted to species defined in the Carbon Bond Mechanism (CBM-IV) (Gery *et al.*, 1989).

European Anthropogenic Emissions

Annual emissions and time functions for Europe were kindly provided by the Freie Universitaet Berlin (FBU). This inventory was jointly developed with the Umweltbundesamt (UBA) and The Netherlands Organisation for Applied Scientific Research (TNO) in the frame of the CITY-DELTA project (Stern, 2003; Builtjes *et al.*, 2002). The inventory includes TSP, PM10, PM2.5, CH_4, CO, NH_3, NMVOC, NO_x and SO_2 for 12 source categories following the

SNAP classification. The spatial resolution of the inventory is 0.25 deg latitude (~28 km) and 0.5 deg longitude (~38 km at 47 deg lat). Reference year is 1995. Factors to extrapolate the data to 2000 are given for each country. Seasonal, weekly and diurnal variations are available as well. TNO provided factors for each SNAP category to convert NMVOCs to CBM-IV species.

Swiss Anthropogenic Emissions

Road traffic

Annual road traffic emissions of NO_x, CO, NMVOC, toluene, benzene and xylene were prepared by INFRAS. Data are split into link and zone emissions. The spatial resolution is 250m, the co-ordinates are based on the Swiss co-ordinate system. Reference year is 2000. An average diurnal variation was provided as well.

Data sets of 2 scenarios were given:

- reference scenario: speed limit on freeways according to current legislation.
- V80 scenario: general speed limit of 80 km/h on all freeways

Figure 2 shows the annual NO_x emissions for the reference case. The difference of the V80 and the reference scenario (not shown) differs from zero only on freeways because of the general speed limits of 80 km/h or less on other roads. Due to the speed limit, NO_x emissions decrease typically by 10 to 20 %, on certain freeway sections by up to 35 %. Averaged over Switzerland, the reductions relative to road traffic and relative to total NO_x emissions are 7.7% and 4.3%, respectively. Conversely, NMVOC emissions are not significantly affected by the speed reduction.

Industrial and residential NO_x

Annual NO_x emissions from residential activities, heating, industry, off-road traffic and agriculture / forestry on a 200 m resolution were provided by Meteotest. Reference year is 2000.

Industrial and residential VOC

In the frame of the air quality project TRACT an emission inventory was developed for September 1992 (Kunz *et al.*, 1995). The resolution is 5 km. From this inventory residential and industrial VOC emissions were extracted. The inventory includes 32 species according to the chemical mechanism RADM. For CAMx this data has to be converted to the CBM-IV mechanism. Using the time projections given by BUWAL (BUWAL, 1995) the emissions were converted to 2000.

NH_3

Ammonia is released mainly by manure, followed by waste treatment and road traffic. Meteotest provided annual NH_3 emissions for 2000 on a 1 km grid.

Anthropogenic emissions were resampled to the grids of the 2 domains. Figure 3 show the gridded emissions of NO of the CAMx coarse domain 1 resampled to 9 km resolution. In the area of the fine domain 2 the data are replaced by the domain 2 data.

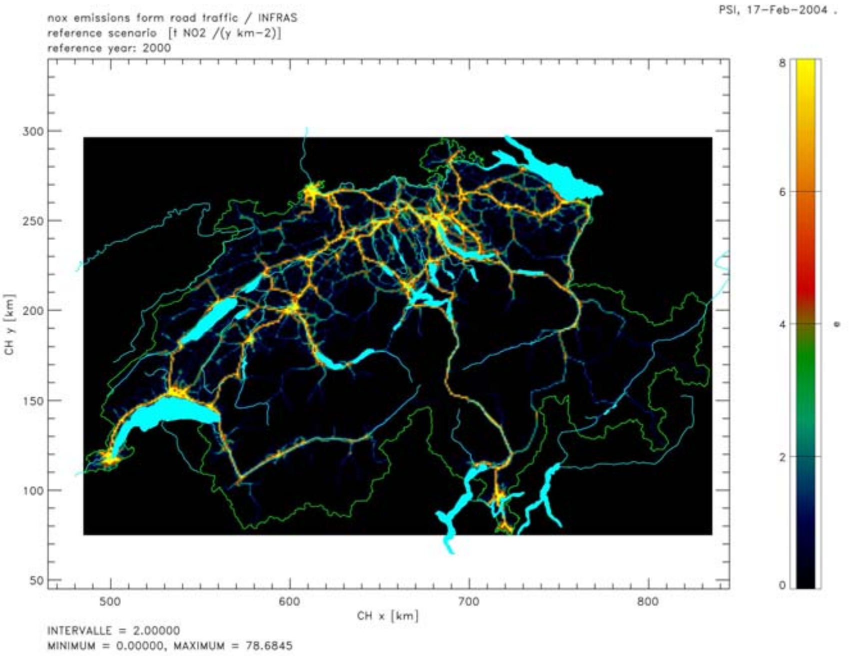

Figure 2: Annual NO_x emissions of road traffic resampled to 1 km resolution ($t\ NO_2$ / km2). Data source: INFRAS

Biogenic Emissions

The most abundant species are monoterpenes, which are released mainly by spruce and fir. Less abundant, but much more reactive is isoprene emitted by oak trees and pasture. NO emissions are caused by bacteriological decomposition in soils. Monoterpene and NO emissions are temperature dependent, whereas the isoprene release is a function of temperature and shortwave irradiance. In Andreani-Aksoyoglu and Keller, 1995 and Keller *et al.*, 1995 a methodology for the estimation of biogenic emissions is given. Gridded biogenic emissions were calculated directly for the CAMx domains. Land use data were taken from the MM5 database, from data of the “Arealstatistik” (100m resolution) issued by the Federal office of Statistics (BFS, 1999) and from forest data (1km resolution) of the “Landesforstinventar” (Mahrer and Vollenweider, 1983). Gridded temperature and shortwave irradiance data were extracted from the MM5 output.

Photochemical Modelling

The Comprehensive Air Quality Model with Extensions (CAMx) is an Eulerian photochemical dispersion model that allows for an integrated “one-atmosphere“ assessment of gaseous and particulate air pollution over many scales ranging from urban to regional (ENVIRON, 2003).

Gas-phase chemistry

There are five gas-phase mechanisms supported in CAMx4 (version CAMx v4.03): four different versions of Carbon Bond Mechanism (CBM-IV, Gery *et al.*, 1989) and SAPRC99 chemical mechanism (Carter, 2000). In this study, CBM-IV mechanism with the extensions for aerosol modelling (mechanism 4) was used. Photolysis rates are derived for each grid cell assuming clear sky conditions as a function of five parameters: solar zenith angle, altitude, total ozone column, surface albedo and atmospheric turbidity. Since the photolysis rates are significantly affected by the presence of clouds, a cloud input file is required in case of cloudy conditions.

Aerosol chemistry

In CAMx4, aerosol processes are linked to the CBM-IV gas-phase mechanism. The gas-phase photochemistry forms aerosol precursors via the OH initiated oxidation of SO_2 to sulphate, production of nitric acid, and formation of condensable organic gases.

Model Setup

The size of the CAMx4 coarse domain is 35 grid cells in the east-west direction and 29 grid cells in the north-south direction with a resolution of 27 km x 27 km, i.e. the same as the MM5 coarse domain. The fine domain contains 68 and 50 grid cells in the east-west and north-south direction, respectively, with a resolution of 9 km x 9 km. This size is slightly smaller than the MM5 domain to assure proper meteorological conditions at the boundaries. There are 10 layers in a terrain-following coordinate system, the first being 30 m above ground. Initial and boundary conditions were calculated using the REM-3 European model output data for the same time period provided by the Meteorological Institute of Freie Universitaet Berlin. REM-3 domain covers almost whole Europe with a resolution of 0.5 x 0.25 degree.

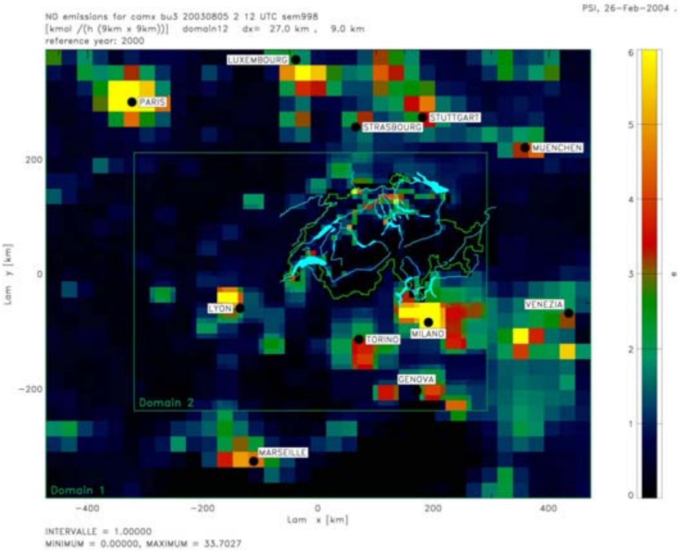

Figure 3: NO emissions in CAMx domain 1 and 2 calculated for 5 August 2003, 12:00 UTC (14:00 CEST) (kmol / h). The data were resampled to a common grid cell size of 9 km. Reference year of the original emission data is 2000. The boundaries of the CAMx domains 1 and 2 are depicted in green.

Emission Scenarios

The following scenarios were selected:

Scenario 1 (base case):
time period for model runs: 4-7 August 2003
reference year for emissions: 2000
current speed pattern on Swiss roads (legal limits 80 / 120 km/h)

Scenario 2:
general speed limit on Swiss highways: 80 km/h

Scenario 3:
50% reduction of NOx and VOC emissions in Switzerland only

Scenario 4:
50% reduction of NOx and VOC emissions in whole Europe

Results

Scenario 1 (base case)

Only the part of fine domain covering Switzerland will be discussed in this section. The highest ozone mixing ratios in the lowest layer were predicted generally in the afternoon between 13:00 and 16:00 UTC (Figure 4). Ozone levels on 5 August are rather high in southern Switzerland, around Lugano, under the influence of southerly winds with polluted Po Basin air.

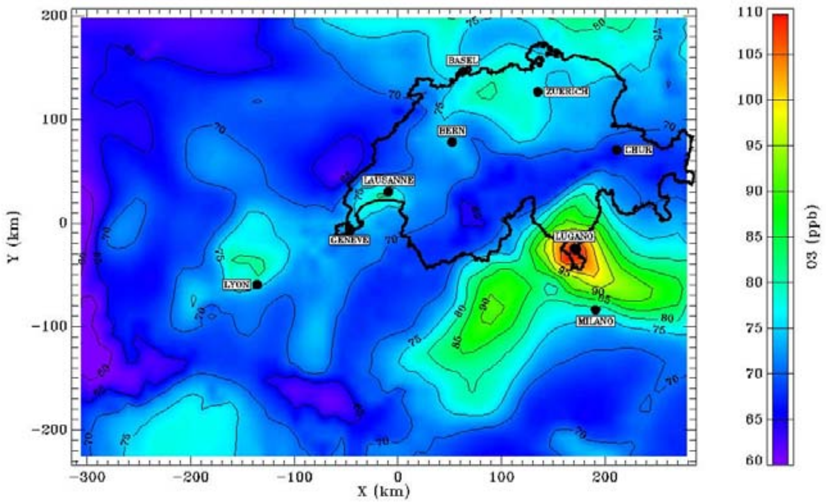

Figure 4: Predicted O_3 mixing ratios (ppb) on 5 August 2003, at 13:00-14:00 UTC.

Scenario 2

In this case, emissions were adjusted to a speed limit of 80 km/h on the freeways. Changes in peak ozone concentrations in the lowest layer due to reduced speed limit are shown as percentages in Figure 5. Blue colour indicates a decrease in ozone mixing ratios in percentage, and red colour shows the increase.

Ozone concentrations increased in the morning along the highways due to the fact that ozone production is usually VOC-limited during the morning hours. On the other hand, ozone decreased in the afternoon when ozone formation becomes more NO_x-limited. This is the case for every day of the studied period.

The decrease in ozone levels due to speed reduction, however, is very small, lower than 1%. Keeping in mind that NO_x emissions decreased only by about 4% and VOC emissions were not significantly affected by speed reduction, the small influence on ozone concentrations is not surprising. Other studies with similar measures indicated the need for emission reductions larger than 50% to achieve considerable decreases of ozone (Umweltbundesamt, 2004).

Scenario 3

The change in peak ozone when reducing NO_x and VOC by 50 % in Switzerland only is shown in Figure 6. Reductions up to 10 % are feasible in the Swiss plateau. In southern Switzerland, however, this abatement strategy is inefficient because of the strong influence of the Po Basin.

Scenario 4

If NO_x and VOC are reduced by 50 % in the whole domain, ozone levels may be reduced by up to 18 % (Figure 7). This effect is strongest in southern Switzerland, due to the reduction in the Milan area.

Conclusions

The influence of the traffic speed reductions to maximum 80 km/h in Switzerland on ozone concentrations is not very high, typically lower than 1%. This can be backed up by a back-of-the-envelope calculation. In the beginning of the 90s, results from the POLLUMET (Pollution and Meteorology) project in Switzerland suggested that around 30% of the ozone concentrations could be controlled by Swiss emissions during summer smog situations (BUWAL, 1996). Due to lower emissions nowadays, a lower amount, around 25%, can be estimated to be controllable today. The Swiss NO_x emissions in the traffic scenario were calculated to be around 4% lower than in the base case. If the response of the ozone production is linear to the NO_x emissions, 4% of 25% yielding 1% of the ozone concentrations could be reduced. This is true for NO_x-limited conditions. The response can be opposite if the ozone production is VOC-limited. This could be shown for the morning hours when the ozone production is usually VOC-limited and the ozone increased in the traffic scenario near the highways. Overall, the traffic speed reduction alone is not enough to significantly reduce the ozone levels. However it should be noted that the NO_x concentrations and the aerosol concentrations also decrease in such a traffic scenario. This leads to a relief in addition to the small ozone reduction during these summer smog conditions.

Larger scale (Central Europe) emission decreases would yield better results than just decreases within Switzerland, but our model runs indicate that also in this case larger emission reductions than speed limitations on highways are necessary to make a detectable difference in ozone. More important for the ozone reductions in Switzerland will be the long-term emission developments in Switzerland, the surrounding countries, and to some extent even in the whole northern hemisphere. The influence of past and possible future emission changes in Switzerland and in the near surroundings will be investigated in a follow-up study.

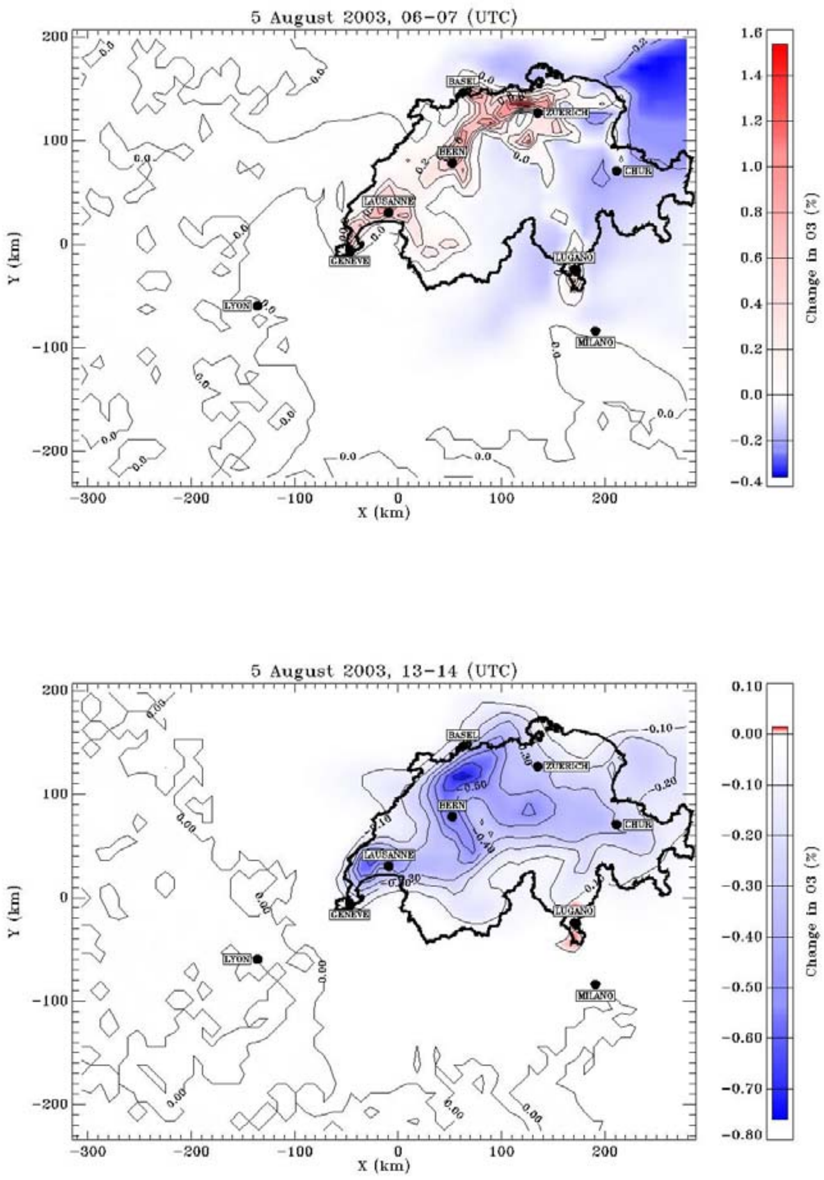

Figure 5: Predicted change in O_3 mixing ratios (%) due to speed limit, on 5 August 2003, at 06:00-07:00 UTC (top), 13:00-14:00 UTC (bottom). Blue colour shows the decrease, red colour shows the increase.

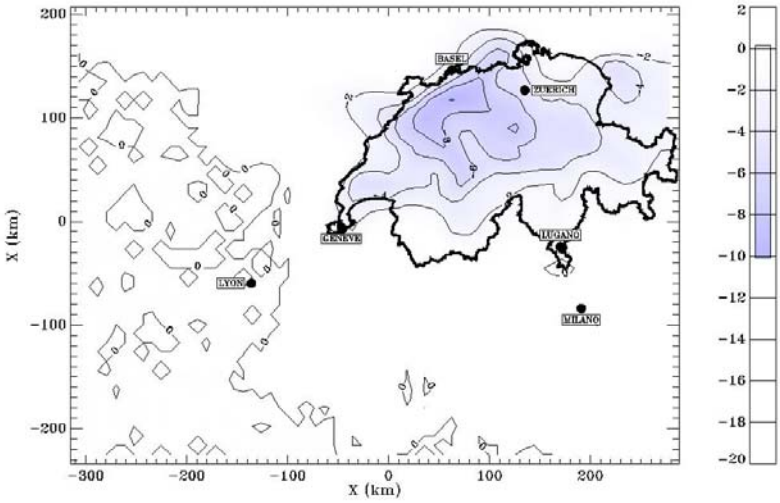

Figure 6: Change in peak ozone level (%) due to a 50% decrease of NO_x and VOC emissions in Switzerland only.

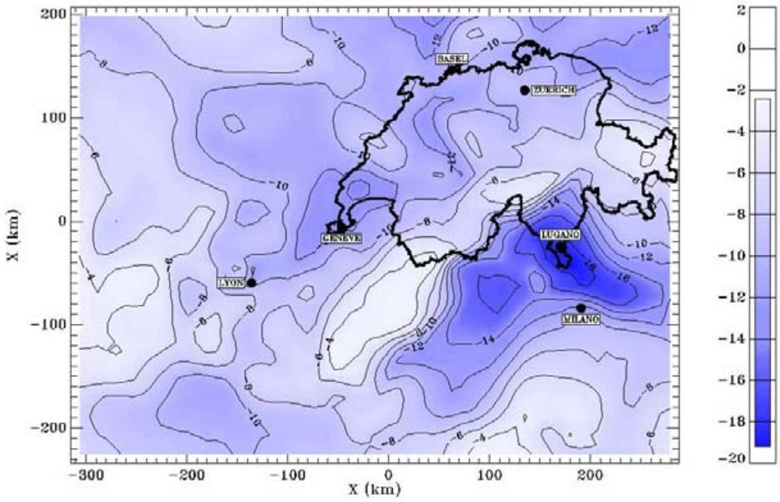

Figure 7: Change in peak ozone level (%) due to a 50% decrease of NO_x and VOC emissions in the whole model domain.

Acknowledgements

This project was financially supported by the Swiss Agency for the Environment, Forests and Landscape, SAEFL (Bundesamt für Umwelt, Wald und Landschaft, BUWAL)

We are grateful to the following people and institutions for providing weather, emission and air quality data within very restricted time limits: F.Schubiger and C. Voisard (MeteoSwiss) for aLMo analysis data, R.Stern (FUB), A.Graff (UBA) and M. van Loon (TNO) for European emissions, R. Zbinden, M. Keller and J. Heldstab (INFRAS) for Swiss road traffic data, Th.

Kuenzle and B.Rihm (METEOTEST) for updated Swiss NO_x and NH_3 data and for the TRACT emission inventory, and J. Flemming (FUB) for REM-3 model output data. We thank also R.Weber (BUWAL) for the fruitful co-operation during the project.

References

Andreani-Aksoyoglu S., Keller J., (1995) Estimates of monoterpene and isoprene emissions from the forests in Switzerland. J. Atmospheric Chemistry 20, 71-87.

BFS, (1999) GEOSTAT Benuetzerhandbuch, Bern.

Builtjes P., van Loon M., Schaap M., Teeuwisse S., Visschedijk A. J. H., Bloos J. P., (2002) The development of an emission data base over Europe and further contributions of TNO-MEP. Freie Universitaet Berlin / Institut fuer Meteorologie und Troposphaerischer Umweltforschung, Berlin.

BUWAL, (1995) Vom Menschen verursachte Luftschadstoffemissionen in der Schweiz von 1900 bis 2010. Schriftenreihe Umwelt Nr.256, BUWAL, Bern.

BUWAL, (1996) Troposphaerisches Ozon. Aktuelle Forschungsergebnisse und ihre Konsequenzen fuer die Luftreinhaltung. BUWAL, Bern.

BUWAL, (2003) Ozonsommer 2003 im Vergleich mit 1993-2002, http://www.umwelt-schweiz.ch/buwal/de/fachgebiete/fg_luft/luftbelastung/publikat/nabel/index.html.

BUWAL, (2004) Luftbelastung 2003, http://www.umwelt-schweiz.ch/buwal/de/fachgebiete/fg_luft/luftbelastung/publikat/nabel/index.html.

Carter W. P. L., (2000) Programs and files implementing the SAPRC-99 mechanism and its associates emissions processing procedures for Models-3 and other regional models, http://pah.cert.ucr.edu/~carter/SAPRC99/s99files.htm.

COSMO, (2002) Newsletter No. 2. Deutscher Wetterdienst, Offenbach (D).

ENVIRON, (2003) User's Guide, Comprehensive Air Quality Model with Extensions (CAMx). Version 4.00. ENVIRON International Corporation, Novato.

Gery M. W., Whitten G. Z., Killus J. P., Dodge M. C., (1989) A photochemical kinetics mechanism for urban and regional scale computer modeling. JOURNAL OF GEOPHYSICAL RESEARCH 94, 925-956.

Keller J., Andreani-Aksoyoglu S., Joss U., (1995) Inventory of natural emissions in Switzerland. In *Air Pollution III, Air Pollution Engineering and Management*, 339-346. Computational Mechanics Publications, Southhampton.

Kunz S., Kuenzle T., Rihm B., Schneider A., Schlaepfer K., (1995) TRACT Emissionsmodell Schweiz. Schlussbericht Maerz 1995. METEOTEST / Carbotech, Bern.

Mahrer F., Vollenweider C., (1983) Landesforstinventar LFI, Eidgenössische Forschungsanstalt für Wald, Schnee und Landschaft (WSL), Birmensdorf.

PSU/NCAR, (2004) MM5 Version 3 Tutorial Presentations, http://www.mmm.ucar.edu/mm5/mm5v3/tutorial/presentations/tut-presentations.html.

Stern R., (2003) Erstellung einer europaweiten Emissionsdatenbasis mit Bezugsjahr 1995 und die Erarbeitung von Emissionsszenarien für die grossraeumige Ausbreitungsrechnungen mit

REM/CALGRID. Freie Universitaet Berlin / Institut fuer Meteorologie und Troposphaerischer Umweltforschung, Berlin.

Umweltbundesamt, (2004) Programme of Control Concepts and Measures for Ozone, http://www.umweltdaten.de/ozon-e/index.htm.

The THOR integrated air pollution forecast system – current status and ongoing developments

Jørgen Brandt, Jesper H. Christensen, Lise M. Frohn, Camilla Geels,
Kaj M. Hansen and Carsten A. Skjøth

National Environmental Research Institute, Department of Atmospheric Environment,
Frederiksborgvej 399, P.O. Box 358, DK-4000 Roskilde, Denmark.

Abstract

The THOR system is a highly integrated model system, capable of performing forecasting of meteorological and chemical weather for the general public as well as air quality scenarios, assessment and management for decision-makers. It consists of several meteorological and air pollution models, developed at NERI during the latest decades and is capable of operating for different applications and at different scales. The main purposes of the THOR system are forecasting, nowcasting, emission reduction scenarios, retrospective analyses and air pollution assessments and management. The system is capable of accurate and high-resolution three-days forecasting of weather and air pollution from regional scale over urban background scale and down to individual street canyons in cities – on both sides of the streets. The coupling of models over different scales makes it possible to account for contributions from local, near-local as well as remote emission sources in order to describe the air quality at a specific location - e.g. in a street canyon or in a park. The system is presently operational for several cities in Denmark and is used for information and warning of the public in cases of high air pollution levels and for policy management (e.g. by emission reduction or traffic scenarios) of many different chemical compounds. The system is also used in connection with both the urban and rural monitoring programs in Denmark. Furthermore, the system is capable of forecasting air pollution from accidental releases as e.g. nuclear power plants, industrial sites and fires.

The THOR Integrated Model System

The general concept of the THOR model system (illustrated in figure 1) is to form a basis for an open framework of model integration. Not only atmospheric models are included in the system, even though these models form the core of the framework, but also e.g. effect models for human exposure, marine models, terrestrial models, and social models. The basic framework idea is the operationalisation of data flow and communication between these different types of models, input data, measurements, results, visualisations, end-users/decision-makers. This means that the system should be ready (operational) to give answers to (any) specific questions or problems within the atmospheric environment besides modelling the chemical weather (Lawrence et al., 2005). The system was initially developed in the spring of 1998 (Brandt et al., 2001a; 2001b; 2001c; 2003) and has been running operational since then. At present the system includes global meteorological data from either NCEP or ECMWF used as initial and boundary conditions for the numerical weather forecast models Eta and/or MM5v3. The weather data is used to drive the air pollution models, including the different versions of the Danish Eulerian Hemispheric Model (DEHM), the Urban Background Model (UBM), the Operational Street Pollution Model (OSPM), the accidental release model (DREAM), the Gaussian plume model (OML) and others. Results from the air pollution models are implemented and used e.g. in models for human exposure, marine models, and economic assessment of impacts on human health. The weather forecast model Eta, and the air pollution models DEHM-REGINA, UBM and OSPM is presently running operationally four times every day, producing three-days air pollution forecasts from European scale, over urban background scale to urban street scale. For every forecast, more than 3000 visualizations are produced for quality analysis and a subset of this information is provided to the public via the Internet, local radio, TV, and newspapers. In the following, the individual models are described. The ozone forecasts from the THOR system was compared with forecast data from other forecast systems in Europe in Tilmes et al., (2002) showing good performance.

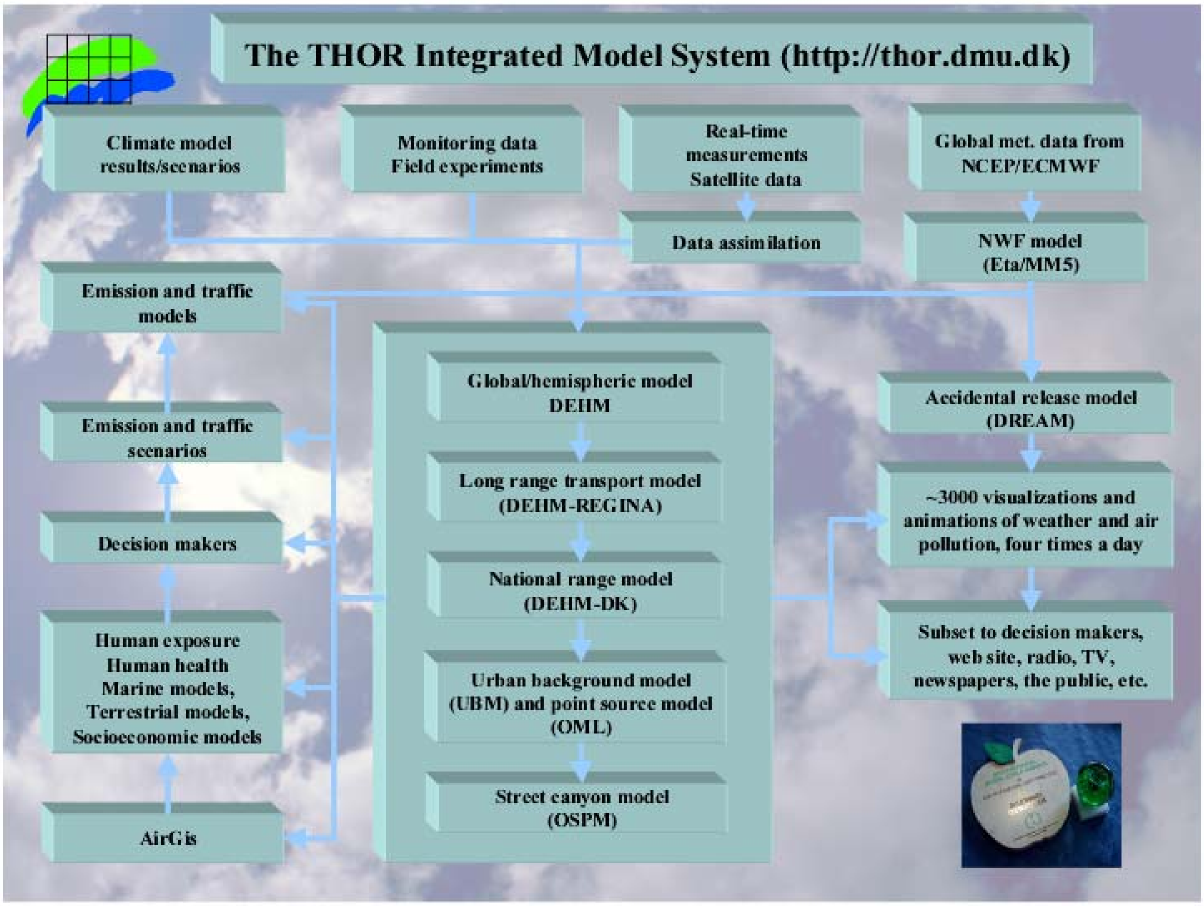

Figure 1. A schematic diagram of the models/modules in the operational THOR system and data flow within the system.

Meteorological models

Two different mesoscale numerical weather prediction models are used as meteorological drivers for the model: the MM5v3 model (Grell et al., 1995) or the Eta model (Janjić, 1994). Global analyzed meteorological data available from 1979 to 2004, used as input to the MM5v3 mesoscale modelling system, are obtained from the European Centre for Medium-range Weather Forecasts (ECMWF), while global analyzed- and forecast data from the National Centers for Environmental Prediction (NCEP) available for the period from 1998 to present is used as input to the Eta model. Data from NCEP global circulation model are the starting point for nearly all weather forecasts in the USA, and for many forecast systems in Europe. An example of output from the Eta model is given in figure 2. The setup and the application of the Eta model in the THOR system is documented in Brandt et al., (2004a; 2004b).

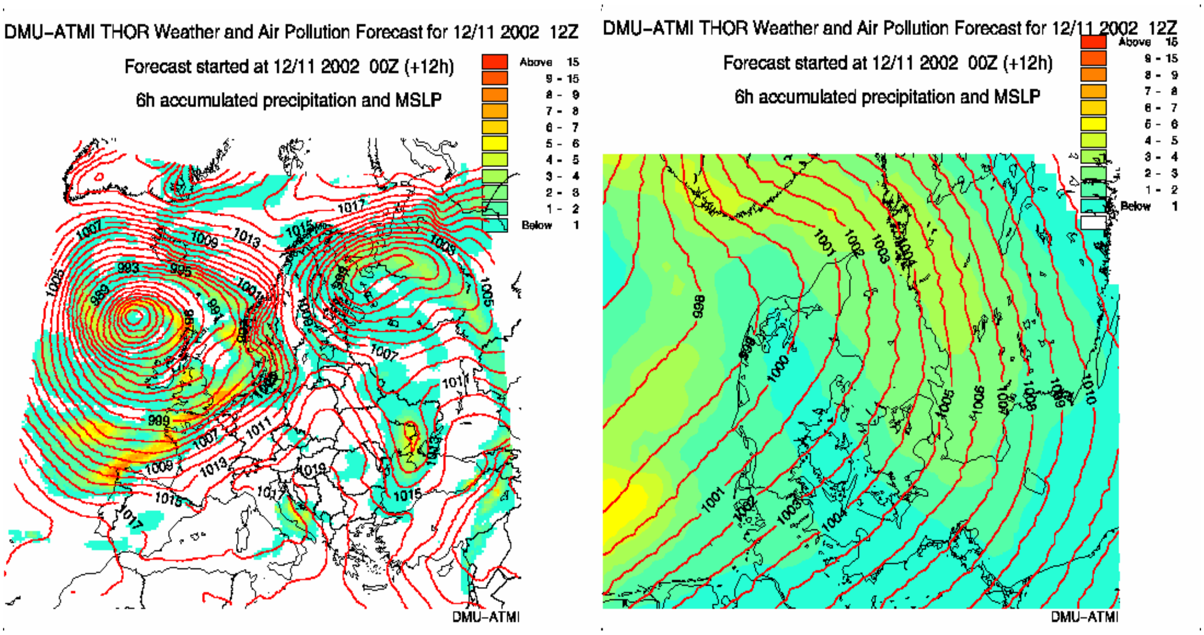

Figure 2. An example of results from the numerical weather forecast model Eta, including the 6 hour accumulated precipitation and mean sea level pressure for Europe (left figure) and Denmark (right figure).

DEHM-REGINA

The weather forecast is used as input to the photo-chemical version of the long-range transport air pollution model the Danish Eulerian Hemispheric Model (DEHM-REGINA) (Frohn et al., 2002) producing air pollution forecasts on regional background scale (e.g. the greater European scale). The operational version of the model calculates transport, dispersion, deposition and chemistry (including photochemistry) of 63 chemical compounds. A chemical scheme similar to the EMEP scheme with 63 species and 120 chemical reactions is included in the model. Three of the species are particulates (PM25, PM10, TSP). Furthermore sea salt is implemented in the model. The model was tested in a model intercomparison exercise, see Loon et al., (2004).

The emissions are based on a combination of the GEIA (Global Emissions Inventory Activity), the EDGAR (Emission Database for Global Atmospheric Research) and the EMEP emissions (European Monitoring and Evaluation Programme). The dry deposition velocities of the species are based on the resistance method. The wet deposition is parameterized by a simple scavenging ratio formulation with different in-cloud and below-cloud scavenging.

DEHM is in general based on a set of coupled full three-dimensional advection-diffusion equations. The original model covers the majority of the Northern Hemisphere with currently one two-way coupled nest over Europe implemented. The horizontal resolution in the mother domain is 150 km x 150 km, and the nesting factor is three giving a resolution in the first nest of 50 km x 50 km. The nested grid is a sub grid of the EMEP 50 km x 50 km grid. The vertical discretization is defined on an irregular grid with 20 layers up to ~15 km. The advection is solved numerically using an Accurate Space Derivatives scheme with non-periodic boundary conditions for the horizontal advection and a finite elements scheme for the vertical advection. The diffusion is solved using the finite elements scheme.

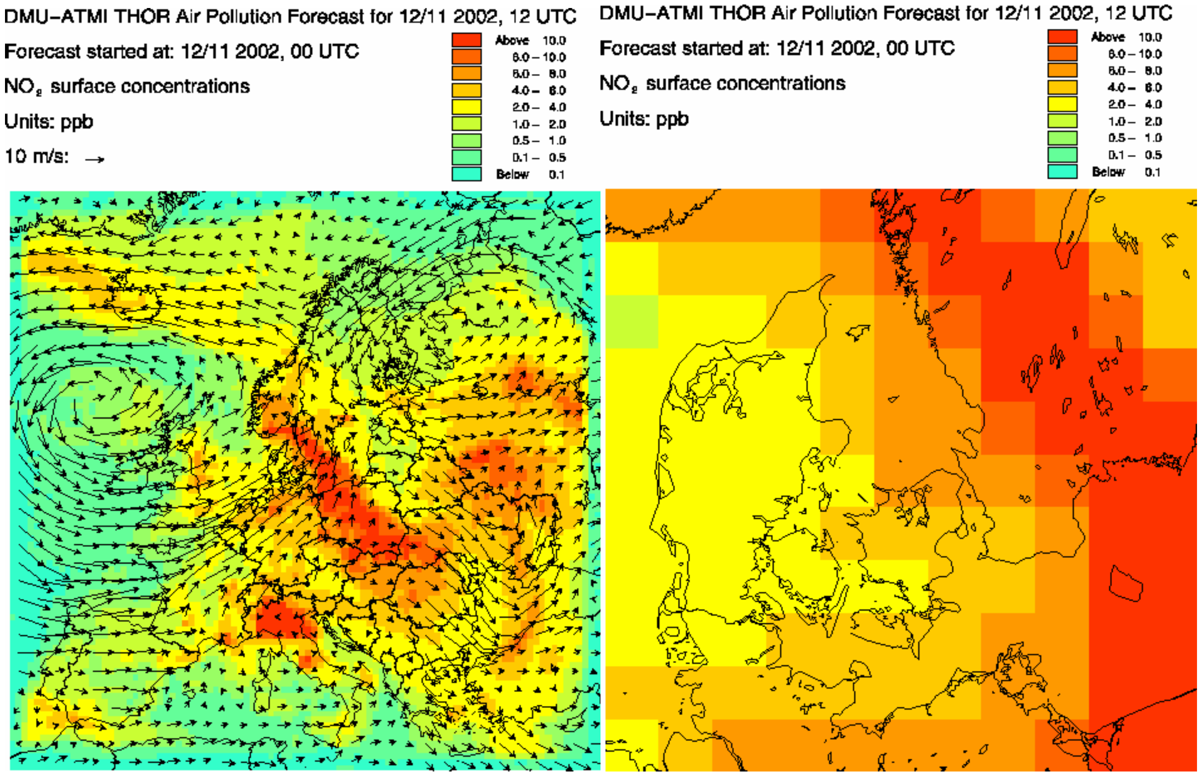

Figure 3. An example of forecasted results from the long range transport model for NO_2 for Europe (left figure) and Denmark (right figure).

Four other versions of DEHM exist: 1) DEHM-CO_2 version, including atmospheric transport and biogenic and anthropogenic fluxes of CO_2 (Geels et al, 2004), 2) DEHM-Hg - a mercury version, including 14 mercury species (Christensen et al., 2004), 3) DEHM-POP, which is presently including α-HCH (Hansen et al., 2004) , and 4) DEHM-Sulphur: SO_2, SO_4 and lead (Christensen, 1997).

Urban background model, UBM

Meteorological data from the weather forecast and air pollution concentrations from the long-range transport model are subsequently used as input to the Urban Background Model, UBM, calculating the urban background air pollution based on emission inventories with a spatial resolution down to one kilometer.

The UBM model is suitable for calculations of urban background concentrations when the dominating source is the road traffic. For this source the emissions take place at ground level, and a good approximation is to treat the emissions as area sources, but with an initial vertical dispersion determined by the height of the buildings. The applied emission data have to be provided on a grid with the same resolution as used in the model. The concentrations calculated by the model include NO, NO_2, NO_x, O_3, CO, benzene and particles. Contributions from the individual area sources, subdivided into a grid with a resolution down to 1 km x 1 km, are integrated along the wind direction path assuming linear dispersion with the distance to the receptor point. Horizontal dispersion is accounted for by averaging the calculated concentrations over a certain, wind speed dependent, wind direction sector, centred on the average wind direction. Formation of the nitrogen dioxide due to oxidation of NO by ozone is calculated using a simple chemical model based on an assumption of photochemical equilibrium on the time scale of the pollution transport across the city area. This time scale governs the rate of entrainment of fresh rural ozone. The model is described in more detail in Berkowicz (1999b).

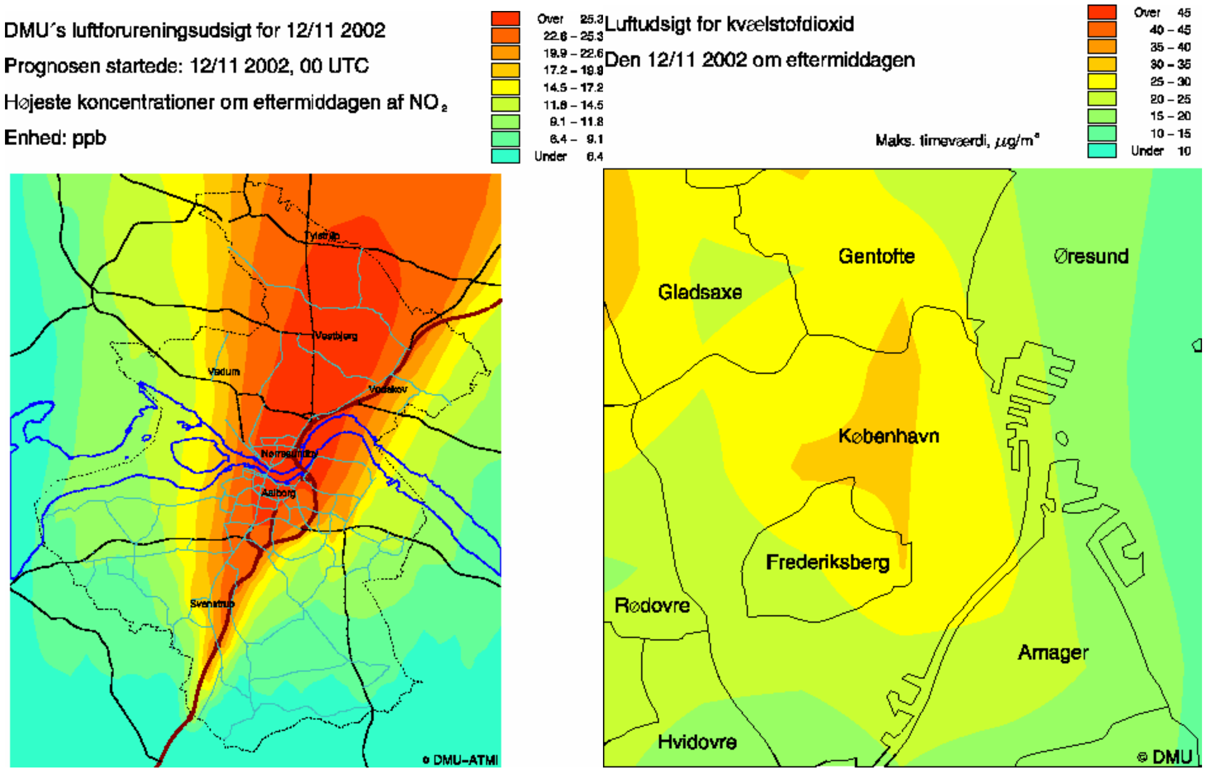

Figure 4. Examples of forecasted maximum afternoon NO_2 concentrations from the Urban background model for the City of Aalborg (left figure) and the City of Copenhagen (right figure) for November 12th, 2002. The forecast started November 12th at 00 UTC. The unit in the left figure is ppb and µg/m^3 in the right figure.

The model is e.g. run operationally for the central city of Copenhagen and for the city area of Aalborg, Denmark, and the results of these calculations are published on the Internet four times each day. Figure shows concentrations of nitrogen-dioxide over the city of Aalborg (left figure) and the city of Copenhagen (right figure).

Operational Street Pollution Model, OSPM

The output from the urban background model is used as input to the Operational Street Pollution Model, OSPM, producing the air pollution concentrations at street level at both sides of the streets in cities. The OSPM model is a parameterized semi-empirical model making use of a priori assumptions about the flow and dispersion conditions in a street canyon. In the model, concentrations of exhaust gases are calculated using a combination of a plume model for the direct contribution and a box model for the recirculating part of the pollutants in the street. Parameterization of flow and dispersion conditions in street canyons was deduced from extensive analysis of experimental data and model tests. Results from these tests have been used to improve the model performance, especially with regard to different street configurations and a variety of meteorological conditions. The model calculates air concentrations of NO, NO_2, NO_x, O_3, CO, benzene and particles in the street canyon at both sides of the street. A schematic diagram showing the principles behind the model is given in figure 5.

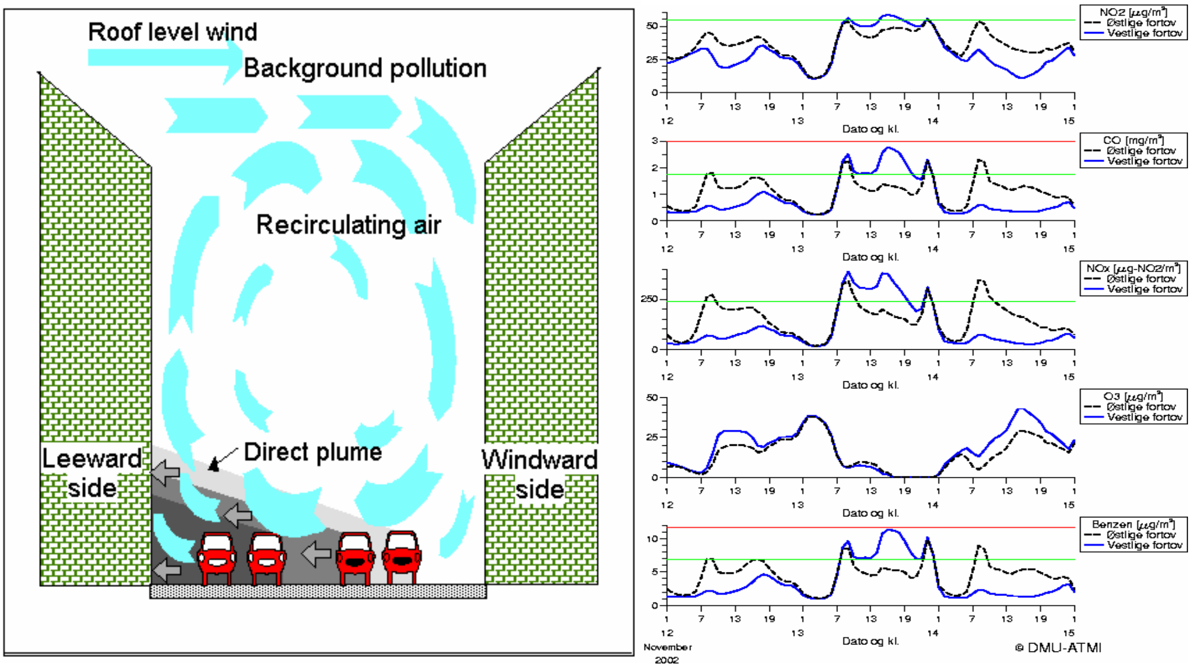

Figure 5. Left figure: A schematic diagram of the vortex in a street canyon. In this situation where the wind is coming from the left at the roof top, the concentrations at the windward side of the street is dominated by the urban background concentrations and the concentrations at the leeward side of the street is dominated by the direct plume from the vehicles. Right figure: An example of a three days forecast of concentrations using the OSPM model for November 2002. The blue line represents the concentrations at the western side of the street and the dotted line represent the concentrations at the eastern side of the street.

Due to the circulation of air in street canyons, the air pollution concentrations can be very different at the two sides of a street. This is illustrated in the figure. The right figure shows a three-day forecast of air pollution concentrations at the eastern and western side of a street in Copenhagen for different chemical compounds. Depending on the meteorological situation, the concentration levels are very different. The OSPM has been successfully tested for many different cities in the world. For a more detailed description of the model, see Berkowicz (1999a).

The DREAM model

The weather forecast also drives the Danish Rimpuff and Eulerian Accidental release Model, DREAM (Brandt 1998; Brandt et al., 2002), used in connection with accidental releases at greater scales as e.g. the Chernobyl accident. DREAM is a combined Lagrangian and

Eulerian model, where the Lagrangian part handles the initial near-source transport and dispersion (up to ~300 km from the source) and the Eulerian part calculates transport and dispersion in an area covering e.g. Europe. The model can be used for any accidental release from power plants, industrial sites, natural and human made fires, etc. Recently, the model was setup and applied for a large fire at a fire-works storage building in the city of Kolding, Denmark.

Examples of validation

The model system has been operational since August 1998, which means that more than six years of data are available for validation and evaluation of the coupled system. Examples of comparison of some model results with measurements given as time series for January 2000 and June 2003 are given in figure 6.

The upper left figure shows a comparison of hourly values of measured meteorological parameters in the city of Aalborg, Denmark, and the weather forecast for January 2000. The figures to the right show a comparison of hourly values of measured concentrations and the air pollution forecast using the Operational Street Pollution Model at the street Vesterbro, Aalborg for January 2000 and June 2003. The lower figure to the left shows results obtained from the UBM model compared to measurements for June 2003. As seen in the figures, the models produce very accurate forecasts of both weather and air pollution parameters.

All weather and air pollution data from the system can be disseminated to the authorities, decision-makers and the public. The raw data can be displayed as maps or as time series. Furthermore, information about exceedances of critical air pollution levels can be extracted and displayed as color codes or given as compressed information, as e.g. "below mean", "mean", "above mean", "high" or "warning".

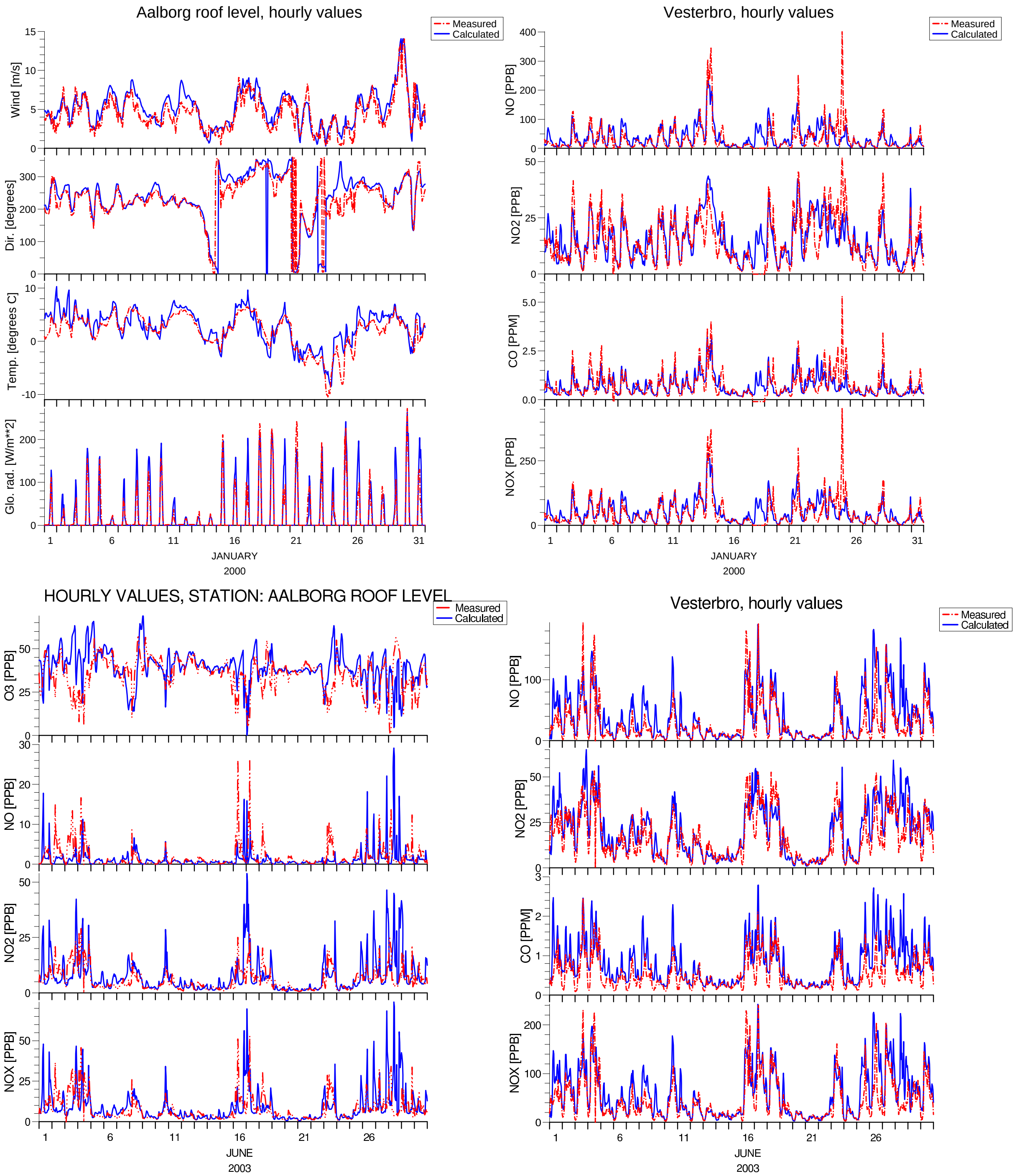

Figure 6. Comparison of hourly values of measured meteorological parameters in the city of Aalborg, Denmark, and the weather forecast for January 2000 (upper left figure). Comparison of hourly values of measured concentrations and the air pollution forecast using the Operational Street Pollution Model at the street Vesterbro, Aalborg for January 2000 and June 2003 (right figures). Results obtained from the UBM model compared to measurements for June 2003 (lower left figure).

Ongoing developments

Ongoing developments of the system include implementation of different data assimilation techniques (4D-var and Optimum Interpolation) for ground based and satellite data in order to improve the air quality forecasts and retrospective model runs at different scales.

Furthermore, scenario data from a global climate model is being included to assess the future impacts of a changing climate within the 21st century on the air pollution concentrations and depositions with focus on the European and Arctic areas.

A new model, DEHM-DK, which is a high-resolution (down to 1 km x 1 km), national scale model, especially designed for modelling air pollution important for eutrophication in terrestrial and marine eco-systems as well as human exposure in cities is under development. The work concerning the inclusion of particles in all models for calculating PM25, PM10, and TSP from regional scale and down to street scale are continuing.

The DEHM-REGINA model together with the OML model forms a basis for assessing costs from air pollution related impacts on human health. Residuals from model runs with and without specific sources (e.g. a power plant) are combined with exposure-response functions to give the impacts. Valuation of the different responses allows estimate of the damage (or "cost"). Currently, comparisons with results from the EcoSense software developed within the ExternE methodology for Danish conditions are carried out. This setup within the THOR system facilitates estimation of costs related to e.g. one specific power plant or industrial unit and will - once completely developed - form a powerful basis for management.

Acknowledgement

The authors greatly acknowledge the National Centers for Environmental Prediction (NCEP), USA, for providing meteorological data. The European Monitoring and Evaluation Programme (EMEP), GEIA (Global Emissions Inventory Activity), and the EDGAR (Emission Database for Global Atmospheric Research) are greatly acknowledged for providing emission data. Part of the work has been funded by the EU-projects FLOODRELIEF (REaL tImE Flood Decision Support System Integrating Hydrological, Meteorological and Radar Technologies (EU 5th framework programme) and CARBOEUROPE-IP including assessment of the European Terrestrial Carbon Balance (6th EU framework programme).

References

Berkowicz, R., 1999a. OSPM - A parameterized street pollution model, 2nd International Conference - Urban Air Quality, Measurement, Modelling & Management, 3-5 March, Madrid, pp. 8.

Berkowicz, R., 1999b. A simple model for urban background pollution, 2nd International Conference - Urban Air Quality, Measurement, Modelling & Management, 3-5 March, Madrid, pp. 8.

Brandt, J., 1998. Modelling transport, dispersion and deposition of passive tracers from accidental releases, PhD Thesis. National Environmental Research Institute, Department of Atmospheric Environment, Frederiksborgvej 399, P.O. Box 358, DK-4000 Roskilde, Denmark, pp. 307.

Brandt, J., J. H. Christensen, L. M. Frohn, F. Palmgren, R. Berkowicz and Z. Zlatev, 2001a: "Operational air pollution forecasts from European to local scale". *Atmospheric Environment*, Vol. 35, Sup. No. 1, pp. S91-S98, 2001.

Brandt, J., J. H. Christensen, L. M. Frohn and R. Berkovicz, 2001b: "Operational air pollution forecast from regional scale to urban street scale. Part 1: system description", *Physics and Chemistry of the Earth (B)*, Vol. 26, No. 10, pp. 781-786, 2001.

Brandt, J., J. H. Christensen, L. M. Frohn, 2001c: "Operational air pollution forecast from regional scale to urban street scale. Part 2: performance evaluation", *Physics and Chemistry of the Earth (B)*, Vol. 26, No. 10, pp. 825-830, 2001d.

Brandt, J., J. H. Christensen and L. M. Frohn, 2002: "Modelling of transport and deposition of caesium and iodine from the Chernobyl accident using the DREAM model". *Atmospheric Chemistry and Physics,* Vol. 2, pp. 397-417, *2002*

Brandt, J., J. H. Christensen, L. M. Frohn and R Berkowicz, 2003: "Air pollution forecasting from regional to urban street scale – implementation and validation for two cities in Denmark". *Physics and Chemistry of the Earth,* Vol. 28, pp. 335-344, 2003.

Brandt, J., C. A. Skjøth, J. H. Christensen, L. M. Frohn and C. Geels, 2004a: "FLOODRELIEF, High-resolution weather forecasting using dynamical downscaling - system description", Contract number EVK1-CT-2002-00117, Deliverable 2.1, pp. 53, 2004.

Brandt, J., C. A. Skjøth, J. H. Christensen, L. M. Frohn, C. Geels and W. Szalinska, 2004b: "FLOODRELIEF, High-resolution weather forecasting using dynamical downscaling - system validation", Contract number EVK1-CT-2002-00117, Deliverable 2.2, pp. 104, 2004.

Christensen, J. H., 1997 The Danish Eulerian Hemispheric Model – a three-dimensional air pollution model used for the Arctic, *Atm. Env.*, 31, 4169–4191.

Christensen, J. H., J. Brandt, L. M. Frohn and H. Skov, 2004: "Modelling of mercury in the Arctic with the Danish Eulerian Hemispheric Model. *Atmospheric Chemistry and Physics*. Vol. 4, pp 2251-2257, 2004.

Geels, C., S. Doney, R. Dargaville, J. Brandt and J. H. Christensen, 2004: "Investigating the sources of synoptic variability in atmospheric CO_2 measurements over the Northern Hemisphere continents – a regional model study". *Tellus*, 56B, pp. 35-50, 2004.

Grell G. A., Dudhia J. and Stauffer D. R. (1995) A Description of the Fifth-Generation Penn State/NCAR Mesoscale Model (MM5). NCAR/TN-398+STR. NCAR Technical Note. June 1995, pp 122. Mesoscale and Microscale Meteorology Division. National Center for Atmospheric Research. Boulder, Colorado.

Hansen, K. M., J. H. Christensen, J. Brandt, L. M. Frohn and C. Geels, 2004: "Modelling atmospheric transport of α-hexachlorocyclohexane in the Northern Hemisphere with a 3-D dynamic model: DEHM-POP". *Atmospheric Chemistry and Physics*, Vol. 4, pp. 1-13, 2004.

Janjić, Z. I., 1994: "The step-mountain Eta coordinate model: Further developments of the convection, viscous sublayer, and turbulence closure schemes", Mon. Weather Rev., 122, 927-945.

Frohn, L. M. J. H. Christensen and J. Brandt, 2002: "Development of a high resolution nested air pollution model – the numerical approach". *Journal of Computational Physics*. Vol. 179, pp. 68-94, 2002.

Lawrence, M. G., Ø. Hov, M. Beekmann, J. Brandt, H. Elbern, H. Eskes, H. Feichter, and M. Takigawa, 2005: "The Chemical Weather", Environmental Chemistry, Featured Paper, Vol 2, pp 6-8, 2005.

Loon, M. van, Roemer, M. G. M., Builtjes, P. J. H., Bessagnet, B., Rouill, L., Christensen, J., Brandt, J., Fagerli, H., Tarrason, L., Rodgers, I., Stern, R., Bergström, R., Langner, J., Foltescu, V., 2004: "Model inter-comparison. In the framework of the review of the Unified EMEP model". TNO-report, TNO-MEPO – R 2004/282, pp. 86, June 2004.

Tilmes, S, Brandt, J., Flatøy, F., Bergström, R., Flemming, J., Langner, J., Christensen, J. H., Frohn, L. M., Hov, Ø., Jacobsen, I., Reimer, E., Stern, R. and Zimmermann, J., 2002: "Comparison of five Eulerian ozone prediction systems for summer 1999 using the German monitoring data". *Journal of Atmospheric Chemistry*, Vol. 42, pp. 91-121, 2002.

Integrated Systems for Forecasting Urban Meteorology, Air Pollution and Population Exposure: Achievements from the FUMAPEX project

Baklanov, A.1), Bjergene, N., Fay, B., Finardi, S., Jantunen, M., Kukkonen, J., Rasmussen, A., Skouloudis, A., Slørdal, L.H., Sokhi, R.S.

1) Coordinator of the project; Danish Meteorological Institute

Introduction

The main problem in forecasting urban air pollution is the prediction of episodes with high pollutant concentrations in urban areas, where most of the well-known methods and models based on in situ meteorological measurements, fail to realistically produce the meteorological input fields for the urban air pollution models.

Urban air pollution models in operational urban air quality information and forecasting systems, as a rule, use simple in-situ meteorological measurements which are fed into meteorological pre-processors (Fig. 1). Lacking an adequate description of physical phenomena and the complex data assimilation and parameterisations of numerical weather prediction (NWP) models, these pre-processors do not achieve the potential of NWP models in providing all the meteorological fields needed by modern urban air pollution models to improve urban air quality forecasts.

During the last decade substantial progress in numerical weather prediction modelling and in the description of urban atmospheric processes has been achieved. Modern nested NWP models are utilising land-use databases down to hundred metres resolution or finer, and are approaching the necessary horizontal and vertical resolution to provide weather forecasts for the urban scale. In combination with the recent scientific developments in the field of urban sublayer atmospheric physics and the enhanced availability of high-resolution urban surface characteristics, the capability of the NWP models to provide high quality urban meteorological data will therefore increase.

Despite the increased resolution of existing operational numerical weather prediction models, urban and non-urban areas mostly contain similar sub-surface, surface, and boundary layer formulations. These do not account for specifically urban dynamics and energy exchange and their impact on the numerical simulation of the atmospheric boundary layer and its various characteristics (e.g. internal boundary layers, urban heat island, precipitation patterns). Additionally numerical weather prediction models are not primarily developed for air pollution modelling and their results need to be designed as input to urban and meso-scale air quality models. Therefore the situation in urban air quality information and forecasting systems is changing and requires a revision of the conventional conception of urban air pollution forecasting.

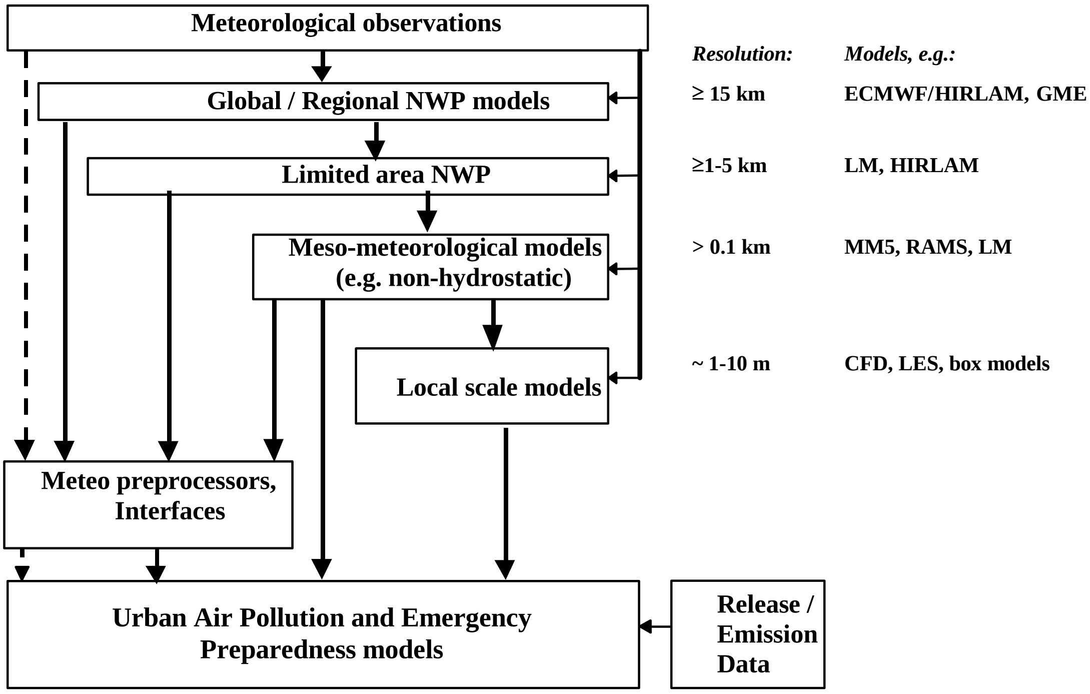

Figure 1. Current regulatory (dash line) and suggested (solid line) ways for systems of forecasting of urban meteorology for urban air quality information and forecasting systems

Project Objectives and Implementation

In response to the above research needs, a new European Union research project Integrated Systems for Forecasting Urban Meteorology, Air Pollution and Population Exposure (FUMAPEX, project web-site: http://fumapex.dmi.dk) was initiated within the COST 715 community, and submitted to the Fifth Framework Programme, Subprogramme: Environment and Sustainable Development, Key Action 4: City of Tomorrow and Cultural Heritage. FUMAPEX started in November 2002 and will continue for a period of three years. It is also a member of the Cluster of European Urban Air Quality Research CLEAR (http://www.nilu.no/clear).

The main objectives of FUMAPEX are to improve meteorological forecasts for urban areas, to connect numerical weather prediction models to urban air pollution and population exposure models, to build improved Urban Air Quality Information and Forecasting Systems, and to demonstrate their application in cities subject to various European climates. The FUMAPEX scheme for the improvement of meteorological forecasts in urban areas, interfaces and integration with urban air pollution and population exposure models for urban air quality information forecasting and information systems (UAQIFS) is presented in Figure 2.

The improvement of urban meteorological forecasts will also provide information to city managers regarding other hazardous or harmful urban climates (e.g. urban runoff and flooding, icing and snow accumulation, high urban winds or gusts, heat or cold stress in growing cities and/or a warming climate). Moreover the availability of reliable urban scale weather forecasts could be of relevant support for the emergency management of fires, accidental toxic emissions, potential terrorist actions etc.

In order to achieve the goal of establishing and implementing an improved new urban air quality information forecasting and information system to assist sustainable urban development, the following steps are being undertaken:

1. improve predictions of the meteorological fields needed by urban air pollution models by refining resolution and developing specific parameterisations of the urban effects in numerical weather prediction models,
2. develop suitable interface/meteorological pre-processors from numerical weather prediction to urban air pollution models,

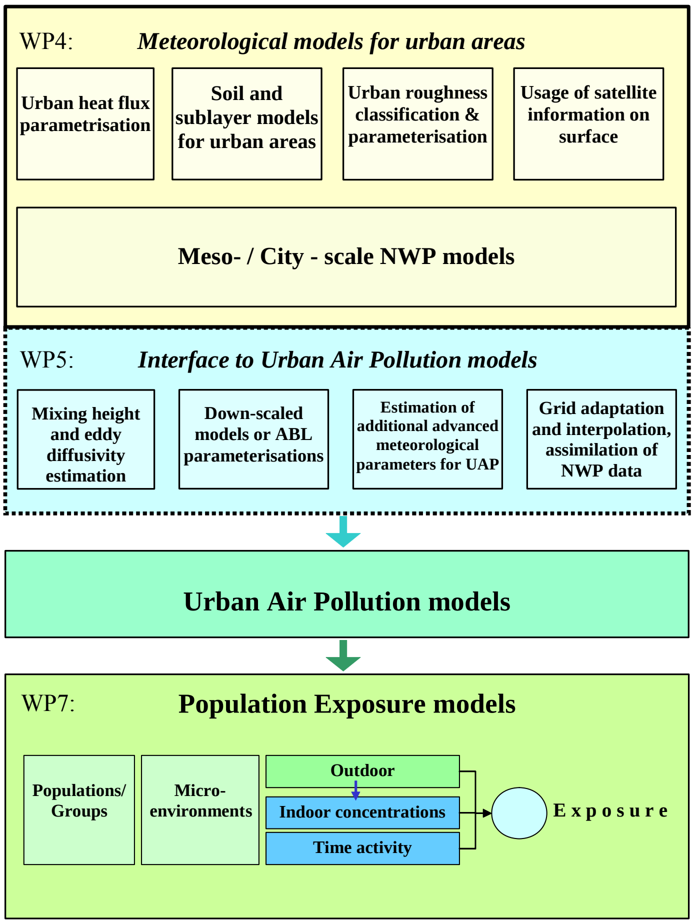

Figure 2. FUMAPEX scheme of the improvements of meteorological forecasts (numerical weather prediction) in urban areas, interfaces and integration with urban air pollution and population exposure models for urban air quality information forecasting and information systems.

3. validate the improvements in numerical weather prediction models and meteorological pre-processors by evaluating their effects on the urban air pollution models against urban measurement data,
4. apply the improved meteorological data to urban air quality information and forecasting systems, emergency preparedness and population exposure models and compare and analyse the results, and

5. link meteorologists and numerical weather prediction modellers with urban air pollution scientists and the end users of urban air quality information and forecasting systems.

The necessary steps are divided in separate, interlinked work packages involving 16 participants and 6 subcontractors (see list below). They represent numerical weather prediction centres, research organisations, and organisations responsible for urban air quality, population exposure forecasts and control, and local authority or city authorities from ten European countries.

The work packages consist of:

1. Analysis and evaluation of air pollution episodes in European cities (led by J. Kukkonen, Finnish Meteorological Institute)
2. Assessment of different existing approaches to forecast urban air pollution episodes (led by R.S. Sokhi, University of Hartfield, UK)
3. Testing the quality of different operational meteorological forecasting systems for urban areas (led by B. Fay, German Meteorological Service DWD)
4. Improvement of parameterisation of urban atmospheric processes and urban physiographic data classification (led by A. Baklanov, Danish Meteorological Institute)
5. Development of interface between urban-scale NWP and urban air pollution models (led by S. Finardi, Arianet, Italy)
6. Evaluation of the suggested system (UAQIFS) to uncertainties of input data for urban air pollution episodes (led by N. Bjergene, Norwegian Meteorological Institute DNMI)
7. Development and evaluation of population exposure models in combination with urban air quality information forecasting and information systems (led by M. Jantunen, National Public Health Institute KTL, Finland)
8. Implementation and demonstration of improved Urban Air Quality Information and Forecasting Systems (led by L.H. Slørdal, Norwegian Institute for Air Research NILU)
9. Providing and dissemination of relevant information (led by A. Skouloudis, EU Joint Research Centre, Ispra)
10. Project management and quality assurance (led by A. Rasmussen, Danish Meteorological Institute).

The project involves the following steps.

Classification of air pollution episodes focusing on relevant meteorological variables

1. Identification and classification of various types of air pollution episodes in cities located in different European climatic and geographic regions.
2. Key pollutants relevant to EU Air Quality Directives and Daughter Directives (EC/96/62; EC/99/30) will be selected for different regions/city characteristics.
3. Classification of meteorological conditions leading to pollution episodes and identification of the more relevant meteorological parameters to define these conditions in various European climatic regions.

4. Compilation and analysis of existing datasets of concentration and meteorological data measured during pollution episodes in different European climatic and geographic regions.

Improvement of the quality of urban meteorological forecasting for urban air pollution and exposure models

1. Improvement of urban weather forecasts and calculation of key meteorological parameters for pollution episodes. A hierarchy of numerical weather prediction models from large-scale global circulation models to local-scale obstacle-resolving meteorological models will be employed (see Figure 11.1).
2. Improvement of boundary layer formulations and parameterisations, and the physiographic data description of urban areas.
3. Development of assimilation techniques with satellite remote sensing data in numerical weather prediction models.
4. Development of interfaces to connect numerical weather prediction to urban air pollution models.

Verification of the improved numerical weather prediction, urban air pollution and population exposure models

1. Evaluation of improved urban meteorological forecast models based on urban air pollution episodes.
2. Estimation of sensitivity of urban air pollution models to uncertainties in meteorological input data.
3. Evaluation of the impact of the improved output of the urban air quality models on simulations of an urban population exposure model.

Application of Urban Air Quality Information Forecasting and Information Systems (UAQIFS) and emergency systems

1. Integration of the improved numerical weather prediction, urban air pollution and population exposure models into urban air quality information and forecasting systems.
2. Implementation of the new improved urban air quality information and forecasting system in air quality forecasting mode to be applied in four target cities, in urban management or public health and planning mode in one selected target city, and of the emergency preparedness system in one selected target city.
3. The six target cities for testing the improved systems implementations in association with end users are: Oslo (Norway), Turin (Italy), Helsinki (Finland), Castellon/Valencia (Spain), Bologna (Italy), and Copenhagen (Denmark).

Current Urban Meteorology Achievements

Testing the quality of different operational meteorological forecasting systems for urban areas

The focus of this aspect of the work is on the description of existing forecasting systems and the evaluation of their capability to forecast key meteorological parameters in urban areas. Partners in FUMAPEX use different operational numerical weather prediction (NWP), or research mesoscale models, for providing the meteorological input data for the urban air pollution models in the urban air quality information and forecasting systems. Therefore the tasks comprise:

1. the description and comparison of the selected operational NWP models
2. the harmonised analysis and evaluation of the model simulations with original, and increased model resolution, but unaltered physics for agreed cities and episodes, and
3. the controlled inter-comparison of the simulations of the various models.

These results provide the basis for explaining and quantifying the model improvements planned in subsequent work and also supply useful information to modellers and regulatory authorities. The numerical weather prediction and meso-meteorological models for which 'urbanisation' are considered include: 1. DMI-HIRLAM model (DMI); 2. Lokalmodell (LM) (DWD); 3. MM5 model (DNMI, UH); 4. RAMS model (CEAM, Arianet); 5. Topographic Vorticity-Mode Mesoscale (TVM) Model (UCL); 6. Finite Volume Model (FVM) (EPFL); 7. SUBMESO model (ECN).

A model overview (Fay, 2003) has been completed of operational mesoscale numerical weather prediction models, plus established research mesoscale models used in four European national weather services, one regional weather service, and in many European and international research centres/universities as operational numerical weather prediction models and as input to air pollution modelling. It contains detailed information on all model aspects including information on the different interfaces, or pre-processors, converting the numerical weather prediction output data into input data for urban air pollution models. For an effective comparison of model characteristics, summary tables are provided for all models concerning model scales, initialisation, nesting capabilities, parameterisations and especially turbulence treatment which is a basic requisite for the work of improving and exchanging parameterisations and for some of the interfaces and pre-processors used.

A model comparison design study has also been completed on model comparison and evaluation (Fay, 2003a). It deals in detail with the choice of cities and episodes, and the various theoretical and applied aspects of evaluation methodology for episode, as well as for longer-term evaluation. The choice of cities, the proposed evaluation strategy, and the harmonised use of the GRADS visualisation software and of the MMAS evaluation tool (FMI) had been discussed and agreed upon. Information has been collected on standard numerical weather prediction evaluation and verification in the European CityDelta, ENSEMBLE and AUTOOIL-II projects.

With focus on winter and spring episodes in Helsinki, simulations have been undertaken using the operational numerical weather prediction/mesoscale models HIRLAM, LM, MM5 and RAMS. Results show improvements with increasing model resolution (down to 1.1 km) but the need for adapted external parameters and urbanised parameterisations was apparent. Harmonised model evaluation and comparison was discussed in detail (Neunhäuserer *et al.*, 2004) and will be performed for all target cities.

Improvement of parameterisation of urban atmospheric processes and urban physiographic data classification

The following urban features can influence the atmospheric flow, microclimate, turbulence regime and, consequently, the transport, dispersion, and deposition of atmospheric pollutants within urban areas:

1. local-scale non-homogeneities, sharp changes of roughness and heat fluxes,
2. the building effect in reducing wind velocity,
3. redistribution of eddies, from large to small, due to buildings,
4. trapping of radiation in street canyons,
5. effect of urban soil structure on diffusivities of heat and water vapour,
6. anthropogenic heat fluxes, including the urban heat island effect,
7. urban internal boundary layers and the urban mixing height,
8. effects of pollutants (including aerosols) on urban meteorology and climate,
9. urban effects on clouds and precipitation.

Accordingly the following aspects of urban effects have been considered in improved urban-scale numerical weather prediction models:

1. higher spatial grid resolution and model downscaling,
2. improved physiographic data and land-use classification,
3. calculation of effective urban roughness,
4. calculation of urban heat fluxes,
5. urban canopy and soil sub-models,
6. simulation of the internal boundary layers and mixing height in urban areas,
7. urban measurement assimilation in numerical weather prediction models.

Since these involve many complexities the FUMAPEX project has decided to concentrate on three main steps, or levels of complexity in NWP urbanisation (Baklanov, 2003):

1. corrections to the surface roughness for urban areas (Baklanov and Joffre, 2003) and to the heat fluxes (by adding an extra urban heat flux, e.g., via heat/energy production/use in the city, heat storage capacity and albedo change) in the existing non-urban physical parameterisations of the surface layer in higher resolution NWP models with improved land-use classification. Furthermore, an analytical model for wind velocity and diffusivity profiles inside the urban canopy is suggested (Zilitinkevich and Baklanov, 2004).
2. improvement and testing of a new flux aggregation technique, suggested by the Risø National Laboratory in co-operation with DMI (Hasager *et al.,* 2003) for urban areas. Recently this module was coupled to the DMI-HIRLAM model for non-urban areas. The approach can be extended for urban canopies as well. However, experimental data are needed to verify parameterisations for urban areas.
3. implementation of special physical parameterisations for the urban sublayer into the numerical weather prediction models. It is planned to incorporate into both the

HIRLAM and LM models a new urban module, developed within FUMAPEX, and based on the following two different urban submodels:

- the urban surface exchange parameterisation, developed by the Swiss team, (the model description is given by Martilli *et al.,* 2002);
- the SM2-U urban area soil submodel, developed by the French team, (the model description is given by Dupont *et al.,* 2002).

At the current stage of progress the following examples of 'urbanisation' within models have been completed (Baklanov *et al.,* 2003).

1. Increased resolution and surface data bases for the roughness length calculation in operational numerical weather prediction models have been tested in DMI-HIRLAM, LM, MM5 and RAMS models. For instance, DMI-HIRLAM has been run semi-operationally for Denmark with a horizontal grid resolution of 1.4 km and 1 km land-use classification including 21 land classes and subclasses of urban areas. DWD finalised and successfully tested the LM2LM that provides initial and boundary values of the local model with coarser resolution needed to calculate the LM with higher resolution. Using the LM2LM, three level nested LM forecasts (7, 2.8, 1.1km) have already been performed.
2. Modified parameterizations and algorithms for roughness parameters in urban areas based on the morphometric method are being developed. Urban database analysis for mapping morphometric and aerodynamic parameters is tested using the St. Jerome case study, from the ESCOMPTE experiment (see Chapters 4 and 5).
3. Improved models for urban roughness sublayer simulation, including (i) effective roughness and flux aggregation techniques, (ii) effect of stratification on the surface resistance over very rough surfaces, (iii) roughness lengths for momentum, heat, and moisture have been suggested.
4. It has been shown that the roughness length depends on the atmospheric temperature stratification, new parameterisations for the effect of stratification on the surface resistance over very rough surfaces are suggested. The roughness lengths for momentum, temperature and moisture are different for urban areas. Several possible parameterisations for the scalar roughness length for urban areas have been recommended for urban-scale numerical weather prediction models, but they need to be verified and improved.
5. As the next step in the 'urbanisation' of numerical weather prediction, it is suggested that the urban roughness sublayer is parameterised by the Martilli model. This method is more advanced than the roughness approach, but more expensive computationally in NWPs. This urban sublayer model, which combines the thermal and dynamical effect of the urban canopy, has already been introduced in the TVM model.
6. Experimental studies of urban roughness inhomogeneity effects on the urban boundary layer development has been undertaken by the University of Hamburg and the results have been made available for model verification.
7. EPFL improved the Martilli's module to simplify its introduction in other models and tested it using the BUBBLE measurements. They are preparing the computer code as a separate module, suitable for implementation into numerical weather prediction models.

8. ECN further developed a 1-dimensional, 2-dimensional and box version of the SM2-U model and implemented SM2-U and a simplified Martilli parameterisation in the MM5 model. ECN tests of SM2-U on CLU-ESCOMPTE Marseilles data are in progress.
9. The sea surface temperature data, obtained from an algorithm based on NOAA satellite high-resolution images, have been incorporated by CEAM into the RAMS model. The land categories (from CORINE and PELCOM datasets) have been reclassified following the USGS categories.

Development of interface between urban scale numerical weather prediction and urban air pollution models

The possibility of obtaining reliable air quality forecasts in urban areas depends on the exploiting appropriately meteorological and air quality models' technical features. To reach this objective the communication between models has to be physically consistent and finalised to practical applications. This includes specifically the need to incorporate the improved description of the urban boundary layer introduced in numerical weather prediction models. The main activity has been to identify interfaces: what physical variables have to be processed or estimated, which computational methods are normally used and what kind of improvements are desired to better exploit the new features of parameterisations and 'urbanised' meteorological models that are under development in the FUMAPEX project (Finardi, 2003).

The analysis of typical output parameters of numerical weather prediction models and their comparison with the urban air pollution models identified the necessary main computations to be performed by interface modules and what improvements in the existing software are desirable and can be achieved. Urban air pollution models have been grouped into four classes for which the interface modules have to perform similar processing of meteorological data. The first class includes statistical models, which do not need any particular calculation from the interface system. They simply need to be given single valued meteorological data extracted from the coupled meteorological model.

A more numerous class of simple models includes all the approaches based on a steady state solution of dispersion equation. The models included in this class normally require meteorological data at a single point or possibly a vertical profile. Moreover they normally require evaluation of turbulence scaling parameters.

A third class of three-dimensional models includes all the models based on Lagrangian description of dispersion phenomena. These models usually need 3-D fields of average quantities (wind, temperature, humidity and possibly turbulent kinetic energy), 2-D surface fields (precipitation, sensible heat flux, friction velocity and Monin-Obukhov length), and 3-D turbulence fields that are usually described by wind variances and Lagrangian time scales. The turbulence describing variables have to be evaluated from mean variables, turbulent kinetic energy or K_H, K_Z and scaling parameters.

The final class includes 3-dimensional Eulerian models. The Eulerian dispersion coefficients (K_H, K_Z) produced by numerical weather prediction models could be directly used by these air quality models. Nevertheless the direct use of dispersion coefficients calculated by NWP models is not always possible or advisable, and therefore, interfaces for Eulerian models have often to implement capabilities to compute turbulence parameters from mean variables and scaling parameters. This last possibility can also use the meteorological data provided by the numerical weather prediction models supplemented by high resolution physiographic data, or even observations.

The possible and desirable improvements for each model interface class have been identified in a preliminary way. Progresses in the description of urban meteorology and turbulence can be obtained from both the urbanisation of meteorological models and from the improvement of the built-in turbulence models implemented by the interface modules. Progress in this domain will be a critical step in enhancing our capabilities to simulate and forecast urban meteorology and air quality.

List of FUMAPEX Partners

Danish Meteorological Institute (DMI) co-ordinator Dr Alexander Baklanov, Alix Rasmussen

German Weather Service (DWD), PO Box 100465, D-63004 Offenbach, Germany, Contact: Barbara Fay

Hamburg University (MIHU), Bundesstrasse 55, D-20146 Hamburg, Germany, Contact: Prof. Michael Schatzmann

Centro De Estudios Ambientales Del Mediterrano (CEAM), Parque Tecnológico, C/Charles R.Darwin, 14, E-46980 (Paterna) Valencia, Spain, Contact: Dr Millàn M. Millàn

Ecole Centrale de Nantes (ECN), B.P. 92101, F-44321 Nantes Cedex 3, France, Contact: Dr. Patrice Mestayer

Finnish Meteorological Institute (FMI), Sahaajankatu 20E, FIN-00810 Helsinki, Finland, Contact: Dr Jaakko Kukkonen

ARIANET Consulting (ARIANET), via Gilino 9, I-20128 Milano, Italy, Contact: Dr Sandro Finardi

Environmental Protection Agency of Emilia-Romagna Region (ARPA), Vviale Silvani 6, I-40122 Bologna, Italy, Contact: Dr Marco Deserti

Norwegian Meteorological Institute (DNMI, met.no), P.O.Box 43, Blindern, N0313 Oslo, Norway, Contacts: Dr Norvald Bjergene

Norwegian Institute for Air Research (NILU), P.O.Box 100, N-2027 Kjeller, Norway, Contact: Dr Leiv Haavard Slordal

University of Hertfordshire (UH), College Lane, Hatfield, AL10 9AB, UK, Contact: Prof. Ranjeet Sokhi

INSA CNRS-Universite-INSA de Rouen (CORIA), Av. de l'Université-BP 8, F-76801 Saint Etienne du Rouvray cedex, France, Contact: Prof. Alexis Coppalle

Finnish National Public Health Institute (KTL), P.O.Box 95, FIN-70701 Kuopio, Finland, Contact: Prof. Matti Jantunen

Environmental Protection Agency of Piedmont (ARPAP), Via della Rocca 49, I-10123 Torino, Italy, Contact: Dr Francesco Lollobrigida

Institute for Environment & Sustainability - Joint Research Center (JRC IES), Ispra (VA), I-21020, Italy, Contact: Dr Andreas N. Skouloudis

Swiss Federal Institute of Technology (ETH), EPFL DGR-LPA, CH-1015 Lausanne, Switzerland, Contacts: Drs Alain Clappier & Mathias Rotach

FUMAPEX subcontractors:

Brockmann Consult, BC (Prof. Sergej S. Zilitinkevich, Uppsala University),

Université catolique de Louvain, UCL (Prof. Guy Schayes),

Danish Emergency Management Agency, DEMA (Mr Steen C. Hoe),

Helsinki Metropolitan Area Council, YTV (Mr Paivi Aarnio),

Norwegian Traffic Authorities, NTA (Mr Pål Rosland),

Municipality of Oslo, MO (Mrs Ingrid Myrtveit).

European Commission Scientific Officer: Dr Viorel Vulturescu, DG Research

FUMAPEX Project Co-ordinator: Dr. Alexander A. Baklanov, Danish Meteorological Institute, e-mail: alb@dmi.dk)

Relevant FUMAPEX References

Published papers

Baklanov, A., A. Rasmussen, B. Fay, E. Berge and S. Finardi (2002) Potential and Shortcomings of Numerical Weather Prediction Models in Providing Meteorological Data for Urban Air Pollution Forecasting. *Water, Air and Soil Poll., Focus*, 2(5-6), 43-60.

Baklanov, A., A. Gross, J.H. Sørensen (2004) Modelling and forecasting of regional and urban air quality and microclimate. *J. Computational Technologies*, 9: 82-97.

Chenevez, J., A. Baklanov, J. H. Sørensen (2004) Pollutant Transport Schemes Integrated in a Numerical Weather Prediction Model: Model description and Verification Results. *Meteorological Applications,* 11(3), 265-275.

Hasager, C.B. Nielsen, N.W., Boegh, E., Jensen, N.O., Christensen, J.H, Dellwik, E. and Soegaard, H. (2003) Effective roughnesses calculated from satellite-derived land cover maps and hedge information and used in a weather forecasting model. *Boundary-Layer Meteorology,* 109: 227-254.

Kitwiroon, N., R. S. Sokhi, L. Luhana and R. M. Teeuw (2002) Improvements in air quality modeling by using surface boundary layer parameters derived from satellite land cover data. *Water, Air and Soil Pollution, Focus*, 2, 29-41.

Kukkonen, J., Partanen, L., Karppinen, A., Ruuskanen, J., Junninen, H., Kolehmainen, M., Niska, H., Dorling, S., Chatterton, T., Foxall, R. and Cawley, G. (2003) Extensive evaluation of neural network models for the prediction of NO2 and PM10 concentrations, compared with a deterministic modelling system and measurements in central Helsinki. *Atmospheric Environment* 37(32), pp. 4539-4550.

Martilli, A., A. Clappier, and, M. W. Rotach (2002) An urban surfaces exchange parameterisation for mesoscale models. *Boundary Layer Meteorol.*, 104, 261-304.

Mestayer, P., R. Almbauer, O. Tchepel (2003) Urban Field Campaigns, Air quality in cities, N. Moussiopoulos, editor. Springer Verlag Berlin Heidelberg (ISBN3-540-00842-x), 2003, pp.51-89

Pohjola, M.A., J. Kukkonen, M. Rantamäki, A. Karppinen and E. Berg (2004) Meteorological evaluation of a severe air pollution episode in Helsinki on 27 - 29 December, 1995. *Boreal Environment Research*, 9: 75-87.

Zilitinkevich, S. and A. Baklanov, (2002) Calculation of the height of stable boundary layers in practical applications. *Boundary-Layer Meteorology*, 105(3): 389-409.

Conference Proceedings

Calori G., De Maria R., Clemente M., Lollobrigida F., Finardi S. and Tinarelli G. (2003) Air quality integrated assessment in Turin urban area using atmospheric transport and dispersion models. Proc. of the 4th Int. Conf. On Urban Air Quality, pp.214-217.

Dupont, S., I. Calmet and P. Mestayer (2002) Urban canopy modelling influence on urban boundary layer simulation. 4th AMS Symposium on Urban Climatology, 20-24 May 2002, Norfolk, VA, Proceedings AMS, pp. 151-152.

Long, N., G. Pigeon, P. Mestayer, P. Durand, C. Kergomard (2003) Correlation between temperature and classification of urban fabric on Marseille during ESCOMPTE. 5th International Conference on Urban Climate, 1-5 Septembre 2003, Lodz, Poland, Proc. O.5.2

Long, N., P. Mestayer, C. Kergomard (2003) Urban database analysis for mapping morphology and aerodynamic parameters, the case of St Jerome suburban area, in Marseille during ESCOMPTE 5th International Conference on Urban Climate, 1-5 Septembre 2003, Lodz, Poland, Proc. O.31.1

Long, N., S. Kermadi, C. Kergomard, P. Mestayer, A. Träbouet (2003) Urban cover modes and thermodynamic parameters from urban database and satellite data: a comparison for Marseille during ESCOMPTE 5th International Conference on Urban Climate, 1-5 Septembre 2003, Lodz, Pologne.

Mestayer, P., P. Durand, P. Augustin, P. Bastin, J.-M. Bonnefond, B. Bénech, B. Campistron, A. Coppalle, H. Delbarre, B. Dousset, P. Drobinski, A. Druilhet, E. Fréjafon, S. Grimmond, D. Groleau, M. Irvine, C. Kergomard, S. Kermadi, J.-P. Lagouarde, A. Lemonsu, F. Lohou, N. Long, V. Masson, C. Moppert, J. Noilhan, B. Offerle, T. Oke, G. Pigeon, V. Puygrenier, J.-M. Rosant, F. Saïd, J. Salmond, M. Talbaut, J. Voogt (2003) UBL/CLU-Escompte , the Urban Boundary Layer Field experiment over Marseille and the data base. 4th International Conference on Urban Air Quality, 25-28 March 2003, Carolinum University, Prague, Czech Republic, Proceedings, 4 pp.

Neunhäuserer, L, Fay B., Baklanov A., Bjergene N., Kukkonen J., Palau J.L., Perez-Landa G., Rantamaki M., Rasmussen A., Valkama I. (2004) Evaluation and comparison of operational NWP and mesoscale meteorological models for forecasting urban air pollution episodes - Helsinki case study. 9th Intern. Conference on Harmonisation within Atmospheric Dispersion Modelling for Regulatory Purposes, 1-4 June 2004, Garmisch-Partenkirchen, Germany.

Rantamäki, M., Pohjola, M., Kukkonen J. and Karppinen, A. (2003) Evaluation of the HIRLAM model against meteorological data during an air pollution episode in southern Finland 27-29 December 1995. In: Sokhi, R.S. and Brechler, J. (eds.), Proceedings of the Fourth International Conference on Urban Air Quality - Measurement, Modelling and Management, Charles University, Prague, Czech Republic, 25-27 March 2003. University of Hertfordshire, Hatfield, United Kingdom, 420-423.

Schatzmann, M., Grawe, D., Leitl, B., Muller, W.J. (2003) Data from an urban street monitoring station and its application in model validation. Proceedings, 26th ITM ‘Air pollution and its applications’, Istanbul, May 2003.

Sokhi, R. S., L Luhana, J Kukkonen, E Berge, L H Slördal and S Finardi (2003) Analysis and Evaluation of PM10 Air Pollution Episodes in European Cities. In: Sokhi, R.S. and Brechler, J.

(eds.), Proceedings of the Fourth International Conference on Urban Air Quality - Measurement, Modelling and Management, Charles University, Prague, Czech Republic, 25-27 March 2003. University of Hertfordshire, Hatfield, United Kingdom, pp. 26-29.

Zilitinkevich, S., A. Baklanov, R. Bornstein, J. Hunt and P. Mestayer (2003) Modelling and Prediction of Urban Climate. Word Climate Change Conference, September 29 – October 3, 2003, Moscow, Russia

Zilitinkevich, S., Esau, I., Baklanov, A., Djolov, G. (2003) Scaling laws and turbulence closures for stable boundary layers. Presentation at EGS-AGU-EUG-2003, Nice, France.

FUMAPEX Reports

Baklanov, A. (editor) (2003) FUMAPEX Integrated Systems for Forecasting Urban Meteorology, Air Pollution and Population Exposure – Project Kick-off Meeting and First Progress Report. DMI Sci. Report 03-12, ISSN 0905-3263. April 2003, 140p., URL: http://www.dmi.dk/f+u/publikation/vidrap/2003/Sr03-12.pdf

Baklanov, A. and S. Joffre (editors) (2003) Improved Models for Computing the Roughness Parameters of Urban Areas. / Baklanov, A., P. Mestayer, M. Schatzmann, S. Zilitinkevich, A. Clappier, etc. D4.4 FUMAPEX Report, November 2003. DMI Sci. Report 03-19, ISBNnr.: 87-7478-495-1, 51 p.

Baklanov, A. and P. Mestayer (editors) (2004) Improvement of parameterisation of urban atmospheric processes and urban physiographic data classification. WP4 FUMAPEX Progress Report, April 2004. DMI Sci. Report.

Batchvarova, E., R. Sokhi, etc. (2003) 'Comparison and analysis of currently employed meteorological approaches for modelling urban air pollutants' and 'Identification of gaps in met data required by UAP models for characterising urban BL'. FUMAPEX D2.3-2.4 Report, December 2003.

Fay, B. (2003) Overview of NPW / wind field models in FUMAPEX. D3.1 report for FUMAPEX, 29 p.

Fay, B. (2003a) Design of model comparison study. D3.2 report for FUMAPEX, 26 p.

Finardi, S. (editor) (2003) Definition of NWP models output products, UAP models input needs and gaps to be filled. FUMAPEX report for M5.1, Arianet, Italy.

Finardi, S. (editor) (2004) Guidelines for the construction of the interfaces from operational NWP models to UAP models. FUMAPEX report for D5.1, Arianet, Italy, January 2004, 47 p.

Millan, M. (editor) (2003) Ozone dynamics in the Mediterranean basin. Air pollution research report 78. EC DG RTD – CEAM. 287 p

Slördal, L.H. (editor) (2003) FUMAPEX: Guidelines of output from UAQIFSs as specified by end-users. FUMAPEX D8.1 report. NILU Report OR 2/2004, Ref: U-102144.

Sokhi, R.S., N. Kitwiroon and L. Luhana (2003) 'FUMAPEX Datasets of Urban Air Pollution Models and Meteorological Pre-processors'. D2.1-2.2 report for FUMAPEX, 41 p.

Valkama, I., J. Kukkonen (2003) Identification and classification of air pollution episodes in terms of pollutants, concentration levels and meteorological conditions. FUMAPEX Deliverable D1.2, Oct. 2003.

Submitted papers

Baklanov, A., A. Kuchin (2003) The mixing height in urban areas: comparative study for Copenhagen. *Atmospheric Chemistry and Physics* (submitted).

Baklanov, A., J.H. Sørensen, S.C. Hoe, B. Amstrup, (2003) Urban meteorological modelling for nuclear emergency preparedness. Submitted to *Journ. Envir. Radioactivity.*

Berthier, E., S. Dupont, H. Andrieu, PG. Mestayer. (2003) Comparison of two evapotranspiration schemes on a suburban site. Submitted to *Journal of Hydrology*, July 2003

Calori G., Clemente M., De Maria R., Finardi S., Lollobrigida F. and Tinarelli G. (2003) Air quality integrated modelling in Turin urban area. Submitted to *Environmental Modelling and Software.*

Dupont, S. E. Guilloteau, P.G. Mestayer, E. Berthier and H. Andrieu (2003) Parameterisation of the Urban Water Budget by Using SM2-U model. Submitted to *Applied Meteorology*, August 2003

Dupont, S., I. Calmet, P.G. Mestayer and S. Leroyer (2003) Parameterisation of the Urban Energy Budget with the SM2-U Model for the Urban Boundary-Layer Simulation. Submitted to *Boundary Layer Meteorology*, September 2003

Kukkonen, J. M., Pohjola, R. S., Sokhi, L., Luhana, N., Kitwiroon, M., Rantamäki, E., Berge, V., Odegaard, L. H., Slørdal, B., Denby and S. Finardi (2003) Analysis and evaluation of local-scale PM10 air pollution episodes in four European cities, Oslo, Helsinki, London and Milan. Submitted to *Atmospheric Environment*, September 2003.

Mestayer, P.G., J.-P. Costes and J.-F. Sini (2002) Inhomogeneous roughness influence on neutral atmospheric boundary layer simulation. Part I, steps, strips, and spots. Submitted to *Boundary-Layer Meteorology*, November 2002

Mestayer, P.G., P. Durand, P. Augustin, S. Bastin, J.-M. Bonnefond, B. Bénech, B. Campistron, A. Coppalle, H. Delbarre, B. Dousset, P. Drobinski, A. Druilhet, E. Fréjafon, S. Grimmond, D. Groleau, M. Irvine, C. Kergomard, S. Kermadi, J.-P. Lagouarde, A. Lemonsu, F. Lohou, N. Long, V. Masson, C. Moppert, J. Noilhan, B. Offerle, T. Oke, G. Pigeon, V. Puygrenier, S. Roberts, J.-M. Rosant, F. Saïd, J. Salmond, M. Talbaut, J. Voogt (2003) The Urban Boundary Layer Field Experiment over Marseille UBL/CLU-Escompte, Experimental Set-up and First Results. Submitted to Boundary-Layer Meteorology, Mai 2003.

Mestayer, P.G., S. Dupont and J.-F. Sini (2002) Inhomogeneous Roughness Influence on Neutral Atmospheric Boundary Layer Simulation. Part II, Regular Checkerboard'. Submitted to *Boundary-Layer Meteorology*, November 2002

Rantamäki, M., Pohjola, M., Kukkonen J., Bremer, P., Karppinen A. (2003) Evaluation of two versions of the HIRLAM model against meteorological data during an air pollution episode in Southern Finland, 27-29 December 1995. Submitted for publication to *Atmos. Environ.*, September 2003.

Zilitinkevich, S., A. Baklanov (2004) A simple model of turbulent mixing and wind profile within urban canopy. Manuscript to be submitted.

Air quality modelling in Portugal

A. Monteiro[1], A. I. Miranda[1], R. Vautard[2] and C. Borrego[1]

[1]Department of Environment and Planning, University of Aveiro, Portugal
[2] Laboratoire de Meteorologie Dynamique, Palaiseau, France

Abstract

Accordingly to the Air Quality Framework Directive 96/62/EC, plans and programmes should be implemented in zones and agglomerations where pollutants ambient air concentrations exceed the limit target values, in order to guarantee its reduction and future law accomplishment. At the national level, the Portuguese Institute of Environment manages the air quality monitoring network, with stations distributed mainly on the coast and concentrated in the large agglomerations. Due to this restricted spatial distribution of the monitoring sites, atmospheric modelling techniques constitute helpful tools for air quality assessment.

The main objective of this study is to perform an air quality long-term simulation for Portugal, using the CHIMERE chemistry transport model. This photochemical model was applied over a 580 x 290 km^2 grid domain covering the Continental Portugal region, with 10 km horizontal resolution, for the 2001 year. The meteorological forcing was given by the European Centre for Medium-Range Weather Forecasts (ECMWF) and the emission inventory obtained from a spatial top-down disaggregation of the EMEP national database updated for the 2001 simulation year.

The evaluation of the model performance was based on statistical comparison between pollutants concentration data measured in the air quality national network and the correspondent simulated values. As a first approach, and despite the coarse resolution used in the simulation, the complex topography and coastal location of Portugal, the results obtained show a modelling system able to reproduce the pollutants concentrations temporal evolution and spatial distribution.

Concerning the fulfilment of the air quality target values, there are exceedances of the human health and vegetation protection limits for NO_2 and SO_2. The ozone is a critical pollutant for vegetation health, with density forest areas being affected by high levels of concentration.

Introduction

Measured concentrations available at given monitoring sites are generally not enough detailed to describe the spatial distribution of air pollutants over wide areas, whereas this information is a crucial factor to evaluate the impact of air pollution on human health and natural ecosystems. Modeling systems can represent suitable tools for these purposes, allowing both the study of air quality with an adequate spatial detail and the assessment of appropriate emission reduction strategies.

In order to assess the air quality at a regional level (β-mesoscale), verifying the fulfillment of the limit targets and thresholds values imposed by the EC Directives, and to understand the causes and origin of air pollution, numerical modelling exercises should be used. Recent works (Tarasson et al., 2001) point out the importance to perform policies analysis on a "climatological" basis rather than focusing on a single critical episode; this approach allows both to better evaluate model performances and to quantify policies effects with respect to long-term air quality standards.

Several ozone modelling studies were already performed for Portugal, but only for β-mesoscale domains and during some specific and episodic days (Barros et al, 2003; Borrego et al, 2000, 2002). The present work represents an important air pollution modelling study for Portugal, since it aims to asses the air quality over the whole continental region of Portugal for the most critical gaseous pollutants (SO_2, CO, NO_2 and O_3) and during the entire year of 2001.

Methodology

Modelling system description

CHIMERE is a three-dimensional chemistry-transport model (CTM), based on the integration of the continuity equation for the concentrations of several chemical species in each cell of a given grid (Schmidt et al, 2001). CHIMERE has been used for several research applications, among which sensitivity to anthropogenic or biogenic emissions (Beekmann and Derognat, 2003; Menut, 2003; Sillmann et al, 2003; Derognat et al, 2003; Schmidt and Martin, 2003), emission diagnostics (Vautard et al, 2003) or photo-oxidant forecasting over Europe and the Paris region (Vautard et al, 2000). From the year 2000 to 2004, a web server displayed these real-time forecasts together with surface observations for verification (http://euler.lmd.polytechnique.fr/pioneer), and this exercise has been extended to the Portuguese Continental region in the last summer. Results showed reasonable skill for ozone daily maxima forecasts with average RMS error of about 10 ppb and 0.8 of correlation, which is in agreement with the ozone forecast model intercomparison experiment described in Tilmes et al (2002).

The model version used here is primarily described in Schmidt et al (2001) and further updates, especially for the smaller-scale version, can be found in Vautard et al (2003) and on the web site http://euler.lmd.polytechnique.fr/chimere where the model can be downloaded with some documentation.

The meteorological input variables are taken, as in Schmidt et al (2001), from the European Centre for Medium-range Weather Forecast (ECMWF): 3D fields of horizontal wind, temperature, specific humidity, cloud liquid water content, and 2D fields of surface pressure, heat fluxes, 2 m temperature and cloud cover. They are linearly interpolated to the CHIMERE grid and linear time interpolation is also applied to obtain hourly values.

Besides the meteorological input, the CHIMERE model needs boundary and initial conditions, emission data and the land-use and topography characterization.

Figure 1 presents a simplified scheme of the CHIMERE model and its inputs/outputs.

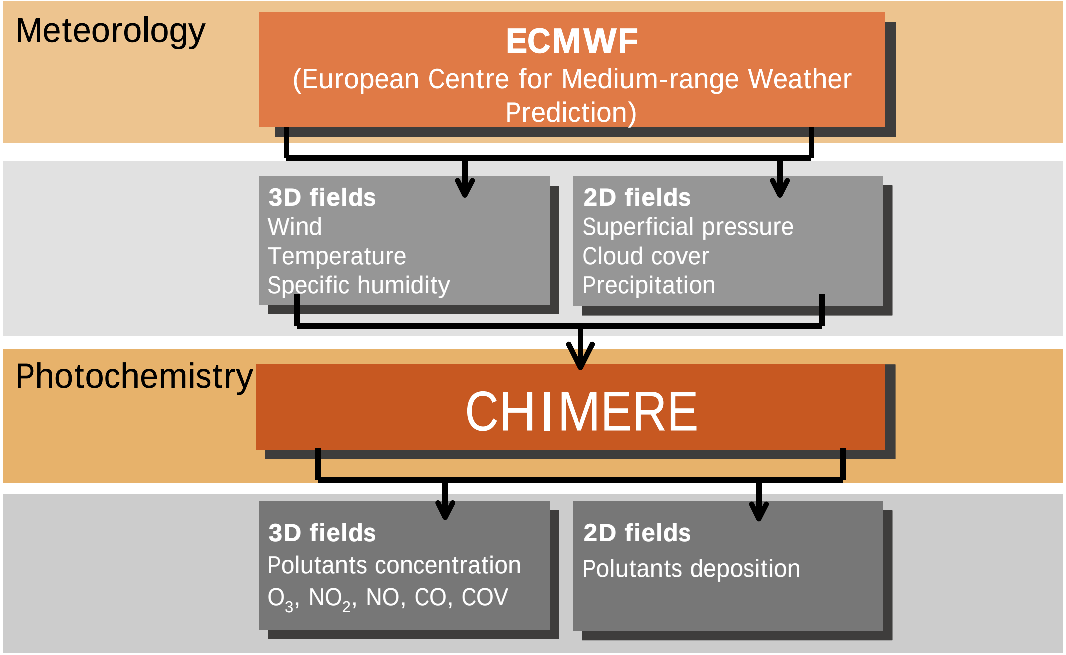

Figure 1. Structure of the modelling system

Modelling system application

The model was applied to the Continental region of Portugal, as shown in Figure 2b, with a horizontal domain of 290 km x 580 km and a 10 km horizontal resolution. Vertical grid consists in 6 hybrid sigma-pressure layers with a model top at 700 hPa. The top altitudes of the layers vary with time, but their approximate values are, from bottom to top: 50, 250, 600, 1200, 2000 and 3000 m.

The Portugal model run is nested within a continental-scale run (Figure 2a), using the same physics and a simple one-way technique: the first long simulation is performed with CHIMERE over a regional area from 10.5W to 22.5E and from 35N to 57.5N. Monthly climatology of O_3, NO_2, CO, PAN, CH_4, C_2H_6, HCHO and HNO_3 issued by the MOZART second-generation model (Horowitz et al., 2003) are forcing this continental-scale simulation at the lateral and top boundaries. The large-scale run concentrations of 22 slow species including ozone and precursors (VOC and reactive nitrogen species) are taken as lateral boundary values for the small-scale run. The top boundary concentrations used are the MOZART monthly climatological values.

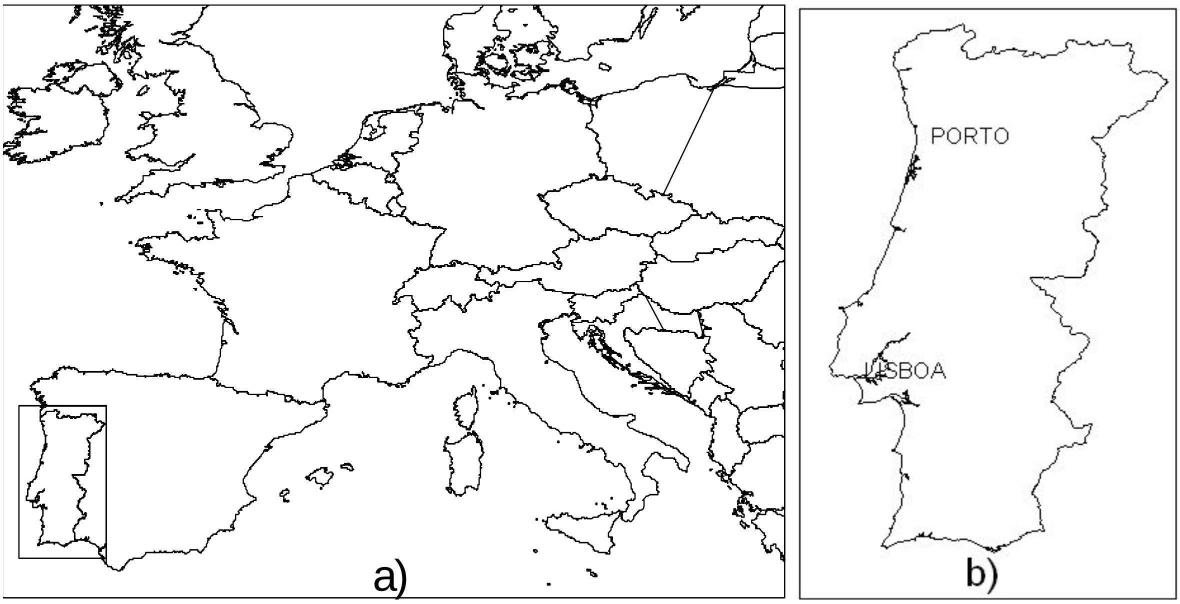

Figure 2. Geographical domains used by the CHIMERE model.

The simulation is continuous in time and a spin-up period of ten days is considered before any statistics on the results are calculated. The spin-up period is also initialized with the MOZART climatological values.

The CHIMERE model requires the input of emission for 15 primary compounds: NO, NO_2, HONO, SO_2, CO, Ethane, n-Butane, Ethene, Propene, Isoprene, a-pinene, o-xylene, Formaldehyde, Acetaldehyde, Methyl ethyl Ketone. At European scale, emissions were derived from the annual totals of the EMEP data base for 1999, through a methodology similar to that described in Schmidt et al. (2001). Over the Portuguese domain, area-sources annual emission data for the four anthropogenic species NO_x, SO_2, CO and NMVOC are obtained from the Portuguese EMEP database for the reference simulation year (2001) for each pollutant activity (traffic, solvents, industrial and residential combustion and others) and then spatially disaggregated in order to obtain the resolution required by the small-scale model. The disaggregation is made in two steps. First emissions are estimated at municipality level (NUT IV) using adequate statistical indicators for each pollutant activity (types of fuel consumption) and then processed applying Census data in order to obtain sub-municipal (NUT V) resolution (Borrego et al., 2002).

Large point sources annual emissions were obtained directly from the available monitoring data of each industrial plant.

Time disaggregation is obtained by application of monthly, weekly and hourly profiles from the University of Stuttgart (GENEMIS, 1994). The NMVOCs are disaggregated into 227 individual VOCs according to the U.K. speciation (Passant, 2002) for each activity sector above referred.

The methodology for biogenic emissions of isoprene and terpenes is described in Schmidt et al. (2001). The land use database comes from the Global Land Cover Facility (Hansen et al., 2000), which, after some processing, provides the cell by cell coverage of coniferous and broadleaf forests. The spatial distribution of tree species within these classes is established following the methodology outlined in Simpson et al. (1999). The Stohl et al. (1996) methodology is used for biogenic emissions of NO from fertilized soils.

Air quality assessment results

In order to perform the air quality assessment for Portugal, the modelling results, for 2001 year, were analysed according to the limit and target values defined by the European Union Directives for each pollutant considered in this study (namely SO_2, NO_2, CO and O_3).

These limit values are listed in Table 1.

Table 1. Limit and target values defined by the European Union Directives for SO_2, NO_2, O_3 and CO.

Parameters	Period	AQ standart ($\mu g.m^{-3}$)	Nº of allowed excedeences	Target date
SO_2 (1999/30/EC)				
Human health protection	Hourly average	350	24 times/year	1 Jan 2005
Human health protection	Daily average	125	3 times/year	1 Jan 2005
Vegetation protection	Anual average	20	-	-
Vegetation protection	Winter average	20	-	-
NO_2 (1999/30/EC)				
Human health protection	Hourly average	200	18 times/year	1 Jan 2010
Human health protection	Anual average	40	-	1 Jan 2010
CO (2000/69/EC)				
Human health protection	8h running average	10 $mg.m^{-3}$	-	1 Jan 2005
O_3 (2002/3/EC)				
Human health protection (target value)	8h running average	120	25 times/year	1 Jan 2010
Vegetation protection (AOT40) (target value)	Hourly average (May-July)	18000 $\mu g.m^{-3}.h$	-	1 Jan 2010
Information threshold	hourly average	180	-	-
Alert threshold	Hourly average	240	3 consecutive h	-

NO_2 results

Figure 3 presents the modelling results for both legislation indicators of human health protection (annual average and the 19th maximum hour of the year) concerning NO_2. In both cases there are areas with exceedances to the limit values during the 2001 year. These areas correspond to the main urban areas of Portugal: Porto and Lisbon metropolitan regions. Since, the remaining area doesn't present any critical values, this suggest that the road traffic is the main responsible activity for the above-mentioned high concentrations of NO_2.

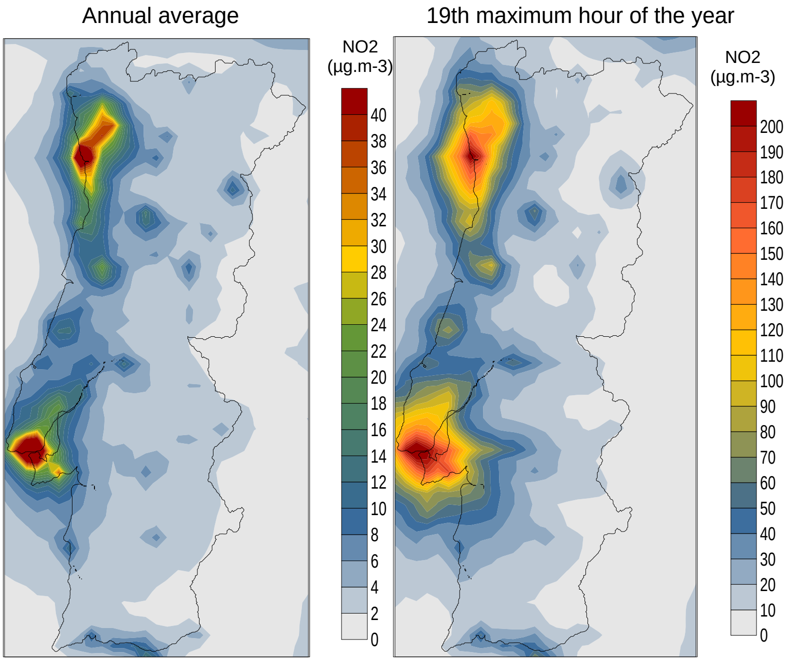

Figure 3. Modelling results for the NO_2 legislated parameter, for the year 2001.

SO_2 results

Figure 4 presents the modelling results for each of the parameters stated in the legislation for the human health and vegetation protection.

For human health protection (daily and hourly averages) there are two areas where the concentrations exceeded the limit values. When analyzing the vegetation protection targets, there are two more different regions with values beyond the limits. All the identified areas correspond to industrial places, suggesting that the industry activity is the main responsible for the bad air quality in these localities.

CO results

Concerning the CO, the legislation establishes a maximum of 10 mg.m^{-3} for the daily 8h averages for the human health protection. Figure 5 shows that there are no areas with concentrations higher than this limit. In fact, the simulation results indicate very low concentration values for this pollutant for the entire region of Portugal.

O_3 results

The 3th Daughter Directive (2002/03/EC), concerning the ozone pollutant, defines the target value of 120 µg.m^{-3} for the 26th maximum 8h daily average and a maximum of 18 000 µg.m^{-3}.h for the AOT40 value. Figure 6 presents the modelling ozone concentration fields for these two parameters. Despite the fulfillment of the target value for human health protection (120 µg.m^{-3}) for all the national territory, there is some risk for vegetation protection on areas with exceedances of the AOT40 threshold. Unfortunately, according to the land-use map, these areas correspond to high density vegetation and forest areas.

These ozone concentration patterns were already forecast and simulated in previous mesoscale modelling studies (Barros et al, 2003; Borrego et al, 2000), where the ozone precursors transport from the urban areas of Porto and Lisbon to the south and interior part of Portugal (by the N-NW dominant winds) is clear and significant.

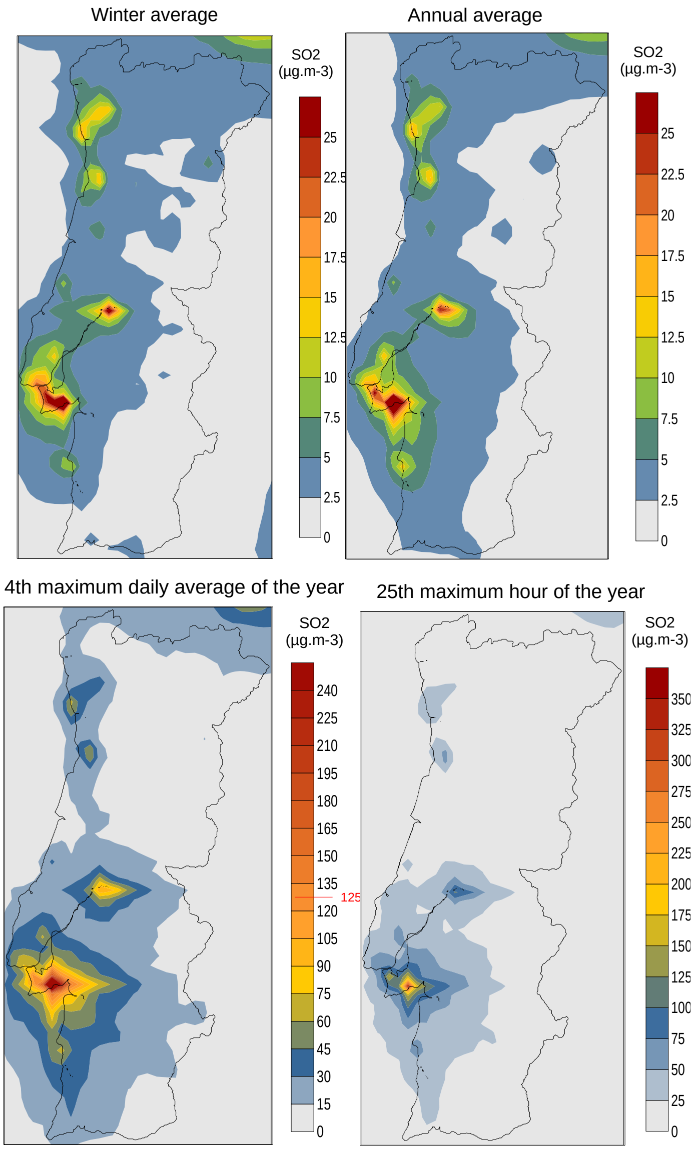

Figure 4. Modelling results for the SO_2 legislated parameter, for the year 2001.

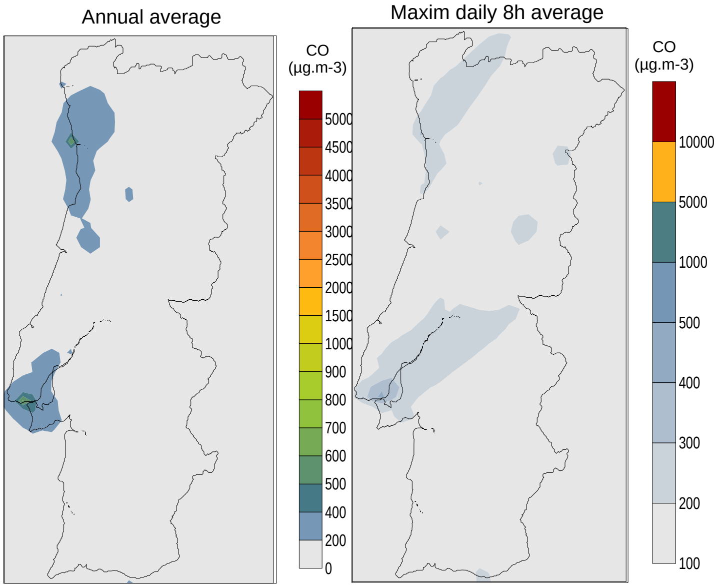

Figure 5. Modelling results for the CO legislated parameter, for the year 2001.

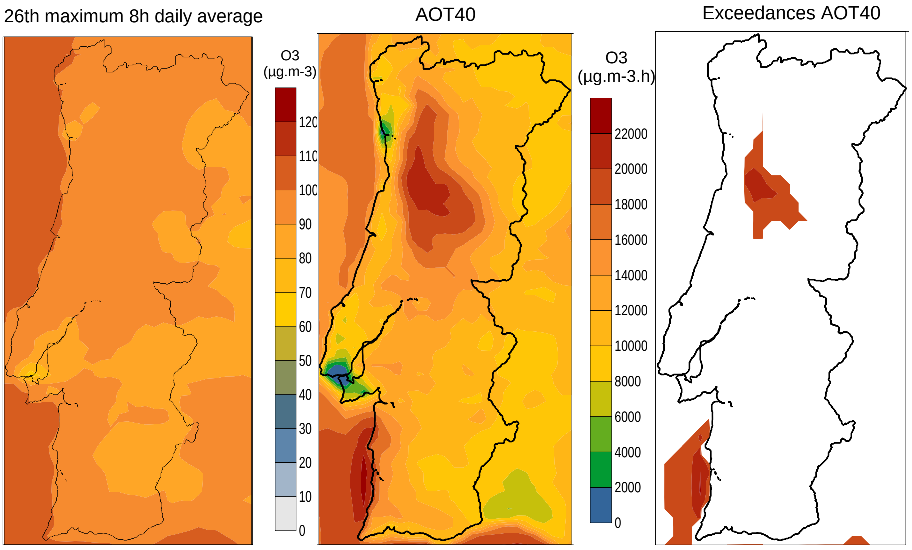

Figure 6. Modelling results for the O_3 legislated parameters, for the year 2001.

Model validation

The model validation was performed through the comparison of the observed and simulated values for the several legislated parameters, for each monitoring station of the Air Quality Portuguese network. Thus, according to the model uncertainty estimation defined by the Framework Directive, an error was calculated for each legislated indicator and for each monitoring site.

This deviation is defined by the following expression, where I_{obs} represents the indicator estimated with the observed values and I_{sim}, calculated from the simulated concentration:

$$Error = \left| \frac{I_{obs} - I_{sim}}{I_{sim}} \right|$$

In Table 2 is presented an average of the all monitoring sites, for each pollutant parameter defined in the respective Daughter Directive.

The analysis of Table 2 shows that the model system is able to reproduce the several legislated indicators, since almost all the deviations are below or equal to 50% (maximum deviation established by the Framework Directive to model evaluation).

An analysis by pollutant specie indicates that the ozone and CO presents the lower deviations. In fact, it should be expected a good model performance for ozone, since the model system was specially developed to simulate oxidant pollutants and photochemistry. In what concerns the CO, the quite chemical inert behavior involves an easier and correct simulation, due to fewer errors in the chemistry-transport modelling.

Table 2. Deviation estimation for each pollutant legislative indicator, considering an average of all the monitoring stations.

Polutant	**Legislated indicators**	**Deviation (%)**
SO_2	Human health protection (25th maximum hourly average)	34
	Human health protection (4th maximum daily average)	57
	Vegetation protection (annual average)	43
	Vegetation protection (winter average)	54
NO_2	Human heath protection (19th maximum hourly average)	48
	Human heath protection (annual average)	50
CO	Human heath protection (maximum 8h daily average)	32
O_3	Human heath protection (26th maximum 8h daily average)	16
	Vegetation protection (AOT40)	59
	(annual average)	40

In opposite to CO, the SO_2 is a very reactive pollutant, participating in a several group of chemical reactions, including aerosols chemistry. The absence of these chemistry reactions in the model version could be the reason of the higher errors for this specific pollutant.

Some conclusions

This work aims to assess the air quality in the Continental part of Portugal, according to the requirements of the new air quality Framework Directive. This first assessment exercise was made for the 2001 year, using the CHIMERE chemistry-transport model, applied to the Continental Portugal domain, and simulating the main critical gaseous pollutants (namely, NO_2, SO_2, CO and O_3).

This model system was then evaluated by comparison with observational data obtained from the national air quality monitoring network. The estimated errors in this validation exercise are relatively small and below the limits established by legislation to model evaluation.

Concerning the fulfillment of the thresholds defined by each Daughter Directive, the modelling results shows that there are exceedances of the human health protection limit of NO_2 in the two main urban areas (Porto and Lisbon), probably associated and due to road traffic emissions. Relatively to SO_2, the concentration fields indicate several small areas with higher values (superior to the human health and vegetation protection limits), all of them located close to large point sources (power plants, more precisely). The ozone is another pollutant with areas in exceedances to the legislated target values, in what concerns vegetation protection. These areas are mainly located in the interior central part and southwest coast of Portugal, not covered by the air quality monitoring Portuguese network. The CO is the unique pollutant that accomplish the limits impose by legislation, with concentration values significantly low in all the study domain.

This air quality assessment work allows to verify the importance of the establishment of several targets values for each air pollutant. In fact, the fulfillment of one of this limits do not imply the accomplishment of all. This can be confirmed with the ozone example, where the human health protection is in agreement with the law, but there are critical areas with concentrations hazardous for vegetation.

Future work will include the air quality assessment for other years and the improvement of the air quality modelling system in several aspects related to the chemistry-transport model, such as the model grid resolution, industrial area emissions estimation and background ozone prediction.

Acknowledgements

The authors wish to thank to the Portuguese Environment Institute for financing and giving access to measured data and to the financial support of the 3rd EU Framework Program and the Portuguese Ministério da Ciência e do Ensino Superior, for the PhD grant of A. Monteiro (SFRH/BD/10922/2002).

References

Barros, N., Borrego, C., Toll, I., Soriano, C., Jiménez, P. and Baldasano, J.M., 2003. Urban photochemical pollution in the Iberian Peninsula: Lisboa and Barcelona airsheds. Air and Waste Management Association 53, 347-359.

Beekmann, M. and Derognat, C., 2003. Monte Carlo uncertainty analysis of a regional-scale transport chemistry model constrained by measurements from the Atmospheric Pollution Over the Paris Area (ESQUIF) campaign, J. Geophys. Res., 108, D17, 8559.

Borrego, C.; Barros, N.; Miranda, A. I.; Carvalho, A. C. and Valinhas, M. J., 2000. Validation of two photochemical numerical systems under complex mesoscale circulations. Air Pollution Modelling and Its Application XIII. Kluwer Academic/Plenum Publishers, S. Gryning & E. Batchvarova, pp. 597-604.

Borrego, C.; Tchepel, O.; Monteiro, A.; Barros, N. and Miranda, A., 2002. Influence of traffic emissions estimation variability on urban air quality modelling. Water, Air and Soil Pollution: Focus 2 (5-6), Kluwer Publishers, pp. 487-499.

Derognat, C.; Beekmann, M.; Baeumle, M.; Martin, D, and Schmidt, H., 2003. Effect of biogenic volatile organic compound emissions on tropospheric chemistry during the Atmospheric Pollution Over the Paris Area (ESQUIF) campaign in the Ile-de-France region, J. Geophys. Res., 108, D17, 8560.

GENEMIS (Generation of European Emission Data for Episodes) Project, 1994. EUROTRAC annual report 1993, Part 5. EUROTRAC International Scientific Secretariat, Garmisch-Partenkirchen.

Hansen, M., DeFries, R., Townshend, J. R. G. and Sohlberg, R., 2000. Global land cover classification at 1km resolution using a decision tree classifier, Intern. Journal of Remote Sensing. 21, 1331-1365

Horowitz, L. W., Walters, S., Mauzerall, D., Emmons, L., Rasch, P., Granier, C., Tie, X., Lamarque, J., Schultz, M. and Brasseur, G., 2003. A global simulation of tropospheric ozone and related tracers: Description and evaluation of MOZART, version 2, J. Geophys. Res., in press.

Menut, L., 2003. Adjoint modelling for atmospheric pollution process sensitivity at regional scale, J. Geophys. Res. 108, No. D17, 8562.

Passant, N., R., 2002. Speciation of U.K. emissions of non-methane VOC, AEAT/ENV/0545 Issue 1.

Schmidt, H. and Martin, D., 2003. Adjoint sensitivity of episodic ozone in the Paris area, to emissions on the continental scale, J. Geophys. Res., 108, D17, 4313.

Schmidt, H., Derognat, C., Vautard, R., and Beekmann, M., 2001. A comparison of simulated and observed ozone mixing ratios for the summer of 1998 in Western Europe. Atmospheric Environment 35, 2449-2461.

Sillman, S., Vautard, R., Menut, L. and Kley, D., 2003. O3-NOx-VOC sensitivity and NOx-VOC indicators in Paris: Results from models and Atmospheric Pollution Over the Paris Area (ESQUIF) measurements. J. Geophys. Res. 108, D17, 8563.

Simpson, D., Winiwarter, W., Börjesson, G., Cinderby, S., Ferreiro, A., Guenther, A., Hewitt, C.N., Janson, R., Khalil, M.A.K., Owen, S., Pierce, T.E., Puxbaum, H., Shearer, M., Skiba, U., Steinbrecher, R., Tarrasón, l. and Öquist, M.G., 1999. Inventorying emissions from nature in Europe. Journal of Geophysical Research 104, 8113-8152.

Stohl, A., Williams, E., Wotawa, G. and Kromp-Kolb, H., 1996. A European inventory for soil nitric oxide emissions and the effect of these emissions on the photochemical formation of ozone, Atmospheric environment 30, 3741-3755.

Vautard, R., Beekmann, M., Roux, J. and Gombert, D., 2000. Validation of a deterministic forecasting system for the ozone concentrations over the paris area. Atmospheric Environment 35, 2449-2461.

Vautard, R., Martin, D., Beekmann, M., Dropbinski, P., Friedrich, R., Jaubertie, A., Kley, D., Lattuati, M., Moral, P., Neininger, B., Theloke, J., 2003. Paris emission inventory diagnostics from the ESQUIF airborne measurements and a chemistry-transport model, J. Geophys. Res., in press.

Tilmes, S., Brandt, J., Flatfy, F., Bergstrom, R., Flemming, J., Langner, J., Christensen, J.H., Frohn, L.M., Hoy, f., Jacobsen, I., Reimer, E., Stern, R. & Zimmermann, J., 2002. Comparison of Five Eulerian Air Pollution Forecasting Systems for the Summer of 1999 using the German Ozone Monitoring Data. Journal of Atmospheric Chemistry 42, 91-121.

A hierarchical Bayesian approach to the spatio-temporal assessment of the CAMx model

G. Barone[1], E. Chianese[1], G. Giunta[2] and A. Riccio[2]

[1]Dept. of Chemistry of the University of Naples “Federico II”
[2]Dept. of Applied Sciences of the University of Naples “Parthenope”
Corresponding address: angelo.riccio@uniparthenope.it

Introduction

The evaluation of the performance of physically-based computer models is of primary importance, from a scientific, as well as regulatory, point of view. Models integrate in a clear conceptual framework our understanding of atmospheric processes and their interactions, and fill in the gap between emission fluxes and atmospheric conditions; for these reasons they are usually exploited for scientific purposes or by policymakers to establish the effectiveness of abatement plans (see the reviews by Dennis et al., 1996, and Peters et al., 1994, on the current state and future direction in the development of eulerian air quality models). According to the USA-EPA, the primary objective of the next generation of air quality models is to improve the environmental community’s ability to evaluate the impact of air quality management practices for multiple pollutants at multiple scales (see the EPA Models-3 project web page at http://www.epa.gov/asmdnerl/models3/).

However, any validation procedure arises several complex statistical issues. Modeled data and measurements are far from being “perfect”. Both datasets are affected by errors of different nature: missing observations are often present, errors connected to the measurement and acquisition devices are practically unavoidable, systematic bias may be present. Modeled data are affected by uncertainties from mis/un-represented physics/chemistry, numerical errors, and so on. It is reasonable to hypothesize that measurements are influenced by local processes which are not equally represented by the model (the “change of support” problem, as defined in the geostatistical literature, Cressie, 1993), due to the implicit and explicit diffusion introduced into the model for numerical/stability reasons; for example McNair et al. (1996) found that *individual concentration measurements only approximately represent the true volume-averaged concentrations within a computational grid cell and that significant spatial variations exist*. This kind of “incommensurability” between point measurements and cell-averaged model values is often ignored in the majority of model evaluation studies. Moreover, measurements are not usually defined at the same spatial locations of the model, so an interpolation procedure is needed, but the interpolation of nonstationary spatio-temporal data, interacting on a wide variety of scales, is still a statistical issue (Guttorp, 2003).

In the following, we device a statistical approach that can be used for comparison and/or assimilation purposes and apply it to validate the output of the CAMx air quality model. In section 2 we introduce our modeling system, describe the main characteristics of the air quality model and its initialization. In section 3 a Bayesian model evaluation/assimilation approach is described; we specify a simple model for both measurements and modeled data in terms of an unobserved ground truth and estimate it in a Bayesian framework to take into account the uncertainties arising in its estimation. We show how to consistently interpolate the measurements from monitoring sites to locations for which modeled data are available. Our approach also takes into account the uncertainties about the different spatial support and the lack of stationarity in the data.

The air quality system

The CAMx (Comprehensive Air Quality Model with eXtensions) is an eulerian air quality photochemical model that allows the simulation of transport and chemical reactions of pollutants in the lower troposphere by solving the set of continuity equations for each chemical species. It is a publicly available software (http://www.camx.com). In this work we used the 4.03 version. The most important physical representations used in this work are summarized in the following.

Meteorological input (wind speed in each horizontal direction, temperature, pressure, relative humidity, water content, turbulent diffusivity) were derived from the MM5 model. The MM5 model was forced by the European Center for Medium Range Weather Forecasting (ECMWF) analysis (TOGA archive). The CAMx grid used the same projection and horizontal grid structure/resolution as MM5 (see figure 1); CAMx simply windowed data from a portion of the MM5 grid and output the subset to the CAMx files. The only interpolation performed was for winds, which need to be moved from the MM5 Arakawa-B configuration to the CAMx Arakawa-C configuration. Thirteen layers were used in the vertical direction with a maximum resolution of about seventy meters near the surface. The turbulent coefficient in the horizontal direction was calculated using the McNider and Pielke (1981) local gradient approach, while the horizontal diffusion coefficients was determined within CAMx using a deformation approach based on the method by Smagorinsky (1963).

The gas-phase chemistry was based in the SAPRC99 chemical mechanism (Carter, 2000). Photolysis rates are derived from the TUV preprocessor (Madronich, 2002) for each grid cell assuming clear sky conditions as a function of solar zenith angle, altitude, total ozone column, surface ultraviolet albedo and haze. Optical depth, needed to scale down photolysis rates for layers within or below clouds to account for UV attenuation, or to scale up the rates for layers above clouds to account for UV reflection, is calculated using the same approach as in RADM (Chang et al., 1987). The SAPRC99 mechanism was adapted to include a “bulk” aerosol chemistry using the module already implemented in CAMx. Aerosol production is initiated by the OH oxidation of SO2 to sulfate, production of nitric acid and condensable organic gases (CG). The aqueous sulfate and nitrate chemistry in resolved clouds is based on the same mechanism implemented in RADM algorithm (Chang et al., 1987). ISORROPIA thermodynamic module (Nenes et al., 1998) is used to partition inorganic components (sulfate, nitrate, ammonium, sodium and chloride) between the gas and particle phases. Four organic gases (CG1÷CG4) were added to the base mechanism in order to allow for the formation of secondary organic aerosol (SOA) using a semi-volatile equilibrium scheme called SOAP (Strader et al., 1998).

The 2001 anthropogenic emission data from the EMEP database have been used. They consist of annual emitted quantities, given for the 11 SNAP activity sectors and NOx , CO, SOx, NMVOC and NH3 families. Spatial emission distribution from the EMEP grid to the CAMx grid has been performed using an intermediate grid at 30'' resolution. Soil type being known on the this grid allowed for a better apportionment of the emissions. VOC speciation has been made according to the AEAT suggested profiles (Passant, 2002). Biogenic emissions for isoprene and terpenes have been computed using vegetation and soil inventories

(Simpson et al.,1999) of the model domain using reference temperature and PAR conditions; then, these emissions were tuned according to the meteorological conditions prevailing during the simulation period.

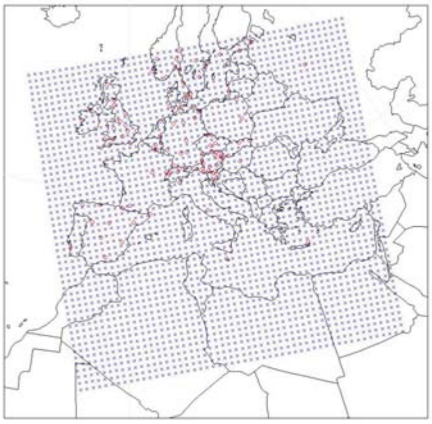

Figure 1. Cell centers of the model grid (crosses) and locations of the EMEP monitoring stations (circles) used for the validation exercise.

The statistical model

Our statistical analysis utilizes two different datasets: measurements, $\mathbf{O} \equiv \{O_t(s) : t = 1,\ldots, T, s = 1,\ldots,S\}$, and modeled data, $\mathbf{M} \equiv \{M_t(x) : t = 1,\ldots, T, \; x = 1,\ldots,M\}$; x and s are two indexes defining the lattices of the measurement network and model grid, respectively (see figure 1); t is the temporal index. In this work **M** represents the ozone data obtained by the CAMx simulation over the Mediterranean region at a nominal spatial resolution of $\approx 81 \times 81$ km^2 and a temporal resolution of 1 hour ranging from 1 to 5 August, 2001; **O** represents ozone observations available from the EMEP database (http://www.emep.int).

Due to their inherent uncertainties, it can be helpful to set up a stochastic framework in order to analyze and compare the properties of the two datasets. We assume that each dataset represents a sample from the same spatio-temporal process; we let

$$\mathbf{Y} \equiv \{Y_t(x) : t = 1,\ldots,T;\; x \in \Omega\} \tag{3.1}$$

where Ω represents the space over which the process is defined. Also, throughout the paper, we use the following notation, popularized by Gelfand and Smith (1990): for a random vector **Y**, let [**Y**] represent the joint probability density function of **Y**, and let [**Y**|**X**] the conditional density of **Y**, given **X**.

Model validation may be based on the use of the two following conditional probability distribution functions:

$$\begin{gathered}[\mathbf{Y}|\mathbf{M}] \\ [\mathbf{Y}|\mathbf{O}]\end{gathered} \tag{3.2}$$

i.e., we reduce modeled data and measurements to the common denominator given by the probability distribution function of the process **Y**; discrepancies between the two datasets may be highlighted by the different statistical properties of the two conditional distribution functions [**Y**|·] in (3.2).

In order to estimate [**Y**] we need to specify its spatio-temporal variability, i.e. how the process of interest evolves in time over the specified spatial domain and how it relates to the two datasets, **M** and **O**. The complex behavior of such dynamical process and the huge amount of data, typical of many environmental problems, make unfeasible a joint approach. However, several recent examples of the application of conditional hierarchical Bayesian space-time models have been reported in the literature: the combination of NSCAT satellite data with NCEP analysis (Wikle and Berliner, 2004), the prediction of surface winds over the tropical region where high resolutions are important for climatological reasons (Wikle et al., 2001), and the modeling of air-sea interaction (Berliner et al., 2003). See also Wikle (2003) for an overview of applications of Bayesian hierarchical models in the environmental sciences.

In essence, this hierarchical approach is based on the formulation of three basic conditional models, coherently linked together by simple probability rules (Berliner, 1996):

Stage 1. Data Model: [Data | Process, θ_1]

Stage 2. Process Model: [Process | θ_2]

Stage 3. Parameter Model: [θ_1, θ_2]

where θ_1 and θ_2 represent generic arrays of parameters introduced in the modeling. Each model can itself be specified as a product of physically-based conditional distributions. Bayesian probability theory ensures us that inference and prediction in the distribution of the process and parameters can be obtained from the so-called "posterior distribution function":

[Process, θ_1, θ_2 | Data] $\propto$ [Data | Process, θ_1] × [Process | θ_2] × [θ_1, θ_2]

The major advantage of this conditional approach is that statistical and physical reasoning can be more easily introduced at each stage of the hierarchy, and the Bayesian framework is ideal for combining the two views, especially in complex settings, i.e. for bringing together physical understanding and statistical modeling to get the best from both, while managing their associated uncertainties in a statistically consistent manner (Berliner, 2003).

In the next subsections we describe the most important characteristics of the conditional models used in this work.

The Data Model

In this work, the data model has been used to represent measurement errors and to accommodate the different supports from the two datasets, **O** and **M**. First, EMEP data were mapped onto the grid locations used by the CAMx model. A reasonable model may be:

$$\vec{O}_t = \mathbf{K}\vec{Y}_t + \vec{\sigma}_1 \qquad (3.3)$$

$\vec{Y}_t$ indicates the array of column-wise ordered values of the process **Y** at time *t* and at the same spatial locations of the CAMx grid cell centers. **K** represents an $S \times M$ matrix of weights mapping the process **Y** onto observations. We used a bi-linear interpolation, i.e. matrix **K** is sparse with only four elements not equal to zero for each row. $\vec{\sigma}_1$ may be interpreted as a combination of measurement and representativeness errors and was modeled as a zero-mean gaussian random noise, i.e. $\vec{\sigma}_1 \sim N(0, \Sigma_1)$, where this notation means that $\vec{\sigma}_1$ is sampled from a normal distribution with mean zero and variance Σ_1. Σ_1 was modeled as a $S \times S$ diagonal matrix, i.e. we assumed that errors were independently distributed in space and time, with a variance that depends only on the spatial location of the measurement station.

In the case of the [**Y** | **M**] distribution function, the data model is

$$\vec{M}_t = \mathbf{I}\vec{Y}_t + \vec{\sigma}_2 \tag{3.4}$$

where $\vec{\sigma}_2 \sim N(0, \Sigma_2)$. Σ_2 was modeled as a $M \times M$ diagonal matrix.

The Process Model

The process model represents the most delicate part of our statistical approach. The goal is to introduce as much knowledge about the statistical and physical behavior of the problem as possible.

To this aim, we used a process model already successful applied for a similar problem (Wikle et al., 1998). The process **Y** was given as conditional on three processes, denoted by μ, S_t and X_t:

$$\vec{Y}_t = \vec{\mu} + \vec{S}_t + \vec{X}_t + \vec{\gamma}_t \tag{3.5}$$

μ represents a site-specific mean, S_t a seasonal component, and X_t the short time scale, dynamical process. The γ_ts are random variables which model noise, and represent the unexplained variations at this second level of the hierarchy.

The mean component of the process model

Since the modeling period is rather short (five days of simulation), we assumed that $\vec{\mu}$ does not depend on time, but only on the spatial location; however, it would be reasonable to assume a temporal dependence (e.g. a seasonal cycle forced by the variability of solar actinic flux) for a longer time period. In order to get a general understanding of the spatial dependence of the mean, we performed a preliminary exploratory analysis (figure 2). We found that there is a large-scale spatial trend from northwest to southeast and a linear dependence on altitude. Similar spatial gradients of background ozone have already been reported (Scheel, 1995). Also, it is generally believed that the higher levels at high elevation sites reflect inputs from the free troposphere (Vingarzan, 2004).

In order to interpolate the ozone measurements from the sparse monitoring locations to the grid locations, $\vec{\mu}$ was specified as a conditionally gaussian Markov Random Model (MRF) with a first-order spatial dependence, i.e. for each grid location (i, j), the mean was specified as

$$\mu(i,j) \mid \{\mu(k,l) : (k,l) \neq (i,j)\} \sim N\left(\mu_0(i,j) + \Delta_\mu, \tau_\mu^2\right) \tag{3.6}$$

where

$$\begin{aligned}\Delta_\mu = \; & \alpha_\mu\left(\mu(i-1,j) - \mu_0(i-1,j) + \mu(i+1,j) - \mu_0(i+1,j)\right) + \\ & \beta_\mu\left(\mu(i,j-1) - \mu_0(i,j-1) + \mu(i,j+1) - \mu_0(i,j+1)\right)\end{aligned} \tag{3.7}$$

models the zonal and meridional MRF spatial dependence, and τ_μ^2 the homogenous variance. $\mu_0(i,j)$ is the conditional mean at the grid point (i, j) and was represented as a simple linearly-dependent spatial trend

$$\mu_0(i,j) = \mu_0^1 + \mu_0^2 \mathrm{lat}(i,j) + \mu_0^3 \mathrm{long}(i,j) + \mu_0^4 \mathrm{altit}(i,j) \tag{3.8}$$

lat(i,j), long(i,j) and altit(i,j) are the latitude, longitude and altitude at grid point (i, j), respectively. μ_0^1, μ_0^2, μ_0^3 and μ_0^4 are four random coefficients.

The seasonal component of the process model

Further exploratory analysis showed a significant diurnal cycle (figure 3). This is a well known characteristic of hourly ozone data, since diurnal fluctuations in ground-level ozone are associated with the diurnal variation of the solar flux and the resulting differences between daytime photochemical production and nighttime removal of ozone as well as the diurnal cycle of boundary layer evolution and decay. The power spectra showed a single significant peak at a period of 24 hr.

From these considerations, the seasonal component was modeled as a diurnal harmonic with amplitudes and phases that vary spatially

$$\vec{S}_t = \vec{g}\cos\left(\frac{2\pi t}{24}\right) + \vec{f}\sin\left(\frac{2\pi t}{24}\right) \tag{3.9}$$

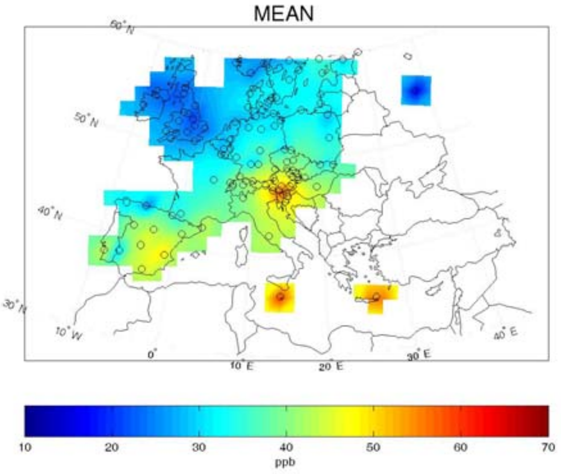

Figure 2. Empirical mean values of ozone concentration interpolated from EMEP data.

where t is the time index and $\vec{g}$ and $\vec{f}$ are two random coefficients that depend of the spatial location

$$g(i,j) = g_0^1 + g_0^2\text{lat}(i,j) + g_0^3\text{long}(i,j) + g_0^4\text{altit}(i,j) \tag{3.10a}$$

$$f(i,j) = f_0^1 + f_0^2\text{lat}(i,j) + f_0^3\text{long}(i,j) + f_0^4\text{altit}(i,j) \tag{3.10b}$$

Equations (3.10a) and (3.10b) introduce our prior knowledge about the spatial pattern of the diurnal cycle. At lower latitudes, the higher actinic flux increases the amplitude of the diurnal cycle; also, at high elevations, in the free troposphere, removal/production processes are not significant and the diurnal ozone concentration is rather flat. However, it is also widely known that the diurnal cycle is influenced by the proximity to emissions sources, since ozone can be steadily titrated by fresh NOx emissions, but this effect has not been taken into account.

The g_0^i's and f_0^i's are eight random coefficients, for which we assumed independent gaussian distributions.

The dynamic component of the process model

In order to capture the dynamic spatial features, we used a first-order Vector AutoRegression (VAR) model

$$\vec{X}_t = \mathbf{H}\vec{X}_{t-1} + \vec{\eta}_t \tag{3.11}$$

where **H** is a matrix of spatial regression coefficients and η_t is a zero-mean random value. We considered the "nearest-neighbor" VAR model, i.e. the value of the dynamic component at the grid cell (*i*, *j*) depends on the value at the same grid cell and on neighbor cells

$$\begin{aligned} X_t(i,j) = \quad & a(i,j)X_{t-1}(i,j) + bX_{t-1}(i+1,j) + cX_{t-1}(i,j+1) \\ & + dX_{t-1}(i-1,j) + eX_{t-1}(i,j-1) + \eta_t(i,j) \end{aligned} \tag{3.12}$$

Note that, in order to introduce a greater flexibility into the model, *a*(*i*,*j*) varies spatially. Furthermore, $\{\eta_t(i,j)\}$ was assumed to be a spatially independent white noise process.

a(*i*, *j*) was represented as a conditionally specified gaussian MRF

$$a(i,j) \mid \{a(k,l):(k,l) \neq (i,j)\} \sim N\left(a_0(i,j) + \Delta_a, \tau_a^2\right) \tag{3.13}$$

where

$$\begin{aligned} \Delta_a = \quad & \alpha_a\left(a(i-1,j) - a_0(i-1,j) + a(i+1,j) - a_0(i+1,j)\right) + \\ & \beta_a\left(a(i,j-1) - a_0(i,j-1) + a(i,j+1) - a_0(i,j+1)\right) \end{aligned} \tag{3.14}$$

$a_0(i,j)$ was also given as a simple linearly-dependent spatial trend

$$a_0(i,j) = a_0^1 + a_0^2\,\mathrm{lat}(i,j) + a_0^3\,\mathrm{long}(i,j) + a_0^4\,\mathrm{altit}(i,j) \tag{3.15}$$

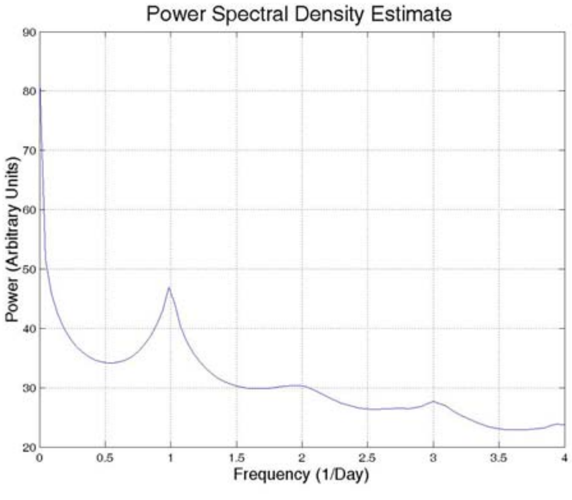

Figure 3. Power spectral density estimate averaged over all EMEP time series

The Parameter Model

To complete the hierarchy we must specify distributions for the parameters from the previous stages. In the past, the choice of the parameter distributions has been the source of the majority of objections to the Bayesian approach, due to its subjectiveness. Of course, such subjectiveness is also present in the data and process models, but the strength of the

Bayesian approach consists in the fact that it provides a coherent probabilistic framework in which to incorporate this subjective judgment. Moreover, during the last years, powerful computational methods have been developed (Gilks et al., 1996), so that even complicated posterior distributions can be easily explored and more complex, physically-based, dynamics can be included in our prior knowledge.

In this work, we used conjugate distributions for all parameters, i.e. inverse gamma distributions for the variances and normal distributions for all other parameters. A Gibbs sampler (Gilks, 1996) was used to explore the conditional posterior distributions for all parameters, with the exception of the MRF spatial dependence parameters (i.e. α_μ, β_μ, α_a, α_b) for which a "pseudo-likelihood" approach was used (Cressie, 1993).

Results

In this preliminary evaluation study, we briefly present the most interesting features of our statistical approach.

The Bayesian approach allows the quantification of all uncertainties in a statistically consistent framework. For example, the posterior distribution function for the **Y** process is (ignoring all other terms that do not explicitly depend on the **Y** values.

$$\begin{aligned}\left[\vec{Y}_t \mid \cdot\right] &\propto \left[\vec{O}_t \mid \mathbf{T}, \vec{Y}_t, \sigma_1^2\right] \times \left[\vec{Y}_t \mid \mu, \vec{S}_t, \vec{X}_t, \sigma_\gamma^2\right] \\ &\propto \exp\left(-\frac{1}{2}\left(\vec{O}_t - \mathbf{K}\vec{Y}_t\right)' \Sigma_1^{-1}\left(\vec{O}_t - \mathbf{K}\vec{Y}_t\right)\right) \\ &\quad \times \exp\left(-\frac{1}{2}\frac{1}{\sigma_\gamma^2}\left(\vec{Y}_t - \vec{\mu} - \vec{S}_t - \vec{X}_t\right)'\left(\vec{Y}_t - \vec{\mu} - \vec{S}_t - \vec{X}_t\right)\right)\end{aligned} \qquad (4.1)$$

Recalling that for a random variable, if $\left[\vec{\theta} \mid \cdot\right] \propto \exp\left\{-\frac{1}{2}\left[\vec{\theta}'\mathbf{A}\vec{\theta} - 2\mathbf{B}\vec{\theta}\right]\right\}$, then $\vec{\theta} \sim N\left(\mathbf{A}^{-1}\mathbf{B}', \mathbf{A}^{-1}\right)$, it can be easily verified that the distribution function for **Y** may be written as

$$\left[Y_t \mid \cdot\right] \sim N\left(\left(\mathbf{K}'\Sigma_1^{-1}\mathbf{K} + \frac{1}{\sigma_\gamma^2}\mathbf{I}\right)^{-1}\left(\vec{O}_t'\Sigma_1^{-1}\mathbf{K} + \frac{1}{\sigma_\gamma^2}\left(\vec{\mu} + \vec{S}_t + \vec{X}_t\right)'\right)', \left(\mathbf{K}'\Sigma_1^{-1}\mathbf{K} + \frac{1}{\sigma_\gamma^2}\mathbf{I}\right)^{-1}\right) \qquad (4.2)$$

Many algorithms exist to sample from this multivariate gaussian distribution. Moreover the Markov chain iterates allow the reconstruction of the full posterior distribution for **Y**, so that any statistical index may be estimated with its uncertainty ranges.

Missing observations may be easily estimated as well, since they are treated as additional parameters. If $\vec{O}_{\mathrm{meas}\,t}$ indicates measurements available at time *t*, then

$$\left[\vec{O}_{\mathrm{meas}\,t}, \vec{O}_{\mathrm{mis}\,t} \mid \cdot\right] \propto \exp\left(-\frac{1}{2}\left(\vec{O}_t - \mathbf{K}\vec{Y}_t\right)' \Sigma_1^{-1}\left(\vec{O}_t - \mathbf{K}\vec{Y}_t\right)\right) \qquad (4.3)$$

so that

$$\left[\vec{O}_{\mathrm{meas}\,t}, \vec{O}_{\mathrm{mis}\,t} \mid \cdot\right] \sim N\left(\mathbf{K}\vec{Y}_t, \Sigma_1\right) \qquad (4.4)$$

It can be shown that the conditional distribution of $\vec{O}_{\text{mis}\,t}$ given $\vec{O}_{\text{meas}\,t}$ may be easily derived (Mardia et al., 1980) from the appropriate partition of matrix Σ_1 and vector $\mathbf{K}\vec{Y}_t$.

The lack of stationarity is implicitly taken into account, since no previous form has been assumed for the covariance of the **Y** data.

As an example of the potentiality of this approach, figure (4) shows the estimated **Y** values, with its uncertainty range. Data from the AT0041 EMEP station (47° 58′ 23′′ N, 13° 0′ 58′′ E, 730 meters of altitude). A deeper quantitative analysis is currently under way.

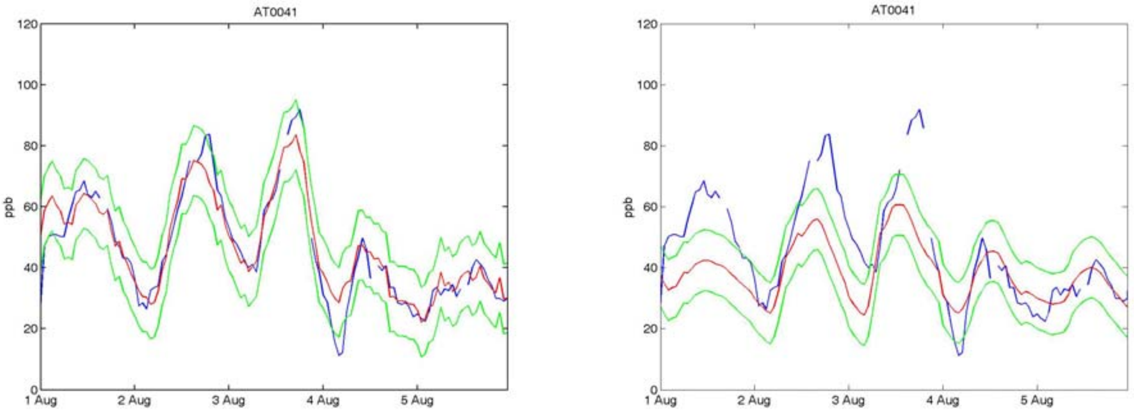

Figure 4. Left: observed concentration (blue line); a sample from the [**Y**|**O**] distribution (red line), plus and minus two times the standard deviation (green line). Right: observed concentration (blue line); a sample from the [**Y**|**M**] distribution (red line), plus and minus two times the standard deviation (green line).

References

Berliner, 2003: Physical-statistical modeling in geophysics, *Journal of Geophysical Research – Atmospheres*, **108**(D24), doi 10.1029/2002JD002865 8776

Berliner, L.M., 1996: Hierarchical Bayesian time series models, in *Maximum Entropy and Bayesian Methods*, 15-22. K. M. Hanson and R.N. Silver (Eds.), Kluwer Academic Publishers.

Berliner, L.M., Milliff, R.F., and C.K. Wikle, 2003: Bayesian hierarchical modeling of air-sea interaction. *Journal of Geophysical Research - Oceans*, **108**(C4):1413-1430

Carter, W.P.L., 2000: Programs and Files Implementing the SAPRC-99 Mechanism and its Associates Emissions Processing Procedures for Models-3 and Other Regional Models. http://pah.cert.ucr.edu/~carter/SAPRC99.htm

Chang, J.S., R.A. Brost, I.S.A. Isaksen, S. Madronich, P. Middleton, W.R. Stockwell, and C.J, Walcek, 1987: A Three-dimensional Eulerian Acid Deposition Model: Physical Concepts and Formulation. *J. Geophys. Res.*, **92**:14,681-14,700.

Cressie, N.A.C., 1993: Statistics for Spatial Data. Wiley and Sons

Dennis, R.L., D.W. Byun, J.H. Novak, K.J. Galluppi, C.J. Coats, and M.A. Vouk, 1996: The next generation of integrated air quality modeling: EPA's Models-3. *Atmospheric Environment*, **30**:1925-1938

Gelfand, A.E. and A.F.M. Smith, 1990: Sampling based approaches to calculating marginal densities. *Journal of the American Statistical Association*, **85**:398--409

Gilks, W.R., S. Richardson and D.J. Spiegelhalter, 1996: Markov Chain Monte Carlo in Practice. Chapman and Hall

Guttorp, P., 2003: Environmental Statistics-A personal view. *International Statistical Review,* **71**: 169-179

Madronich, S., 2002: The Tropospheric Visible Ultra-violet (TUV) model web page. National Center for Atmospheric Research, Boulder, CO. http://www.acd.ucar.edu/TUV/

Mardia, K., S. Kent and J. Bibby, 1980: Multivariate analysis, Academic Press

McNair, L.A., R.A. Hurley and A.G. Russell, 1996: Spatial inhomogeneity in pollutant concentrations, and their implications for air quality model evaluation. *Atmospheric Environment*, **30**:4291-4301

McNider, R.T. and R.A. Pielke, 1981: Diurnal boundary layer development over sloping terrain, *J. Atmos. Sci.*, **38**:2198-2212

Nenes, A, C. Pilinis, and S.N. Pandis, 1998: ISORROPIA: A New Thermodynamic Model for Multiphase Multicomponent Inorganic Aerosols, *Aquatic Geochemistry*, **4**:123-152

Passant, N.R., 2002: Speciation of UK emissions of NMVOC. AEAT/ENV/R/0545 Report

Peters, L.K., C.M. Berkowitz, G.R. Carmichael, R.C. Easter, G. Fairweather, S.J. Ghan, J.M. Hales, L.R. Leung, W.R. Pennell, F.A. Potra, R.D. Saylor and T.T. Tsang, 1995: The current state and future direction of Eulerian models in simulating the tropospheric chemistry and transport of trace species: a review. *Atmospheric Environment*, **29**:189-222

Smagorinsky, J., 1963: General Circulation Experiments with the Primitive Equations: I. The Basic Experiment. *Mon. Wea. Rev.*, **91**:99-164.

Scheel, H.E., H. Areskoug, H. Geiss, B. Gomiscel, K. Granby, L. Haszpra, L. Klasinc, D. Kley, T. Laurila, T. Lindskog, M. Roemer, R. Schmitt, P. Simmonds, S. Solberg and G. Toupance, 1997: On the spatial distribution and seasonal variation of lower troposphere ozone over Europe. *Journal of Atmospheric Chemistry*, **28**:45-59.

Simpson, D., W. Winiwarter, G. Borjesson, S. Cinderby, A. Ferreiro, A. Guenther, C.N. Hewitt, R. Janson, M.A.K. Khalil, S. Owen, T.E. Pierce, H. Puxbaum, M. Shearer, S. Steinbrecher, B.H. Svennson, L. Tarrason, M.G. Oquist, 1999: Inventorying emissions from nature in Europe. *Journal of Geophysical Research* **104**:8113:8152

Strader, R., C. Gurciullo, S.N. Pandis, N. Kumar, and F.W. Lurmann, 1998: Development of gas-phase chemistry, secondary organic aerosol, and aqueous-phase chemistry modules for PM modeling. Final report for CRC Project A21-1 prepared for the Coordinating Research Council, Atlanta, GA by Sonoma Technology, Inc., Petaluma, CA, STI-97510-1822-FR

Vingarzan, R., 2004: A review of surface ozone background levels and trends. *Atmospheric Environment*, **38**:3431-3442

Wikle, C.K., 2003: Hierarchical models in environmental science. *International Statistical Review,* **71**: 181-199

Wikle, C.K., L.M. Berliner and N. Cressie, 1998: Hierarchical Bayesian space-time models. *Environmental and Ecological Statistics*, **5**:117-154

Wikle, C.K. and L.M. Berliner, 2004. Combining information across spatial scales. In review

Wikle, C.K., Milliff, R.F., Nychka, D., and L.M. Berliner, 2001: Spatiotemporal hierarchical Bayesian modeling: Tropical ocean surface winds. *Journal of the American Statistical Association*, **96**:382-397

Implementation issues related to variational data assimilation: some preliminary results and conclusions

Zahari Zlatev [1)], Jørgen Brandt [1)] and Ágnes Havasi [2)]

[1)] National Environmental Research Institute
Frederiksborgvej 399, P. O. Box 358, DK-4000 Roskilde, DENMARK
[2)] Department of Meteorology, Eötvös Loránd University
Pazmany P. setany 1/C, Budapest, H1117, HUNGARY

Abstract

The variational data assimilation approach could be viewed as an attempt to adjust globally the results obtained by a given model to a set of available observations. This approach has the theoretical **advantage** of providing **consistency** between the dynamics of the model and the final results of the assimilation. The idea was probably applied for the first time in 1971 in a paper written by P. Morel, G. Lefebre and G. Rabreau (Morel et al., 1971). They defined and implemented a procedure in which the assimilating model is repeatedly integrated forward and backward in time, the observations being constantly introduced in the model. The **heuristic** idea behind that procedure, supported by a number of numerical results, was that repeated calculations and corrections of model results would converge to a solution which would be **compatible,** at least to a certain degree of accuracy, with the observations.

Results from some preliminary investigations (based mainly on running simple tests) will be presented in this paper. Several conclusions will be drawn. Data assimilation techniques will normally lead to huge computational tasks, which implies that one should try to find out, a priori, whether to apply data assimilation or not in a particular study. The important problem of formulating a set of conditions under which the data assimilation approach will probably not give good results (these conditions have to be checked carefully before applying the data assimilation procedure) will be discussed. Plans for future work will be outlined.

Basic ideas

Assume that observations are available at time-points $\mathbf{t_p}$, where $\mathbf{p} \in \{0,1,2,\ldots,\mathbf{P}\}$. These observations can be taken into account in an attempt to improve the results obtained by a given model. This can be done by minimizing the value of the following functional (see, for example, Lewis and Derber, 1985):

$$\textbf{(1.1)} \qquad \mathbf{J}\{\bar{\mathbf{c}}_0\} = \frac{1}{2} \sum_{\mathbf{p}=0}^{\mathbf{P}} \left\langle \mathbf{W}(\mathbf{t_p})\left(\bar{\mathbf{c}}_\mathbf{p} - \bar{\mathbf{c}}_\mathbf{p}^{\mathbf{obs}} \right),\ \bar{\mathbf{c}}_\mathbf{p} - \bar{\mathbf{c}}_\mathbf{p}^{\mathbf{obs}} \right\rangle ,$$

where the functional $\mathbf{J}\{\bar{\mathbf{c}}_0\}$ depends on the initial value $\bar{\mathbf{c}}_0$ of the vector of the concentrations, $\mathbf{W}(\mathbf{t_p})$ is a matrix containing some weights and $\langle\ ,\ \rangle$ is an inner product in an appropriately defined Hilbert space (it will be assumed in this paper that the usual vector space is used, i.e. that $\overline{\mathbf{c}} \in \Re^{s}$ where $\mathbf{s}$ is the number of chemical species involved in the model). It is seen that the functional $\mathbf{J}\{\overline{\mathbf{c}}_0\}$ depends on both the weights and the differences between calculated by the model concentrations $\overline{\mathbf{c}}_{\mathbf{p}}$ and observations $\overline{\mathbf{c}}_{\mathbf{p}}^{\mathbf{obs}}$ at the time-levels $\{0, 1, \ldots, \mathbf{P}\}$ at which observations are available. $\mathbf{W}(\mathbf{t}_{\mathbf{p}})$ will be assumed to be the identity matrix $\mathbf{I}$ in this study, but in general weights are to be defined in some way.

The task is to find an improved initial field $\overline{\mathbf{c}}_0$, which minimizes the functional $\mathbf{J}\{\overline{\mathbf{c}}_0\}$. This can be achieved by using some optimization algorithm. Most of the optimization algorithms are based on the application of the gradient of $\mathbf{J}\{\overline{\mathbf{c}}_0\}$. The adjoint equation has to be defined and used in the calculation of the gradient of $\mathbf{J}\{\overline{\mathbf{c}}_0\}$.

It is clear that the same procedure, as that used to improve the concentration field $\overline{\mathbf{c}}_0$, can successively be used to improve the next concentration fields $\{\overline{\mathbf{c}}_1, \overline{\mathbf{c}}_2, \ldots\}$.

It should be stressed that other formulations of $\mathbf{J}\{\overline{\mathbf{c}}_0\}$ can be used (see Daescu and Navon, 2004, Daescu et al., 2003, Le Dimet et al., 2002, Elbern and Schmidt, 1999, 2001, Elbern et al., 1997, 1999, 2000, Talagrand and Courtier, 1987). It is assumed here that data assimilation techniques are applied to improve an initial field of concentrations, but data assimilation can be applied for other purposes too. Other applications are (i) improving emission fields, (ii) checking boundary conditions and, in a more general context, (iii) checking the sensitivity of the concentrations to variation of different parameters. More details can be found in Akella and Navon, 2004, Alekseev and Navon, 2005, Daescu et al., 2003, Elbern et al., 2000, Sandu et al., 2003, 2004, Wang et al., 2001). The relationship between the use of data assimilation and the use of a Kalman filter is studied in (Li and Navon, 2001).

Calculating the gradient of the functional

It is convenient to explain the basic ideas that are used when the gradient of the functional $\mathbf{J}\{\overline{\mathbf{c}}_0\}$ is calculated by the following very simple example. Assume that observations are available at five time-points: $\mathbf{t}_0, \mathbf{t}_1, \mathbf{t}_2, \mathbf{t}_3, \mathbf{t}_4$. The gradient of the functional can be calculated by using the scheme Fig. 2.1. The calculations have to be performed in five steps.

Step 1. Use the "model" to calculate $\overline{\mathbf{c}}_1$ (performing integration, in a forward mode, from time-point $\mathbf{t}_0$ to time-point $\mathbf{t}_1$). Calculate the adjoint variable $\overline{\mathbf{q}}_1 = \overline{\mathbf{c}}_1 - \overline{\mathbf{c}}_1^{\mathbf{obs}}$. Form the adjoint equation (corresponding to the model used in the forward mode). Perform backward integration (by applying the adjoint equation) from time-point $\mathbf{t}_1$ to time-point $\mathbf{t}_0$ to calculate the vector $\overline{\mathbf{q}}_0^1$, where the lower index shows that $\overline{\mathbf{q}}_0^1$ is calculated at time-point $\mathbf{t}_0$, while the upper index shows that $\overline{\mathbf{q}}_0^1$ is obtained by using $\overline{\mathbf{q}}_1 = \overline{\mathbf{c}}_1 - \overline{\mathbf{c}}_1^{\mathbf{obs}}$ as an initial vector.

Step 2 – Step 4. Perform the same type of calculations as in Step 1 to obtain $\overline{\mathbf{q}}_0^2$, $\overline{\mathbf{q}}_0^3$ and $\overline{\mathbf{q}}_0^4$.

Step 5. The sum of $\overline{\mathbf{q}}_0^1$, $\overline{\mathbf{q}}_0^2$, $\overline{\mathbf{q}}_0^3$, $\overline{\mathbf{q}}_0^4$ obtained in Step 1 – Step 4 and $\overline{\mathbf{q}}_0^0 = \overline{\mathbf{q}}_0 = \overline{\mathbf{c}}_0 - \overline{\mathbf{c}}_0^{\mathbf{obs}}$ gives the required gradient of the functional $\mathbf{J}\{\overline{\mathbf{c}}_0\}$.

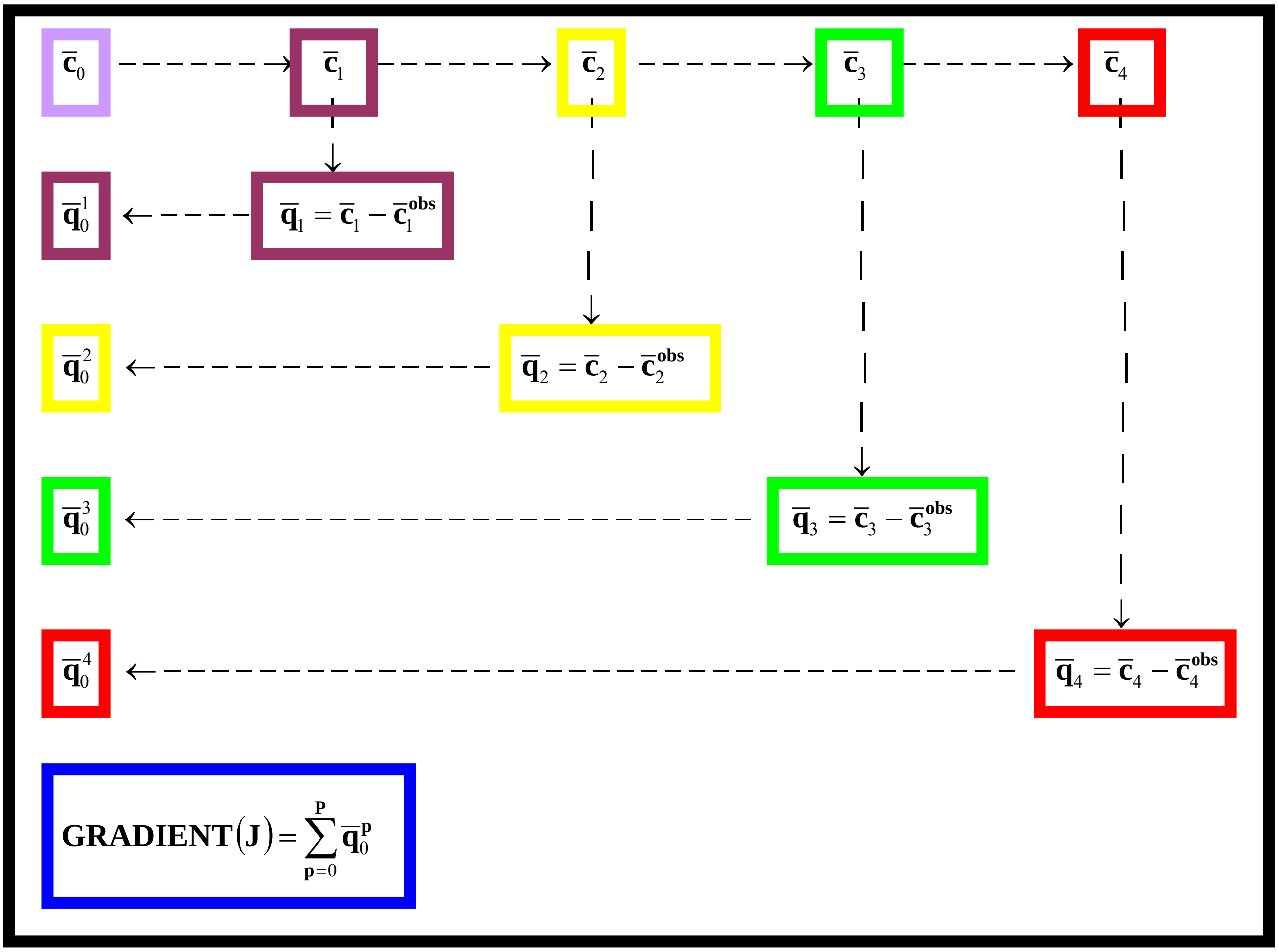

Figure 2.1 Computing the gradient of the functional when observations are available in five time-points.

It is seen from Fig. 2.1 that the gradient of $\mathbf{J}\{\bar{\mathbf{c}}_0\}$ can be calculated by performing one forward step from time-point $\mathbf{t}_0$ to time-point $\mathbf{t}_\mathbf{p}$ and $\mathbf{p}$ backward steps from time-points $\mathbf{t}_\mathbf{p}$, $\mathbf{p} = \mathbf{1}, \mathbf{2}, \ldots, \mathbf{P}$, to time-point $\mathbf{t}_0$. This explains the main idea in a very clear way, but it is expensive when $\mathbf{P}$ is large. In fact, the computational work can be reduced, performing only one backward step as shown in Appendix 1. Unfortunately, there is a price for this reduction of the computational work: one has to store all intermediate vectors $\bar{\mathbf{c}}_\mathbf{p}$, $\mathbf{p} = \mathbf{1}, \mathbf{2}, \ldots, \mathbf{P}$, which will lead to a very considerable increase of the storage needed when $\mathbf{P}$ is large. Thus, there is a trade off here between storage requirements and computational work: the decrease of the computational work leads to an increase of the storage needed and vice versa.

Forming the adjoint equations

Assume that the model is linear, given by

$$(3.1) \quad \frac{\partial \bar{\mathbf{c}}}{\partial \mathbf{t}} = \mathbf{A}\bar{\mathbf{c}}\,.$$

Let $\bar{\mathbf{q}} = \bar{\mathbf{c}} - \bar{\mathbf{c}}^{\mathbf{obs}}$ be the adjoint variable. Then the adjoint equation is defined by

(3.2) $$\frac{\partial \overline{\mathbf{q}}}{\partial \mathbf{t}} = -\mathbf{A}^{\mathbf{T}}\overline{\mathbf{q}},$$

where the superscript $\mathbf{T}$ means that the matrix by which the adjoint operator $\mathbf{A}^{\mathbf{T}}$ is represented is transposed to the matrix representing operator $\mathbf{A}$.

If the model is non-linear, then it is first necessary to produce a linearized version. In other words, the non-linear model

(3.3) $$\frac{\partial \overline{\mathbf{c}}}{\partial \mathbf{t}} = \mathbf{B}(\overline{\mathbf{c}})$$

is rewritten as

(3.4) $$\frac{\partial (\delta \overline{\mathbf{c}})}{\partial \mathbf{t}} = \mathbf{B}'(\delta \overline{\mathbf{c}})\delta \overline{\mathbf{c}}$$

where $\boldsymbol{\delta}\overline{\mathbf{c}}$ is some small variation of $\overline{\mathbf{c}}$ and $\mathbf{B}'$ is a linear operator obtained by differentiation of $\mathbf{B}$. The adjoint equation of the linear model (3.4) can be formed in the following way:

(3.5) $$\frac{\partial(\boldsymbol{\delta}\overline{\mathbf{q}})}{\partial \mathbf{t}} = -(\mathbf{B}'(\boldsymbol{\delta}\overline{\mathbf{q}}))^{\mathbf{T}}\,\boldsymbol{\delta}\overline{\mathbf{q}}.$$

It is not necessary to go into further details for the purposes of this paper. More details about adjoint equations can be found in (Marchuk, 1995, Marchuk et al., 1996, Wang et al., 2001). We shall finish this section with two remarks.

Remark 1. Adjoint equations of the continuous models have been discussed above. Sometimes it is more appropriate to form the adjoint equations of the discretised model (see, for example, Lewis and Derber, 1985). Such formulations will be given in one of the next sections.

Remark 2. Very often splitting techniques are used in connection with large-scale models (Hundsdorfer and Verwer, 2003, Zlatev, 1995). If splitting is used, then one normally forms the adjoint equations corresponding to the obtained by the splitting procedure chosen sub-models; see, for example, (Elbern and Schmidt, 1999, Sandu et al., 2003).

Algorithmic representation of a data assimilation algorithm

A data assimilation algorithm can be represented by applying the procedure described in Fig. 4.1. An optimization procedure is needed for the calculations in the green box (roughly speaking, the direction of the "steepest descent" is normally to be found and then the value of parameter RHO that gives the largest decrease in the direction found is to be used to improve the current solution). In practice, it is only necessary here to find a good **standard** minimization subroutine. In our experiments we used the subroutine E04DGF from the NAG Numerical Library (see NAG Numerical Library, 2004). It should be easy to call another appropriate subroutine.

Nearly all optimization subroutines need the value of the functional $\mathbf{J}\{\overline{\mathbf{c}}_0\}$ and its gradient. The calculation of these values is given in the red box in Fig. 4.1. This is the major part of the computational work and is based on scheme described in Fig. 2.1. Let us reiterate here that the repeated backward steps can be avoided (see the end of Section 2).

Data assimilation for some 1-D examples

It is relatively easy to understand the main ideas on which the variational data assimilation is based by studying the process for simple one-dimensional transport equations. Assume that the unknown variable $\bar{\mathbf{c}} \in \Re$ is the concentration of a given chemical compound and $\mathbf{V}$ is some function ("wind velocity field"), which may depend on $\mathbf{t}, \mathbf{x}$ and $\bar{\mathbf{c}}$. Numerical experiments with (a) constant $\mathbf{V}$, (b) $\mathbf{V}$ depending on $\mathbf{x}$ and/or $\mathbf{t}$ and (c) $\mathbf{V} = \bar{\mathbf{c}}$ have been carried out. In all cases the analytic solution was known, which allowed us to check easily the correctness of both the calculated results and the implementation of the algorithms. Only results obtained by $\mathbf{V}$ depending on $\mathbf{x}$ will be presented in this paper.

The three cases, (a), (b) and (c), can be described by the following partial differential equation (PDE):

$$\textbf{(5.1)} \qquad \frac{\partial \bar{\mathbf{c}}}{\partial \mathbf{t}} = -\mathbf{V}\frac{\partial \bar{\mathbf{c}}}{\partial \mathbf{x}}, \qquad \mathbf{x} \in [\mathbf{a}, \mathbf{b}], \qquad \mathbf{t} \in [0, \mathbf{T}], \qquad \mathbf{c}(\mathbf{x}, 0) = \mathbf{f}(\mathbf{x}).$$

If the spatial interval, the initial value conditions and function $\mathbf{V}$ are chosen to be

$$\textbf{(5.2)} \qquad [\mathbf{a}, \mathbf{b}] = [0, 2\pi], \qquad \mathbf{f}(\mathbf{x}) = \mathbf{sin}(\mathbf{x}), \qquad \mathbf{V(x)} = \frac{6}{(2\pi)^2}\mathbf{x}(2\pi - \mathbf{x}),$$

then (5.1) becomes identical to one of the examples, which are studied in (Lewis and Derber, 1985). Its analytical solution is given by

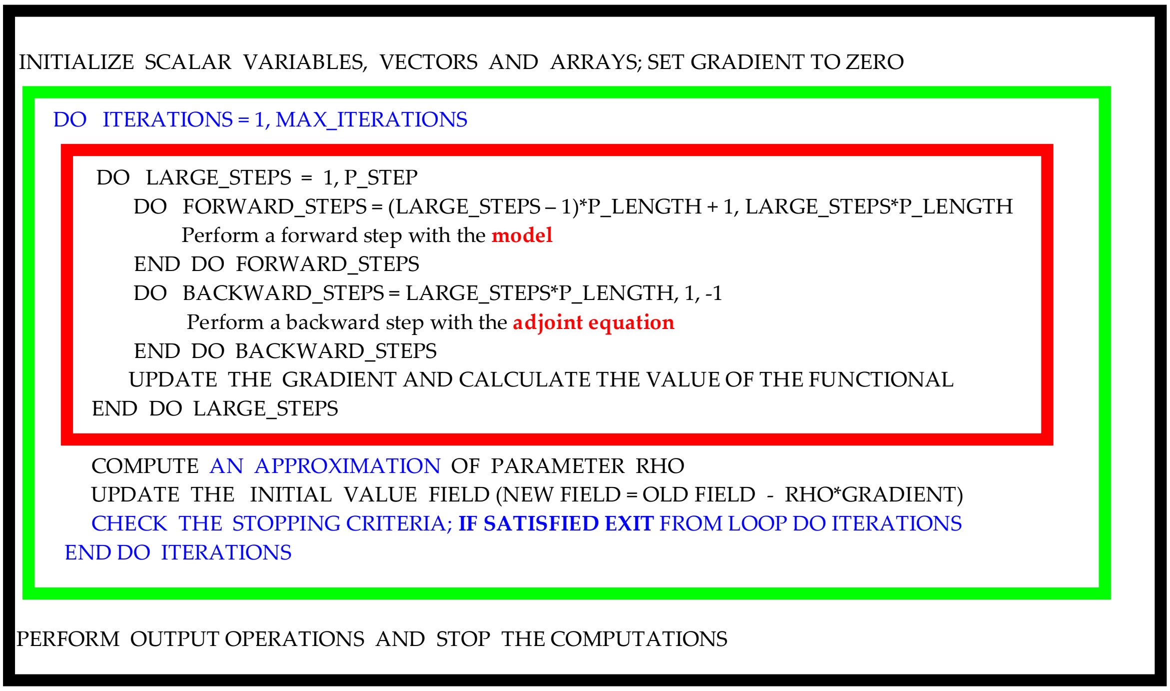

```
INITIALIZE SCALAR VARIABLES, VECTORS AND ARRAYS; SET GRADIENT TO ZERO
  DO ITERATIONS = 1, MAX_ITERATIONS
    DO LARGE_STEPS = 1, P_STEP
      DO FORWARD_STEPS = (LARGE_STEPS – 1)*P_LENGTH + 1, LARGE_STEPS*P_LENGTH
        Perform a forward step with the model
      END DO FORWARD_STEPS
      DO BACKWARD_STEPS = LARGE_STEPS*P_LENGTH, 1, -1
        Perform a backward step with the adjoint equation
      END DO BACKWARD_STEPS
      UPDATE THE GRADIENT AND CALCULATE THE VALUE OF THE FUNCTIONAL
    END DO LARGE_STEPS
    COMPUTE AN APPROXIMATION OF PARAMETER RHO
    UPDATE THE INITIAL VALUE FIELD (NEW FIELD = OLD FIELD - RHO*GRADIENT)
    CHECK THE STOPPING CRITERIA; IF SATISFIED EXIT FROM LOOP DO ITERATIONS
  END DO ITERATIONS
PERFORM OUTPUT OPERATIONS AND STOP THE COMPUTATIONS
```

Figure 4.1 An algorithm for performing data assimilation

$$(5.3) \qquad \bar{c}(x, t) = \sin\left(\frac{2\pi x}{x + (2\pi - x)\exp\left(\frac{3t}{\pi}\right)}\right).$$

Consider the grids:

(5.4) $$\mathbf{G_x} = \{\, \mathbf{x_i} \,|\, \mathbf{i} = 0, 1, \ldots, \mathbf{N_x}, \quad \mathbf{x}_0 = 0\,, \mathbf{x}_{\mathbf{N_x}} = 2\pi \ \textbf{and} \ \mathbf{x_i} - \mathbf{x_{i-1}} = \Delta\,\mathbf{x} \quad \textbf{for} \quad \mathbf{i} = 1, 2, \ldots, \mathbf{N_x} \}$$

and

(5.5) $$\mathbf{G_t} = \{\, \mathbf{t_n} \,|\, \mathbf{n} = 0, 1, \ldots, \mathbf{N_t}, \quad \mathbf{t}_0 = 0 \quad \textbf{and} \ \mathbf{t_n} - \mathbf{t_{n-1}} = \Delta\,\mathbf{t} \quad \textbf{for} \quad \mathbf{n} = 1, 2, \ldots, \mathbf{N_t} \}$$

Let $\mathbf{x_i} \in \mathbf{G_x}$ and $\mathbf{t_n} \in \mathbf{G_t}$. Different numerical methods can be used to calculate approximations

(5.6) $$\mathbf{c_{i,n}} \approx \bar{\mathbf{c}}(\mathbf{x_i}\,, \mathbf{t_n})$$

of the exact solution at point $(\mathbf{x_i}\,, \mathbf{t_n})$.

The formula given below can be obtained by using the notation $\mathbf{w_i} = (\mathbf{V(x_i)}\,\Delta\mathbf{t}) / (4\Delta\mathbf{x})$ and simple finite differences:

(5.7) $$-\mathbf{w_i}\ \mathbf{c_{i-1,n+1}} + \mathbf{c_{i,n+1}} + \mathbf{w_i}\ \mathbf{c_{i+1,n+1}} = \mathbf{w_i}\ \mathbf{c_{i-1,n}} + \mathbf{c_{i,n}} - \mathbf{w_i}\ \mathbf{c_{i+1,n}}\,.$$

Dirichlet boundary conditions can be introduced (by the use of the analytical solution) by the following formulae:

(5.8) $$\bar{\mathbf{c}}(0,\mathbf{t}) = 0\,, \qquad \bar{\mathbf{c}}(2\pi,\mathbf{t}) = 0\ .$$

By applying (5.8), formula (5.7) can be rewritten for $\mathbf{i} = 1$ as

(5.9) $$\mathbf{c_{1,n+1}} + \mathbf{w}_1\,\mathbf{c_{2,n+1}} = \mathbf{c_{1,n}} - \mathbf{w}_1\,\mathbf{c_{2,n}}$$

and for $\mathbf{i} = \mathbf{N_x} - \mathbf{1}$ as

(5.10) $$-\mathbf{w_{N_x-1}}\,\mathbf{c_{N_x-2,n+1}} + \mathbf{c_{N_x-1,n+1}} = \mathbf{w_{N_x-1}}\,\mathbf{c_{N_x-2,n}} + \mathbf{c_{N_x-1,n}}\ .$$

Denote

(5.11) $$\bar{\mathbf{c}}_\mathbf{n} = (\mathbf{c_{1,n}}, \mathbf{c_{2,n}}, \ldots, \mathbf{c_{N_x-1,n}})^\mathbf{T}.$$

By using the notation introduced by (5.11), it is possible to rewrite (5.7), (5.9) and (5.10) in a matrix form:

(5.12) $$(\mathbf{I} - \mathbf{A})\bar{\mathbf{c}}_{\mathbf{n}+1} = (\mathbf{I} + \mathbf{A})\bar{\mathbf{c}}_\mathbf{n} \qquad \Rightarrow \qquad \bar{\mathbf{c}}_{\mathbf{n}+1} = \mathbf{D}\,\bar{\mathbf{c}}_\mathbf{n}\,, \qquad \mathbf{D} = (\mathbf{I} - \mathbf{A})^{-1}(\mathbf{I} + \mathbf{A}),$$

where $\mathbf{I}$ is the identity matrix and $\mathbf{A}$ is a matrix which has non-zero elements only on the two diagonals that are adjacent to the main diagonal (and, more precisely, $-\mathbf{w_i}$ on the diagonal below the main diagonal and $\mathbf{w_i}$ on the diagonal above the main diagonal). If $\bar{\mathbf{c}}_\mathbf{n}$ has already been calculated, then (5.12) can be used to proceed with the calculation of $\bar{\mathbf{c}}_{\mathbf{n}+1}$. Thus, if an initial field, $\bar{\mathbf{c}}_\mathbf{0}$ is given, then (5.12) can be used to calculate successively, step-by-step, approximations of the exact solution.

As mentioned above, it is necessary to calculate the gradient $\mathbf{Grad}\{\mathbf{J}\}$ of the functional $\mathbf{J}\,\{\bar{\mathbf{c}}_0\}$ from (1.1) in order to find an improved initial field $\bar{\mathbf{c}}_0$. Assume as in Section 1 that observations are available at times $\{\mathbf{t_p} \,|\, \mathbf{p} = 0, 1, \ldots, \mathbf{P}\}$. Assume also that the calculations by formula (5.12) for some $\mathbf{n} + 1 = \mathbf{p}$ have been completed. It is necessary to form the "adjoint" variable

$$(5.13) \qquad \bar{\mathbf{q}}_\mathbf{p} = \overline{\mathbf{W}}_\mathbf{p} \left(\bar{\mathbf{c}}_\mathbf{p} - \bar{\mathbf{c}}_\mathbf{p}^\mathbf{obs}\right)$$

and to use it as a starting value in the integration of the "adjoint" equation backward from $\mathbf{t} = \mathbf{t}_\mathbf{p}$ to $\mathbf{t} = \mathbf{t}_0$ (let us reiterate that in this paper we have $\overline{\mathbf{W}}_\mathbf{p} = \mathbf{I}$). The backward calculations can be carried out by using the following formula, which is the discrete adjoint equation corresponding to (5.12):

$$(5.14) \qquad \bar{\mathbf{q}}_\mathbf{n} = \mathbf{D}^\mathbf{T}\, \bar{\mathbf{q}}_{\mathbf{n}+1}, \qquad \mathbf{n} = \mathbf{p}-1, \mathbf{p}-2, \ldots, 0.$$

Numerical results

Several numerical experiments were designed in the efforts to check the correctness of the implementation of the variational data assimilation modules. The following issues were tested during these experiments:

- the correct implementation of the forward module,
- the effects of using different grids,
- the application of unbiased perturbations of the initial values,
- the insertion of biased perturbations in the initial values,
- the effects of reducing the number of observations

and

- the variation of the number of analyses (or, in other words, the variation of the number of time-points at which observations are available).

Checking the module for forward integration

One of the major requirements (at least for the special case treated here) is that the module for performing forward integration should be able to improve the accuracy of the results when the discretization is refined (i.e. when the grid-points in space and time are increased). Results obtained in an experiment where the values of the parameters $\mathbf{N}_\mathbf{x}$ and $\mathbf{N}_\mathbf{t}$ are successively increased (both by a factor of ten) are given in Table 6.1. It is seen that the module is performing as it should. The global error is decreased by a factor of approximately 100 (or, in other words, the accuracy is increased by a factor approximately equal to 100). Of course, one has to pay something for the increased accuracy; the figures in the last column show that the computing time is increased by a factor approximately equal to 100 when the grids are refined.

Table 6.1 Results obtained when the module for forward integration is checked.

N_x	N_t	Global error	Rate of improving	Time	Rate of increase
11	100	$3.01*10^{0}$	-	0.00124	-
101	1000	$4.29*10^{-3}$	701.63	0.0127	102.42
1001	10000	$4.33*10^{-5}$	99.08	1.44	113.39
10001	100000	$4.34*10^{-7}$	99.77	178.89	124.23
100001	1000000	$4.28*10^{-9}$	101.40	18855.19	105.40
1000001	10000000	$2.04*10^{-9}$	2.10	562389.65	298.27

The same perturbation parameter applied on different grids

The next important issue is to check the potential ability of the data assimilation algorithm to improve the initial values of the concentrations when sufficiently many accurate observations are available. This can be done in the following way. Assume that the initial values $\bar{\mathbf{c}}(\mathbf{x},0) = \mathbf{sin}(\mathbf{x})$ are perturbed by using the formula:

$$(6.1) \qquad \mathbf{c}_{i,0} = \{1 - [0.5 - \mathbf{DRAND}(0)]\alpha\}\,\mathbf{sin}(\mathbf{x}_i),$$

where **DRAND** is a UNIX generator of random number in the interval $[0,1]$ and α is a parameter which can freely be chosen in the interval $[0,1]$. It is easily seen that (a) if $\alpha = 0$, then the initial values of the solution are not perturbed and (b) if $\alpha = 0.1$ (as in Table 6.2 below), then the perturbations of the initial values are in the interval [-5%, 5%] without any bias. In the forward mode the calculations are carried out by using the perturbed with (6.1) initial values. The values of the adjoint variable used in the backward mode are obtained as the differences between the calculated with the perturbed initial condition values and the exact values at the grid-points, i.e. the exact values play the role of the observations in (5.13). It is seen from Table 6.2 that

- the global $\mathbf{ERR_{global}}$ error in the forward solution obtained with perturbed initial values is large and cannot be improved by refining the grids,
- the error $\mathbf{ERR_0^{impr}}$ in the initial solution can be improved significantly by the data assimilation algorithm when the resolution is sufficiently good compare the corresponding values of $\mathbf{ERR_0}$ and $\mathbf{ERR_0^{impr}}$),
- The error $\mathbf{ERR_{global}^{impr}}$ of the forward mode carried out with the improved (by the data assimilation algorithm) initial values is clearly becoming smaller when the grid is refined. Moreover, the errors are of the same order of magnitude as those obtained when exact initial values are used (Table 6.1). This means that we are getting an optimal result, which cannot be further improved when the numerical method and the grid are already chosen.

Table 6.2 Results obtained in the checks of the performance of the variational data assimilation algorithm when the initial values are perturbed by random errors in the range [-5%, 5%]. $\mathbf{ERR}_0$ is the error induced by the random perturbations, $\mathbf{ERR}_{\mathbf{global}}$ is the global error when the forward integration is performed with the perturbed initial field, $\mathbf{ERR}_0^{\mathbf{impr}}$ is the error in the improved by the variational data assimilation algorithm initial field, $\mathbf{ERR}_{\mathbf{global}}^{\mathbf{impr}}$ is the global error when the forward integration is performed with the improved by the variational data assimilation algorithm initial field.

$\mathbf{N}_\mathbf{x}$	$\mathbf{N}_\mathbf{t}$	$\mathbf{ERR}_0$	$\mathbf{ERR}_{\mathbf{global}}$	$\mathbf{ERR}_0^{\mathbf{impr}}$	$\mathbf{ERR}_{\mathbf{global}}^{\mathbf{impr}}$
11	100	$4.55 * 10^{-2}$	$2.93 * 10^{-1}$	$1.94 * 10^{-1}$ (0.22)	$1.94 * 10^{-1}$
101	1000	$4.47 * 10^{-2}$	$7.53 * 10^{-2}$	$2.62 * 10^{-3}$ (17.06)	$2.62 * 10^{-3}$
1001	10000	$4.99 * 10^{-2}$	$1.10 * 10^{-1}$	$2.64 * 10^{-5}$ (1890.15)	$2.64 * 10^{-5}$
10001	100000	$4.99 * 10^{-2}$	$1.44 * 10^{-1}$	$2.64 * 10^{-7}$ (189015.15)	$2.64 * 10^{-7}$

Results obtained with different values of parameter α

The results given in Table 6.2 are obtained, as stated in the previous sub-section, by using $\alpha = 0.1$. This means that the perturbations are rather small. Therefore, it is necessary to investigate the case where the perturbations are larger. Larger perturbations can be created by increasing the value of α. Results obtained with $\mathbf{N}_\mathbf{x} = 1001$, $\mathbf{N}_\mathbf{t} = 10000$ and different values of parameter α are given in Table 6.3. It is clearly seen that the magnitude of the errors in the forward mode obtained with the improved initial values are practically not depending on the size of parameter α.

Results obtained when the perturbations created some bias

The perturbations used in Sub-section 6.2 and Sub-section 6.3 are not creating any bias. Bias could be simulated by using the following formulae:

$$\textbf{(6.2)} \qquad \mathbf{c}_{\mathbf{i},0} = \{1 + \mathbf{DRAND(0)}\, \alpha\} \mathbf{sin}(\mathbf{x}_\mathbf{i}), \quad \textbf{production of over – estimated initial values},$$

$$\textbf{(6.3)} \qquad \mathbf{c}_{\mathbf{i},0} = \{1 - \mathbf{DRAND(0)}\, \alpha\} \mathbf{sin}(\mathbf{x}_\mathbf{i}), \quad \textbf{production of under – estimated initial values}.$$

Table 6.3. Results obtained in the checks of the performance of the variational data assimilation algorithm when $\mathbf{N_x} = 1001$, $\mathbf{N_t} = 10000$ and parameter α is varied in the range $[0.1, 1.0]$ with step 0.1. $\mathbf{ERR}_0$, $\mathbf{ERR_{global}}$, $\mathbf{ERR}_0^{\mathbf{impr}}$ and $\mathbf{ERR}_{\mathbf{global}}^{\mathbf{impr}}$ are defined in Table 6.2.

α	$\mathbf{ERR}_0$	$\mathbf{ERR_{global}}$	$\mathbf{ERR}_0^{\mathbf{impr}}$	$\mathbf{ERR}_{\mathbf{global}}^{\mathbf{impr}}$
0.1	$4.99*10^{-2}$	$1.10*10^{-1}$	$2.64*10^{-5}$	$2.64*10^{-5}$
0.2	$9.94*10^{-2}$	$2.31*10^{-1}$	$2.64*10^{-5}$	$2.64*10^{-5}$
0.3	$1.47*10^{-1}$	$3.28*10^{-1}$	$2.64*10^{-5}$	$2.64*10^{-5}$
0.4	$2.00*10^{-1}$	$4.14*10^{-1}$	$2.64*10^{-5}$	$2.64*10^{-5}$
0.5	$2.46*10^{-1}$	$5.83*10^{-1}$	$2.64*10^{-5}$	$2.64*10^{-5}$
0.6	$2.99*10^{-1}$	$6.79*10^{-1}$	$2.64*10^{-5}$	$2.64*10^{-5}$
0.7	$3.43*10^{-1}$	$9.47*10^{-1}$	$2.64*10^{-5}$	$2.64*10^{-5}$
0.8	$3.96*10^{-1}$	$8.55*10^{-1}$	$2.64*10^{-5}$	$2.64*10^{-5}$
0.9	$4.49*10^{-1}$	$1.07*10^{-0}$	$2.64*10^{-5}$	$2.64*10^{-5}$
1.0	$4.90*10^{-1}$	$1.02*10^{-0}$	$2.64*10^{-5}$	$2.64*10^{-5}$

Results obtained by producing perturbations in the initial value by using (6.2) are given in Table 6.4. The error in the improved initial field as well as the global error in the forward mode do not depend on the value of α (as a matter of fact, the rounded to the third significant decimal numbers are the same for all values of α). Results obtained by using (6.3) instead of (6.2) are quite similar to the results shown in Table 6.4.

Results obtained with reduced number of observations

The results given in the previous sections were obtained by using "observations" (exact values of the solution) at all spatial grid-points $\mathbf{x_i}$, $\mathbf{i = 0,1,\ldots N_x}$ at the time-points $\mathbf{p} = 1, 2, \ldots, \mathbf{P}$ (i.e. at every point where backward calculations are initiated). In the practical situations **the number of observations will be limited.** Therefore, it is necessary to investigate the accuracy of the results when the number of observations is reduced. Two different cases should be investigated:

- the adjoint variable is set to zero if there is no observation at spatial grid-points under consideration.

and

- an attempt to get "observations" at all spatial grid-points (by interpolation) is made.

Table 6.4 Results obtained in the checks of the performance of the variational data assimilation algorithm when $\mathbf{N_x} = 1001$, $\mathbf{N_t} = 10000$ and parameter α is varied in the range $[0.1, 1.0]$ with step 0.1. $\mathbf{ERR}_0$, $\mathbf{ERR}_{\mathbf{global}}$, $\mathbf{ERR}_0^{\mathbf{impr}}$ and $\mathbf{ERR}_{\mathbf{global}}^{\mathbf{impr}}$ are defined in Table 6.2.

α	$\mathbf{ERR}_0$	$\mathbf{ERR}_{\mathbf{global}}$	$\mathbf{ERR}_0^{\mathbf{impr}}$	$\mathbf{ERR}_{\mathbf{global}}^{\mathbf{impr}}$
0.1	$1.00*10^{-1}$	$1.77*10^{-1}$	$2.64*10^{-5}$	$2.64*10^{-5}$
0.2	$1.99*10^{-1}$	$3.63*10^{-1}$	$2.64*10^{-5}$	$2.64*10^{-5}$
0.3	$2.96*10^{-1}$	$5.37*10^{-1}$	$2.64*10^{-5}$	$2.64*10^{-5}$
0.4	$4.00*10^{-1}$	$7.08*10^{-1}$	$2.64*10^{-5}$	$2.64*10^{-5}$
0.5	$4.95*10^{-1}$	$8.97*10^{-1}$	$2.64*10^{-5}$	$2.64*10^{-5}$
0.6	$5.98*10^{-1}$	$1.00*10^{0}$	$2.64*10^{-5}$	$2.64*10^{-5}$
0.7	$6.98*10^{-1}$	$1.33*10^{0}$	$2.64*10^{-5}$	$2.64*10^{-5}$
0.8	$7.89*10^{-1}$	$1.40*10^{0}$	$2.64*10^{-5}$	$2.64*10^{-5}$
0.9	$8.95*10^{-1}$	$1.65*10^{0}$	$2.64*10^{-5}$	$2.64*10^{-5}$
1.0	$9.87*10^{-1}$	$1.88*10^{0}$	$2.64*10^{-5}$	$2.64*10^{-5}$

The adjoint variable is set to zero when no observation is available

It is easy to apply this possibility. Some results are given in Table 6.5. It is assumed that "observations" are available at every second spatial grid-point. This is a very restrictive assumption when refined grids are used. Nevertheless, it is seen that the results are much less accurate than those presented in Table 6.2 (where "observations" in all grid-points were used in the calculations). The results indicate that if the spatial grid is fine (100 or more grid-points), then the results can be improved by using data assimilation by a factor approximately equal to 2. The results shown in Table 6.6 indicate that this statement seems to be true also when the magnitude of the perturbations is increased by varying parameter α. Comparing the results in Table 6.6 with the corresponding results in Table 6.3, it is seen that (a) the results in the third and the fourth columns are identical in the two tables and (b) while the errors given in the fifth and the sixth columns in Table 6.3 do not depend on parameter α, the corresponding errors in Table 6.6 grow when the value of α is increased.

Using interpolation to obtain "observations" at all spatial points

The results in Sub-section 6.5.1 show that it is not advisable to set the adjoint variable to zero when no observation is available at the spatial grid-point under consideration. It will be shown now that it might be more profitable, in some situations at least, to try to calculate approximations to the missing observations by using some interpolation rules. For our purposes, the application of simple rules for linear interpolation is quite sufficient and such rules will be used in this section. However, some more advanced interpolation rules (as, for example, cubic splines) may be more successful in some other situations.

Table 6.5 Results obtained in the checks of the performance of the variational data assimilation algorithm when the initial values are perturbed by random errors in the range [-5%, 5%] and when "observations" are available in every second spatial grid-point. The adjoint variable is set to zero at the points where "observations" are not available. $\mathbf{ERR}_0$, $\mathbf{ERR}_{\mathbf{global}}$, $\mathbf{ERR}_0^{\mathbf{impr}}$ and $\mathbf{ERR}_{\mathbf{global}}^{\mathbf{impr}}$ are defined in Table 6.2.

$\mathbf{N}_{\mathbf{x}}$	$\mathbf{N}_{\mathbf{t}}$	$\mathbf{ERR}_0$	$\mathbf{ERR}_{\mathbf{global}}$	$\mathbf{ERR}_0^{\mathbf{impr}}$	$\mathbf{ERR}_{\mathbf{global}}^{\mathbf{impr}}$
11	100	$4.55*10^{-2}$	$2.93*10^{-1}$	$1.01*10^{-1}$ (0.45)	$2.28*10^{-1}$
101	1000	$4.47*10^{-2}$	$7.53*10^{-2}$	$2.47*10^{-2}$ (1.81)	$3.97*10^{-2}$
1001	10000	$4.99*10^{-2}$	$1.10*10^{-1}$	$2.54*10^{-2}$ (1.96)	$5.56*10^{-2}$

Table 6.6 Results obtained in the checks of the performance of the variational data assimilation algorithm when $\mathbf{N}_{\mathbf{x}} = 1001$, $\mathbf{N}_{\mathbf{t}} = 10000$, parameter α is varied in the range $[0.1, 1.0]$ with step 0.1 and when "observations" are available at every second spatial grid-point. $\mathbf{ERR}_0$, $\mathbf{ERR}_{\mathbf{global}}$, $\mathbf{ERR}_0^{\mathbf{impr}}$ and $\mathbf{ERR}_{\mathbf{global}}^{\mathbf{impr}}$ are defined in Table 6.2.

α	$\mathbf{ERR}_0$	$\mathbf{ERR}_{\mathbf{global}}$	$\mathbf{ERR}_0^{\mathbf{impr}}$	$\mathbf{ERR}_{\mathbf{global}}^{\mathbf{impr}}$
0.1	$4.99*10^{-2}$	$1.10*10^{-1}$	$2.54*10^{-2}$	$5.56*10^{-2}$
0.2	$9.94*10^{-2}$	$2.31*10^{-1}$	$5.00*10^{-2}$	$1.16*10^{-1}$
0.3	$1.47*10^{-1}$	$3.28*10^{-1}$	$7.38*10^{-2}$	$1.62*10^{-1}$
0.4	$2.00*10^{-1}$	$4.14*10^{-1}$	$1.00*10^{-1}$	$2.07*10^{-1}$
0.5	$2.46*10^{-1}$	$5.83*10^{-1}$	$1.28*10^{-1}$	$2.94*10^{-1}$
0.6	$2.99*10^{-1}$	$6.79*10^{-1}$	$1.52*10^{-1}$	$3.43*10^{-1}$
0.7	$3.43*10^{-1}$	$9.47*10^{-1}$	$1.72*10^{-1}$	$4.72*10^{-1}$
0.8	$3.96*10^{-1}$	$8.55*10^{-1}$	$2.00*10^{-1}$	$4.26*10^{-1}$
0.9	$4.49*10^{-1}$	$1.07*10^{-0}$	$2.31*10^{-1}$	$5.37*10^{-1}$
1.0	$4.90*10^{-1}$	$1.02*10^{-0}$	$2.46*10^{-1}$	$5.15*10^{-1}$

The results in Table 6.7 are obtained using the same parameters as those used to calculate the results in Table 6.5 with the only exception that linear interpolation is used to obtain "approximations of the observations" in the spatial grid-points at which "observations" are not available.

Some results for $\mathbf{ERR}_{\mathbf{global}}^{\mathbf{impr}}$ obtained when both the number of "available observations" and parameter α are varied are given in Table 6.8. It is seen that the results become poorer when the number of "observations" is decreased. However, the accuracy of the results is very insensitive to variations of α (i.e. the variations of the magnitude of the perturbations inserted in the initial values).

Table 6.7 Results obtained in the checks of the performance of the variational data assimilation algorithm when the initial values are perturbed by random errors in the range [-5%, 5%] and when "observations" are available in every second spatial grid-point. Linear interpolation is used to obtaine approximations of the observations at the points where "observations" are not available. $\mathbf{ERR}_0$, $\mathbf{ERR}_{\mathbf{global}}$, $\mathbf{ERR}_0^{\mathbf{impr}}$ and $\mathbf{ERR}_{\mathbf{global}}^{\mathbf{impr}}$ are defined in Table 6.2.

$\mathbf{N}_{\mathbf{x}}$	$\mathbf{N}_{\mathbf{t}}$	$\mathbf{ERR}_0$	$\mathbf{ERR}_{\mathbf{global}}$	$\mathbf{ERR}_0^{\mathbf{impr}}$	$\mathbf{ERR}_{\mathbf{global}}^{\mathbf{impr}}$
11	100	$4.55 * 10^{-2}$	$2.93 * 10^{-1}$	$1.01 * 10^{-1}$ (0.45)	$2.28 * 10^{-1}$
101	1000	$4.47 * 10^{-2}$	$7.53 * 10^{-2}$	$2.61 * 10^{-3}$ (17.12)	$3.17 * 10^{-3}$
1001	10000	$4.99 * 10^{-2}$	$1.10 * 10^{-1}$	$2.64 * 10^{-5}$ (1890.15)	$3.21 * 10^{-5}$
10001	100000	$4.99 * 10^{-2}$	$1.44 * 10^{-1}$	$2.64 * 10^{-7}$ (168421.57)	$2.64 * 10^{-7}$

Table 6.8 Values of $\mathbf{ERR}_{\mathbf{global}}^{\mathbf{impr}}$ (see the captions in Table 6.2) obtained by using the variational data assimilation algorithm with $\mathbf{N}_{\mathbf{x}} = 1001$, $\mathbf{N}_{\mathbf{t}} = 10000$ when parameter α is varied in the range $[0.1, 1.0]$ with step 0.1 and when the number of "observations" **N_OBS** is varied.

α	**N_OBS=1000**	**N_OBS=500**	**N_OBS=125**	**N_OBS=20**	**N_OBS=5**
0.1	$2.64 * 10^{-5}$	$3.21 * 10^{-5}$	$3.39 * 10^{-4}$	$1.34 * 10^{-2}$	$2.05 * 10^{-1}$
0.2	$2.64 * 10^{-5}$	$3.21 * 10^{-5}$	$3.39 * 10^{-4}$	$1.34 * 10^{-2}$	$2.05 * 10^{-1}$
0.3	$2.64 * 10^{-5}$	$3.21 * 10^{-5}$	$3.39 * 10^{-4}$	$1.34 * 10^{-2}$	$2.05 * 10^{-1}$
0.4	$2.64 * 10^{-5}$	$3.21 * 10^{-5}$	$3.39 * 10^{-4}$	$1.34 * 10^{-2}$	$2.05 * 10^{-1}$
0.5	$2.64 * 10^{-5}$	$3.21 * 10^{-5}$	$3.39 * 10^{-4}$	$1.34 * 10^{-2}$	$2.05 * 10^{-1}$
0.6	$2.64 * 10^{-5}$	$3.21 * 10^{-5}$	$3.39 * 10^{-4}$	$1.34 * 10^{-2}$	$2.05 * 10^{-1}$
0.7	$2.64 * 10^{-5}$	$3.21 * 10^{-5}$	$3.39 * 10^{-4}$	$1.34 * 10^{-2}$	$2.05 * 10^{-1}$
0.8	$2.64 * 10^{-5}$	$3.21 * 10^{-5}$	$3.39 * 10^{-4}$	$1.34 * 10^{-2}$	$2.05 * 10^{-1}$
0.9	$2.64 * 10^{-5}$	$3.21 * 10^{-5}$	$3.39 * 10^{-4}$	$1.34 * 10^{-2}$	$2.05 * 10^{-1}$
1.0	$2.64 * 10^{-5}$	$3.21 * 10^{-5}$	$3.39 * 10^{-4}$	$1.34 * 10^{-2}$	$2.05 * 10^{-1}$

Varying the number of analyses (the numbers of time-points at which observations are available

In all experiments in the previous sub-sections the number of time-steps per analysis was fixed (i.e. after performing 10 time-steps the adjoint variable was formed and a new analysis was calculated by performing backward integration to the initial time-point $\mathbf{t}_0$). This might be very expensive (in terms of computing time). On the other hand (and this may be much more important in practice), observations are often available at a few time-points. Therefore, it is worthwhile to investigate the behaviour of the variational data assimilation when the number of analyses is varied. It is desirable to be able to use as many as possible time-steps per analysis (or, in other words, to reduce the number of analyses as much as possible). Some results, which are obtained by using $\mathbf{N_x} = 1001$, $\mathbf{N_t} = 10000$, $\alpha = 0.1$ and different numbers of analyses ($\mathbf{P\_STEP}$), are given in Table 6.9.

Table 6.9 Values of $\mathbf{ERR^{impr}_{global}}$ (see the captions in Table 6.2) obtained by using the variational data assimilation algorithm with $\mathbf{N_x} = 1001$, $\mathbf{N_t} = 10000$, $\alpha = 0.1$, five different values of **N_OBS** and different numbers of analyses $\mathbf{P\_STEP}$.

P_STEP	**N_OBS=1000**	**N_OBS=500**	**N_OBS=125**	**N_OBS=20**	**N_OBS=5**
1000	$2.64*10^{-5}$	$3.21*10^{-5}$	$3.39*10^{-4}$	$1.34*10^{-2}$	$2.05*10^{-1}$
100	$2.66*10^{-5}$	$3.20*10^{-5}$	$3.48*10^{-4}$	$1.34*10^{-2}$	$2.06*10^{-1}$
10	$2.90*10^{-5}$	$3.04*10^{-5}$	$3.91*10^{-4}$	$1.50*10^{-2}$	$2.15*10^{-1}$
1	$5.27*10^{-5}$	$5.27*10^{-5}$	$5.87*10^{-4}$	$2.75*10^{-2}$	$3.55*10^{-1}$

Conclusions

The test-example defined by (5.1)-(5.2) is very simple. Therefore, it is only possible to make conclusions about the cases in which (a) it is quite certain that the data assimilation algorithm is not performing well and (b) there is some hope that the data assimilation algorithm will perform well, but more experiments with test examples that are closer to real cases are necessary.

When will the data assimilation algorithm not work?

The experiments in Section 6 indicate that there are at least two cases, in which the data assimilation algorithm will not lead to a substantial improvement of the results. These cases are:

- the discretization is crude

and

- the number of observations is very small.

This implies that two requirements should be imposed when data assimilation algorithms are to be used: (a) the discretizations should be sufficiently accurate and (b) the number of available observations should be sufficiently large. We are not discussing here the reliability of the observations, i.e. it was assumed that the observations are reliable. In the real case the reliability of the observations is an important topic, which should be taken into account when data assimilation algorithms are to be used.

When will the data assimilation algorithm likely work well?

It is clear from the experiments in Section 6 that one should expect the data assimilation algorithm to work satisfactorily well in the several cases when the following conditions are satisfied:

- If there are sufficiently many observations, then the results will be substantially improved even if the initial values are quite crude (see Table 6.3). This is also true when there is some bias of the errors in the initial values (see Table 6.4).

- Assume that the number of observations is less than the number of spatial grid-points (which will be always the case in real situations). In this case, it might be useful to calculate (by applying some interpolation rules) "approximate observations" in the grid-points where there are not observations (compare the results in Table 6.5 and Table 6.6 with the results in Table 6.7 and Table 6.8).
- The results seem to be rather insensitive to the number of analyses that are actually used (see Table 6.9). It is important to check further whether this nice property holds in more complicated cases, because the data assimilation procedure will become extremely expensive if many analyses are needed.
- It is important to improve the performance of the data assimilation algorithm with regard to computing time (it is seen that there are problems with the computing time even for the simple one-dimensional example treated in this paper). Parallel algorithms, similar to those used in (Alexandrov et al., 2004) and (Dimov et al., 2004b) might lead to a considerable improvement of the performance.

How to continue this research?
It is clear that, before applying data assimilation algorithms in studies involving large-scale air pollution models, it is necessary to eliminate the cases in which these algorithms will not work well. In this study it was shown, by using a simple example that there are at least two such cases (see Sub-section 7.1). In the further investigations the following situations must carefully be studied:

- Two and three-dimensional test examples should also be studied.
- Chemical reaction schemes are treated.
- The impact of operational splitting, which is practically unavoidable in real applications; see, for example, (Dimov et al., 2004a), on the data assimilation algorithms should be investigated.

Appendix 1: Reducing the computational work in calculating $\mathbf{Grad}\{\mathbf{J}\}$

Let $\mathbf{W}(\mathbf{t_p})$, $\mathbf{p}=0,1,\ldots,\mathbf{P}$, be the identity matrix. Assuming that the ordinary inner product is used in (1.1), the scalar to be minimized in the variational data assimilation procedure is

$$\textbf{(A.1)}\qquad \mathbf{J}\{\bar{\mathbf{c}}_\mathbf{0}\} = \frac{\mathbf{1}}{\mathbf{2}} \sum_{\mathbf{p}=0}^{\mathbf{P}} \left(\bar{\mathbf{c}}_\mathbf{p} - \bar{\mathbf{c}}_\mathbf{p}^\mathbf{obs}\right)^2 .$$

We can consider $\mathbf{J}$ as a function of the concentrations $\bar{\mathbf{c}}_\mathbf{p}$ at $\mathbf{t_0},\mathbf{t_1},\ldots,\mathbf{t_P}$:

$$\textbf{(A.2)}\qquad \mathbf{J} = \mathbf{J}(\bar{\mathbf{c}}_\mathbf{0},\bar{\mathbf{c}}_\mathbf{1},\ldots,\bar{\mathbf{c}}_\mathbf{P}), \qquad \mathbf{J}:\Re^{\mathbf{s(P+1)}} \to \Re .$$

Denote the solution operator used at the p-th time-step by $\mathbf{M_p}$. Clearly, $\mathbf{M_p}:\Re^{\mathbf{s}} \to \Re^{\mathbf{s}}$. Moreover, since $\mathbf{M}_0 = \mathbf{I}$, we have:

$$\textbf{(A.3)}\qquad \mathbf{J} = \mathbf{J}(\bar{\mathbf{c}}_\mathbf{0},\bar{\mathbf{c}}_\mathbf{1},\ldots,\bar{\mathbf{c}}_\mathbf{P}) = \mathbf{J}(\bar{\mathbf{c}}_0, \mathbf{M}_1(\bar{\mathbf{c}}_\mathbf{0}),\ \mathbf{M}_2\mathbf{M}_1(\bar{\mathbf{c}}_\mathbf{0}),\ \ldots,\ \mathbf{M_P}\cdots\mathbf{M}_2\mathbf{M}_1(\bar{\mathbf{c}}_\mathbf{0})).$$

Let $\mathbf{M}:\bar{\mathbf{c}}_\mathbf{0} \mapsto (\bar{\mathbf{c}}_\mathbf{0},\bar{\mathbf{c}}_\mathbf{1},\ldots,\bar{\mathbf{c}}_\mathbf{P})^\mathbf{T}$. Obviously,

$$\mathbf{M} = (\mathbf{I},\ \mathbf{M}_1,\ \mathbf{M}_2\mathbf{M}_1,\ \ldots,\ \mathbf{M}_P \cdots \mathbf{M}_2\mathbf{M}_1)^{\mathbf{T}}, \qquad \mathbf{M}: \Re^s \rightarrow \Re^{s(P+1)}. \tag{A.4}$$

The minimization of $\mathbf{J}$ requires the evaluation of the gradient of the composition $\mathbf{J} \circ \mathbf{M}$ at $\bar{\mathbf{c}}_0$, because we have:

$$\mathbf{Grad}\{\mathbf{J}(\bar{\mathbf{c}}_0)\} = (\mathbf{J} \circ \mathbf{M})'(\bar{\mathbf{c}}_0). \tag{A.5}$$

By using the chain rule of differentiating on the right-hand side, we obtain that

$$\mathbf{Grad}\{\mathbf{J}(\bar{\mathbf{c}}_0)\} = (\mathbf{M}'(\bar{\mathbf{c}}_0))^{\mathbf{T}}(\mathbf{J}'(\mathbf{M}(\bar{\mathbf{c}}_0))). \tag{A.6}$$

Here $\mathbf{M}'(\bar{\mathbf{c}}_0)$ stands for the derivative of $\mathbf{M}$ at $\bar{\mathbf{c}}_0$ (a linear operator of type $\Re^s \rightarrow \Re^{s(P+1)}$) and the superscript T refers to the adjoint (i.e., the transpose of the corresponding matrix). This means that, to compute the above gradient, $(\mathbf{M}'(\bar{\mathbf{c}}_0))^{\mathbf{T}}$ should be applied to the vector

$$\mathbf{J}'(\mathbf{M}(\bar{\mathbf{c}}_0)) = \mathbf{J}'(\bar{\mathbf{c}}_0, \bar{\mathbf{c}}_1, \ldots, \bar{\mathbf{c}}_P) \in \Re^{s(P+1)}. \tag{A.7}$$

As stated above, $\mathbf{M}'(\bar{\mathbf{c}}_0): \Re^s \rightarrow \Re^{s(P+1)}$. Therefore, $(\mathbf{M}'(\bar{\mathbf{c}}_0))^{\mathbf{T}}: \Re^{s(P+1)} \rightarrow \Re^s$. Consider $\bar{\mathbf{q}} = (\bar{\mathbf{q}}_0, \bar{\mathbf{q}}_1\ \ldots, \bar{\mathbf{q}}_P)$, where $\bar{\mathbf{q}}_p = \bar{\mathbf{c}}_p - \bar{\mathbf{c}}_p^{\mathbf{obs}}$, $\mathbf{p} = 0, 1, \ldots, \mathbf{P}$. It is readily seen that $\bar{\mathbf{q}} \in \Re^{s(P+1)}$ and the following equality holds:

$$(\mathbf{M}'(\bar{\mathbf{c}}_0))^{\mathbf{T}}(\bar{\mathbf{q}}) = (\bar{\mathbf{q}}_0,\ \mathbf{M}_1^{\mathbf{T}}(\bar{\mathbf{q}}_1), \mathbf{M}_1^{\mathbf{T}}\mathbf{M}_2^{\mathbf{T}}(\bar{\mathbf{q}}_2), \ldots, \mathbf{M}_1^{\mathbf{T}}\mathbf{M}_2^{\mathbf{T}} \cdots \mathbf{M}_P^{\mathbf{T}}(\bar{\mathbf{q}}_P)) \tag{A.8}$$

with $\mathbf{M}_p^{\mathbf{T}}: \Re^{\mathbf{s}} \rightarrow \Re^{\mathbf{s}}$, p = 1, 2, …, P. Here we used the rule about the transpose of a product of matrices.

Clearly,

$$\mathbf{J}'(\bar{\mathbf{c}}_0, \bar{\mathbf{c}}_1, \ldots, \bar{\mathbf{c}}_P) = (\bar{\mathbf{q}}_0, \bar{\mathbf{q}}_1, \ldots, \bar{\mathbf{q}}_P) = (\bar{\mathbf{c}}_0 - \bar{\mathbf{c}}_0^{\mathbf{obs}}, \bar{\mathbf{c}}_1 - \bar{\mathbf{c}}_1^{\mathbf{obs}}, \ldots, \bar{\mathbf{c}}_P - \bar{\mathbf{c}}_P^{\mathbf{obs}}) \in \Re^{s(P+1)}. \tag{A.9}$$

Now the desired gradient can be obtained by using (A.6), (A.8) and (A.9):

$$\mathbf{Grad}\{\mathbf{J}(\bar{\mathbf{c}}_0)\} = (\mathbf{M}'(\bar{\mathbf{c}}_0))^{\mathbf{T}}(\mathbf{J}'(\mathbf{c}_0, \bar{\mathbf{c}}_1, \ldots, \bar{\mathbf{c}}_P)) \tag{A.10}$$

$$= (\bar{\mathbf{c}}_0 - \bar{\mathbf{c}}_0^{\mathbf{obs}}) + \mathbf{M}_1^{\mathbf{T}}(\bar{\mathbf{c}}_1 - \bar{\mathbf{c}}_1^{\mathbf{obs}}) + \mathbf{M}_1^{\mathbf{T}}\mathbf{M}_2^{\mathbf{T}}(\bar{\mathbf{c}}_2 - \bar{\mathbf{c}}_2^{\mathbf{obs}}) + \ldots + \mathbf{M}_1^{\mathbf{T}} \cdots \mathbf{M}_P^{\mathbf{T}}(\bar{\mathbf{c}}_P - \bar{\mathbf{c}}_P^{\mathbf{obs}}).$$

The right-hand side of (A.10) can be rewritten as

$$(\bar{\mathbf{c}}_0 - \bar{\mathbf{c}}_0^{\mathbf{obs}}) + \mathbf{M}_1^{\mathbf{T}}(\bar{\mathbf{c}}_1 - \bar{\mathbf{c}}_1^{\mathbf{obs}} + \mathbf{M}_2^{\mathbf{T}}(\bar{\mathbf{c}}_2 - \bar{\mathbf{c}}_2^{\mathbf{obs}} + \mathbf{M}_3^{\mathbf{T}}(\bar{\mathbf{c}}_3 - \bar{\mathbf{c}}_3^{\mathbf{obs}} + \ \ldots\ ))), \tag{A.11}$$

which allows us the reduce considerably the computational work. Namely, instead of computing the terms one by one on the right-hand side of (A.10), we should, according to (A.11), use the following algorithm:

evaluate the difference $\bar{\mathbf{c}}_P - \bar{\mathbf{c}}_P^{\mathbf{obs}}$,

apply $\mathbf{M}_P^{\mathbf{T}}$ to this difference, evaluate the difference $\mathbf{\bar{c}_{P\text{-}1}} - \mathbf{\bar{c}^{obs}_{P\text{-}1}}$, and add it to the result of Step 2,

apply $\mathbf{M^{T}_{P\text{-}1}}$ to the result,

perform successively steps 1-4 for $\mathbf{p} = \mathbf{P} - 1, \mathbf{P} - 2, \ldots, 1, 0$.

This is equivalent to applying only once backward integration of the adjoint model, which means that the computing time can be reduced when the above algorithm is used. On the other hand, however, since the adjoint variables are used in reverse order, it is necessary to store all of them during the forward mode, which leads to an increase of the storage needed.

References

S. Akella and I. M. Navon: *"Documentation of the TLM and adjoint models of the Lin-Rood spherical shallow water finite volume model"*. Report. CSIT and Department of Mathematics, Florida State University, Tallahassee, Florida, USA, 2004.

A. K. Alekseev and I. M. Navon: *"A posteori pointwise error estimation for compressible fluid flows using addjoint parameters and Lagrange remainder"*. International Journal for Numerical Methods in Fluids, 47 (2005), 45-74.

V. N. Alexandrov, W. Owczarz, P. G. Thomsen and Z. Zlatev: *"Parallel runs of a large air pollution model on a grid of Sun computers"*. Mathematics and Computers in Simulation, 65 (2004), 557-577.

D. N. Daescu and I. M. Navon: *"Adaptive observations in the context of 4D-Var data assimilation"*. Meteorology and Atmospheric Physics, 85 (2004), 205-226.

D. N. Daescu, A. Sandu and G. R. Carmichael: *"Direct and adjoint sensitivity analysis of chemical kinetic systems with KPP: II – numeical validation and applications"*. Atmospheric Environment, 37 (2003), 5097-5114.

F.-X. Le Dimet, I. M. Navon and D. N. Daescu: *"Second order information in data assimilation"*. Monthly Weather Review, 130 (2002), 629-648.

I. Dimov, I. Faragó, Á. Havasi and Z. Zlatev: *"Operator splitting and commutativity analysis in the Danish Eulerian Model"*, Mathematics and Computers in Simulation, 67 (2004a), pp. 217-233.

I. Dimov, K. Georgiev, Tz. Ostromsky and Z. Zlatev: *"Computational challenges in the numerical treatment of large air pollution models"*, Ecological Modelling, 179 (2004b), pp. 187-203.

H. Elbern and H. Schmidt: *"A four-dimensional variational chemistry data assimilation scheme for Eulerian chemistry transport modeling"*. Journal of Geophysical Research, 104 (1999), 18583-18598.

H. Elbern and H. Schmidt: *"Ozone episode analysis by four-dimensional variational chemistry data assimilation"*. Journal of Geophysical Research, 106 (2001), 3569-3590.

H. Elbern, H. Schmidt and A. Ebel: *"Variational data assimilation for tropospheric chemistry modeling"*. Journal of Geophysical Research, 102 (1997), 15967-15985.

H. Elbern, H. Schmidt and A. Ebel: *"Implementation of a parallel 4D-Var chemistry data assimilation scheme"*. Environmental Management and Health, 10 (1999), 236-244.

H. Elbern, H. Schmidt, O. Talagrand and A. Ebel: *"4D-variational data assimilation with an adjoint air quality model for emission analysis"*. Environmental Modeling Software, 15 (2000), 539-548.

W. H. Hundsdorfer and J. G. Verwer: *"Numerical solution of time-dependent advection-diffusion-reaction equations"*. Springer, Berlin, 2003.

J. M. Lewis and J. C. Derber: *"The use of adjoint equations to solve a variational adjustment problem with advective constraints"*. Tellus, 37A (1985), 309-322.

Z. Li and I. M. Navon: *"Optimality of 4D-Var and its relationship with the Kalman filter and the Kalman smoother"*. Quarterly Journal of the Royal Meteorological Society, 127B (2001), 661-684.

G. I. Marchuk: *"Adjoint equations and analysis of complex systems"*. Kluwer Academic Publishers, Dordrecht, 1995.

G. I. Marchuk, P. V. Agoshkov and I. V. Shutyaev: *"Adjoint equations and perturbation algorithms in nonlinear problems"*. CRC Press, New York, 1996.

P. Morel, G. Lefevre and G. Rabreau: *"On initialization and non-synoptic data assimilation"*. Tellus, 23 (1971), 197-206.

NAG Numerical Library: *"E04 – minimizing and maximizing a function"*. http://www.nag.co.uk, 2004.

A. Sandu, D. N. Daescu and G. R. Carmichael: *"Direct and adjoint sensitivity analysis of chemical kinetic systems with KPP: I – theory and software tools"*. Atmospheric Environment, 37 (2003), 5083-5096.

A. Sandu, D. N. Daescu, G. R. Carmichael and T. Chai: *"Adjoint sensitivity analysis of regional air quality models"*. Journal of Computational Physics, 2004; to appear.

O. Talagrand and Ph. Courtier: *"Variational assimilation of meteorological observations with the adjoint vorticity equation. I: Theory"*. Quarterly Journal of the Royal Meteorological Society, 113 (1987), 1311-1328.

K. Y. Wang, D. J. Lary, D. E. Shallcross, S. M. Hall and J. A. Pyle: *"A review on the use of the adjoint method in four-dimensional atmospheric-chemistry data assimilation"*. Quarterly Journal of the Royal Meteorological Society, 127B (2001), 2181-2204.

Z. Zlatev: *"Computer Treatment of large air pollution models"*. Kluwer Academic Publishers, Dordrecht, 1995.

Assessing the reliability of aerosol simulations with the EURAD model system

M. Memmesheimer[1], E. Friese[1], H. J. Jakobs[1], S. Wurzler[2], H. Feldmann[1],
C. Kessler[1] and A. Ebel[1]

[1]Rhenish Institute for Environmental Research at the University of Cologne (RIU), Aachener Str. 201 – 209, 50931 Cologne, Germany.
[2]Landesumweltamt Nordrhein-Westfalen, Wallneyer Str. 6 , 45023 Essen, Germany.

Introduction

The EURAD model system has been applied to episodic and long-term studies of atmospheric aerosols in Europe and smaller domains using the method of sequential nesting. Much of the simulations have been focussing on the conditions in North Rhine-Westphalia (NRW). Monitoring data for PM10 and/or TSP from this domain has primarily been used to check the applicability and assess the reliability of the simulated aerosol parameters. Considering the uncertainties, which still exist with respect to aerosol emission and formation, the results look promising in general, so that the model complemented by the aerosol module MADE2 can well be used as a supporting tool for the analysis of spatial and temporal variability of atmospheric particulate matter.

At the same time comparisons between observations and calculations provide valuable hints to weaknesses in our understanding and mathematical representation of the complex atmospheric aerosol system. This holds for deviations of spatial distributions as well as of temporal changes. It is an ongoing task of model development to identify such weaknesses, improve the algorithms used in the model and thus increase its reliability. A major problem of comparisons of modelled aerosol parameters with observations is the availability of more sophisticated measurements beyond just aerosol mass, e. g. observations of composition or detailed size distributions. Therefore, peculiar strategies for reliability tests have to be developed building among others on sensitivity and plausibility checks and/or model comparisons. The latter way was chosen in studies by Hass et al. (2003) and van Loon et al. (2004). This study is more concerned with the exploitation of sensitivity arguments in connection with statistical evaluation.

Availability of atmospheric aerosol data for model evaluation

Table 1 is a tentative estimate which aerosol data is available for comprehensive ABL air quality model evaluation and has been used for this purpose. Evidently, only PM and TSP monitoring station networks appear to generate enough data allowing reliable testing of simulated horizontal distributions of these parameters. As regards spatial coverage in Europe, some regional networks (like the one in North Rhine-Westphalia used in this study, Fig. 1) are available. Nevertheless, large gaps still exist causing serious limitations of evaluation studies. Apparently, vertical profile measurements, e. g. from lidar networks, have not yet been systematically employed for model evaluation.

Table 1: Use of atmospheric aerosol data for complex model evaluation

DATA	APPLIED?
routine measurements of PM10, PM2.5, inorg. comp. (horizontal distribution)	yes rare
special measurement programmes (spectra, compos. etc)	not really
lidar (vertical distribution)	no (?)
turbidity	not yet
satellite measurements (AOD)	(?)
laboratory data	

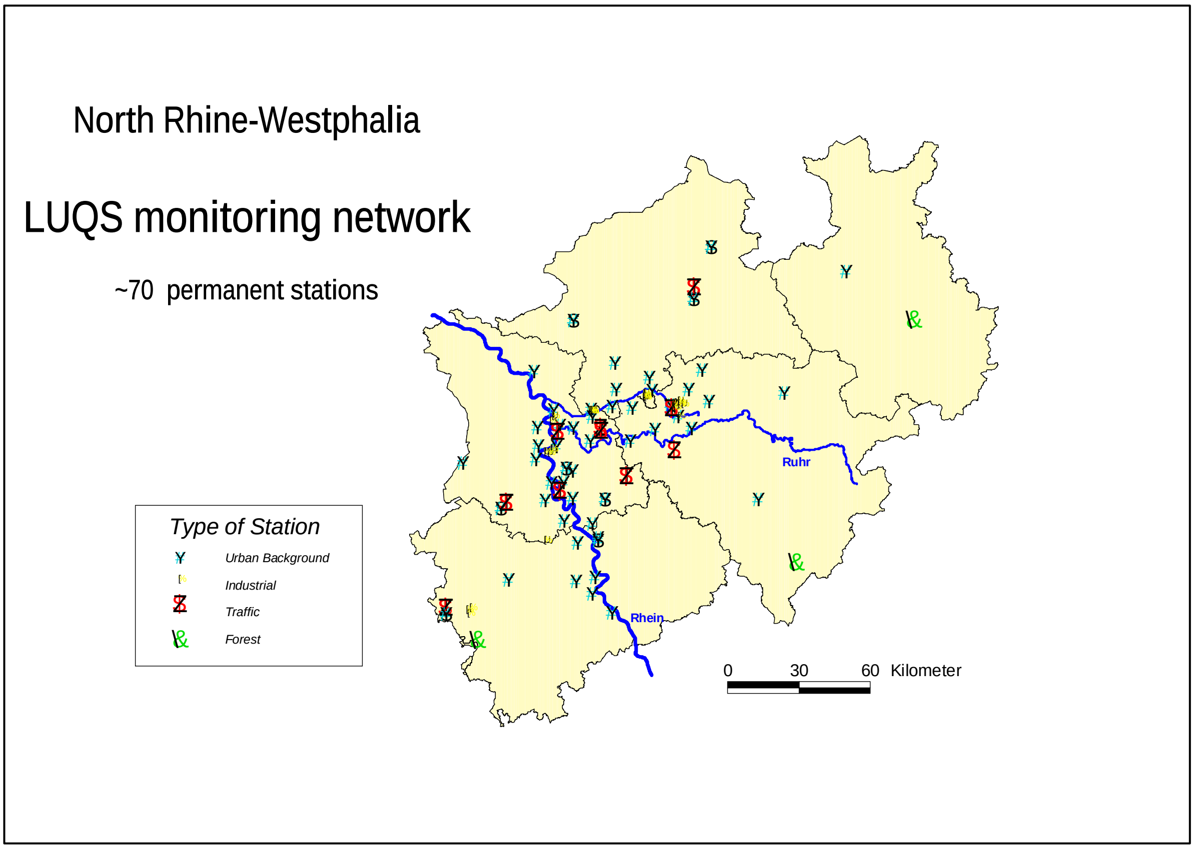

Figure 1. LUQS air quality monitoring network of North Rhine-Westphalia 2001

Comparison with observations

Long-term simulations of aerosol in NRW have been carried out for 1997 and 2002. The results have been compared with measured time series from the monitoring network (example in Fig. 2, summer 1997), scatter diagrams (Fig. 3) and hit rate estimates (Figs. 4) have been employed for statistical evaluation. Significant differences may be obtained for the hit

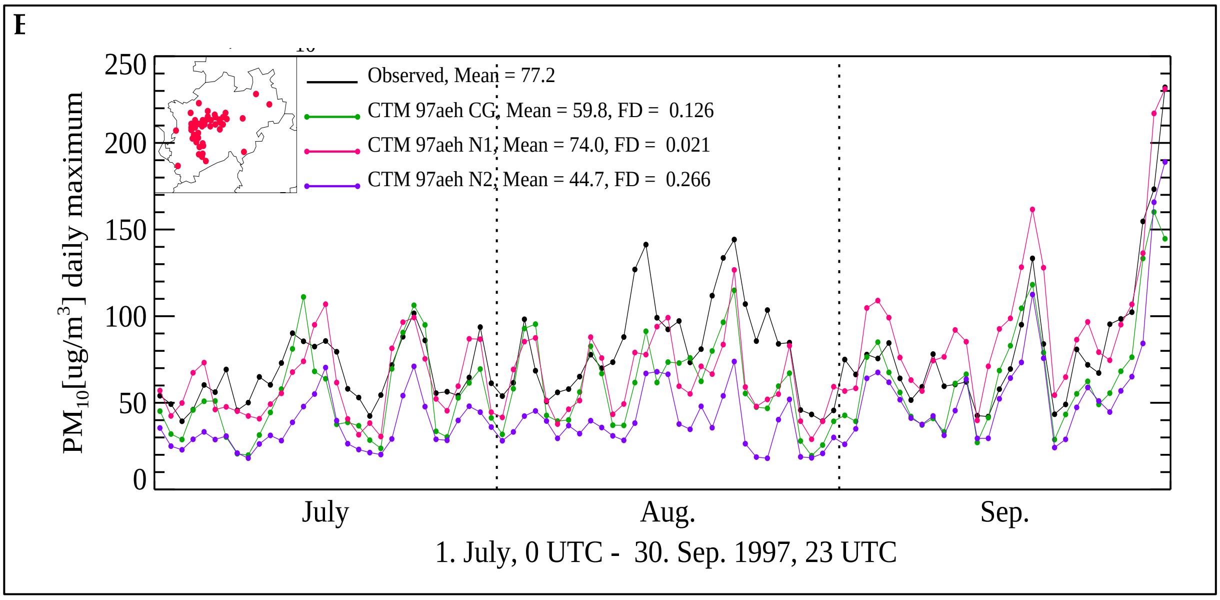

Figure 2. Time series, PM10 daily maxima. Calculated maxima from hourly values as obtained for different horizontal resolution by sequential nesting (CG = 125 km, N1 = 25 km, N2 = 5 km). NRW air quality monitoring network (LUQS) averages are shown.

SCATTER DIAGRAMM PM10

Daily average

Based on hourly values

PM10 from NRW stations only

PM10 = 0.83*TSP

(Nest 2 results, 5 km grid res.)

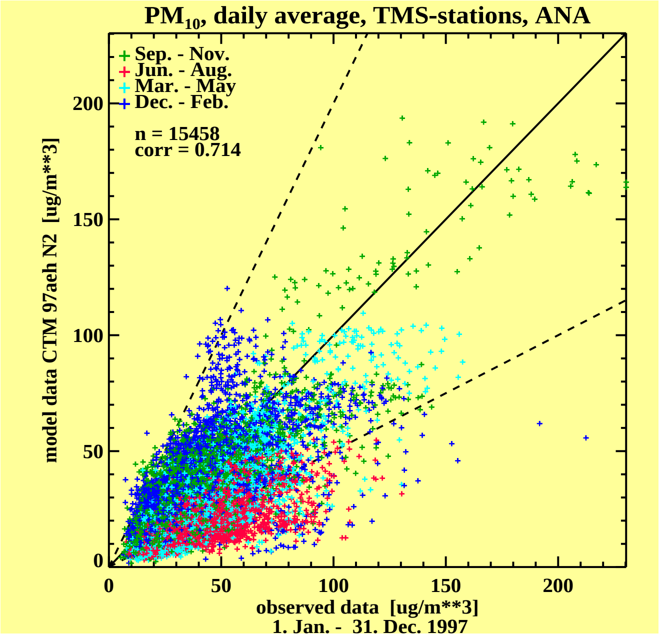

Figure 3. Comparison of measured and calculated daily averages of PM10 in NRW, year 1997

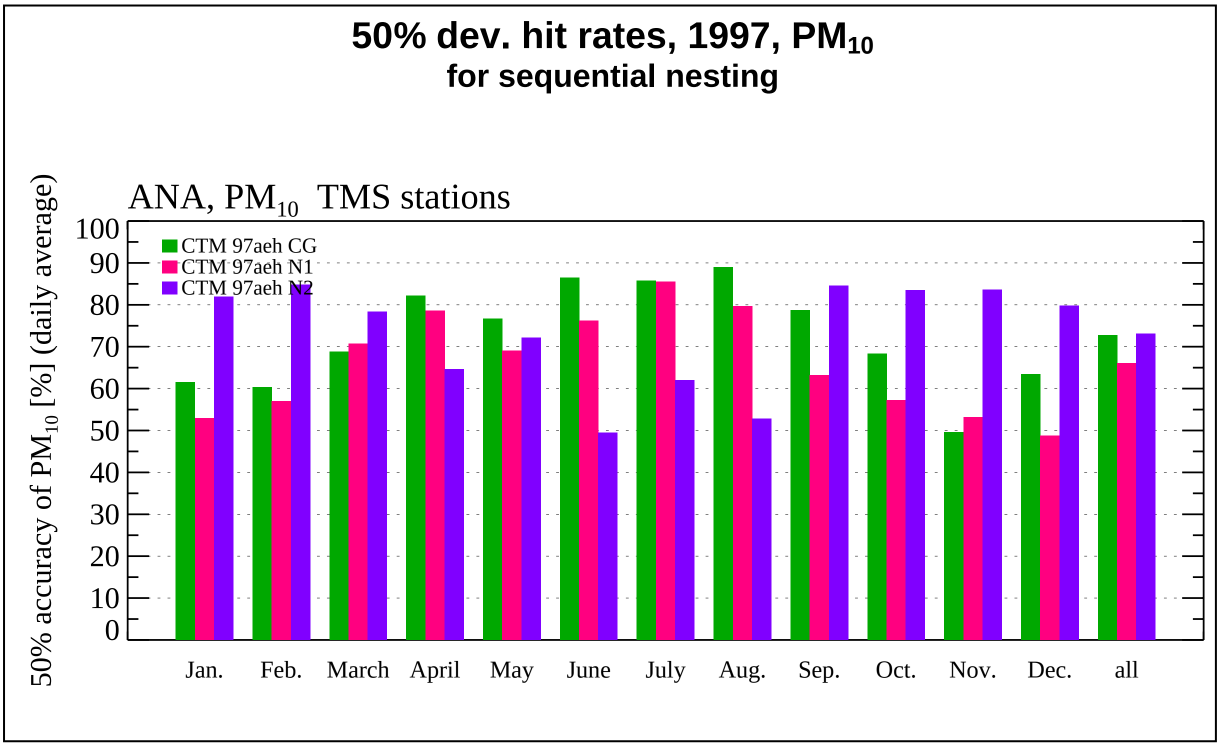

Figure 4. Hit rates 1997, NRW

rates in different years. An obvious deficit of the calculations is the underestimation of PM10 as well as TSP in summer clearly showing up in the scatter plot (Fig. 3) and also indicated by the hit rates. Interestingly, this summer effect is more pronounced in the simulations with finer resolution (nest 2). Since a special emission inventory has been chosen for this nest (NRW) shortcomings of the inventory (e. g., the difficult assessment of emissions by non-point sources) may have caused the underestimation. Uncertainties of aerosol chemistry parameterizations may also contribute.

Sensitivity considerations

A peculiar way to check the performance of a model is the comparison of calculated results with expectations regarding the role of processes relevant for aerosol formation and distribution. For instance, the sensitivity of aerosol distribution to frontal passages and clouds could be exploited in this way. This has the advantage that one can extend model tests far beyond experimental and financial limits of comprehensive atmospheric aerosol distribution and composition measurements. This compensates to a great deal the softness of plausibility arguments which have to be applied in this case.

Dealing with the problem of vertical aerosol distribution which is rarely studied in air quality simulations (though it is an important factor for the transport and deposition of particulate matter) one expects typical changes during days with high pressure conditions which should

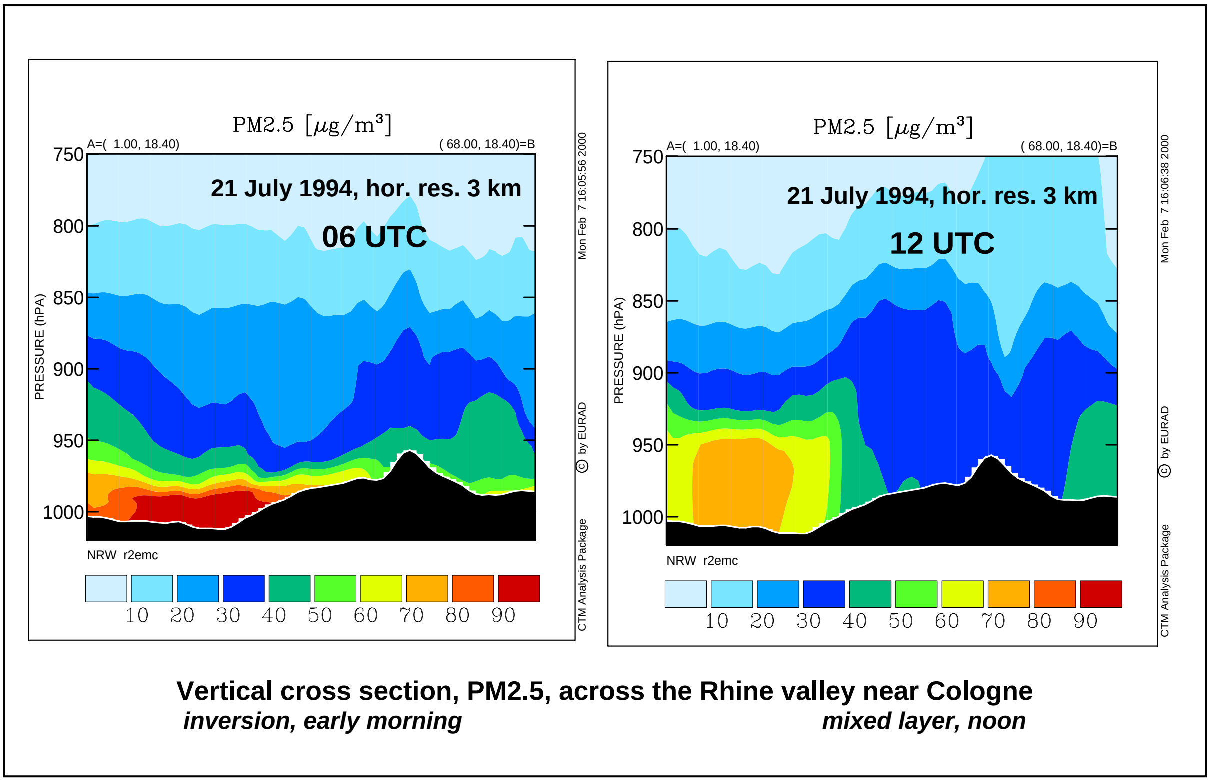

Figure 5. Vertical distribution of PM2.5 during anticyclonic weather conditions

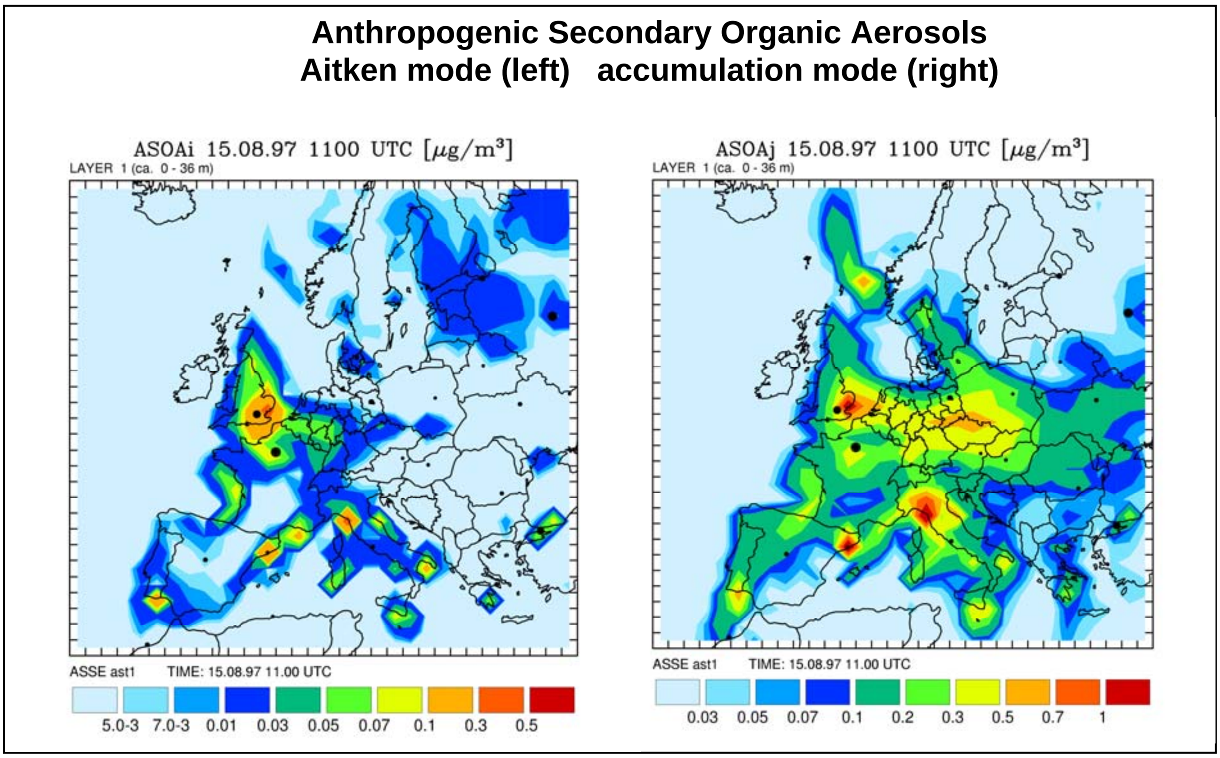

Figure 6. Horizontal distribution of anthropogenic secondary organic aerosols

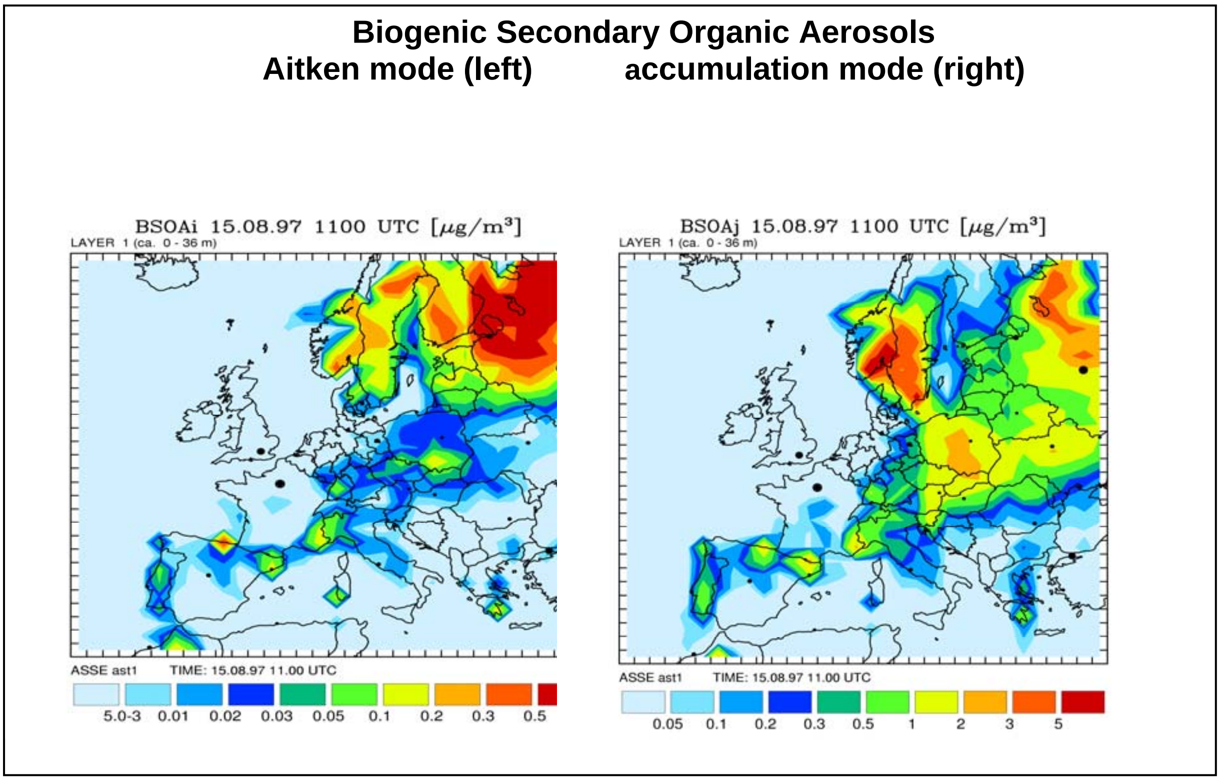

Figure 7. Horizontal distribution of biogenic secondary organic aerosols

be reproduced by a reliable model in a reasonable way (Fig. 5). Secondary aerosols should develop peculiar horizontal structures depending on the distribution of sources of precursors which are different for biogenic and anthropogenic emissions. Examples for the Aitken and accumulation modes are shown in Figs. 6 and 7.

A quite promising way of assessing the plausibility of aerosol simulations in air quality models is the analysis of aerosol composition and expectations for it in different seasons and at different locations. Fig. 8 shows that rather detailed information can be obtained from a complex model which should be exploited for reliability studies much more in future.

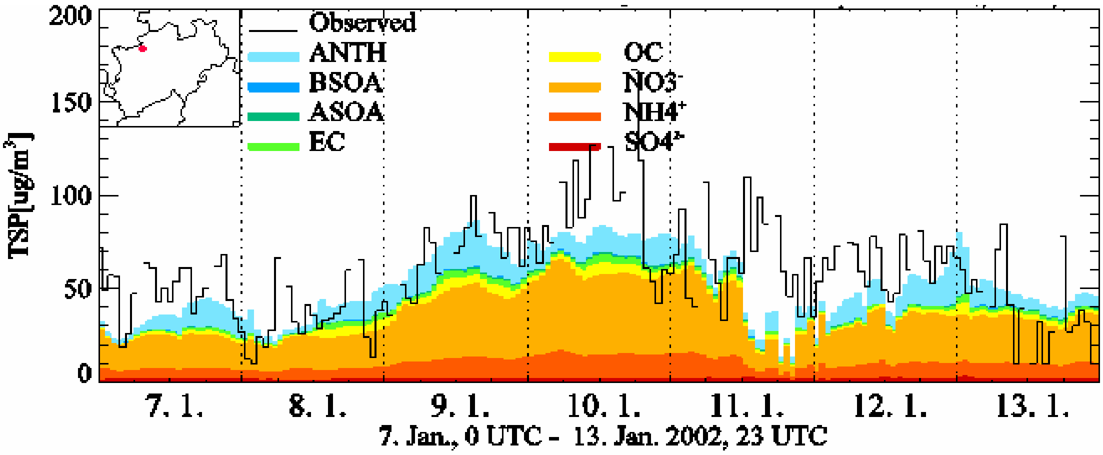

Figure 8. Composition of simulated total suspended matter (TSP) and observed TSP at station Borken, NRW. Model resolution 5 km.

Conclusion

Comprehensive aerosol simulation models are important tools for assessing the air quality and possible adverse effects of particulate matter in the atmosphere. Our experimental knowledge is quite limited in many respects and models can help to bridge the existing gaps through smart strategies of their application. Examples of sensitivity and plausibility tests presented in this short paper may give some hints how to proceed.

Acknowledgement.

The authors gratefully acknowledge funding of projects, on which this article is based, by the German Ministry of Education and Research (BMBF) and the State Environmental Agency (LUA) of North Rhine-Westphalia. Data used in the study have kindly been provided by ECMWF and NCEP (meteorology), TNO, Netherlands, (emissions) and LUA (emissions, monitoring data).

References

H. Hass, M. van Loon, C. Kessler, R. Stern, J. Matthijsen, F. Sauter, Z. Zlatev, J. Langner, V. Foltescu, M. Schaap, *Aerosol modelling: results and intercomparison from European regionasl-scale modelling systems,* EUROTRAC-2/GLOREAM, Munich, Germany, 2003

M. van Loon, M. G. M. Roemer, P. J. H. Builtjes, B. Bessagnet, L. Rouil, J. Christensen, J. Brandt, H. Fagerli, L. Tarrason, I. Rodgers, I. Taesdale, R. Stern, R. Bergström, J. Langner, V. Foltescu, *Model-inter-comparison in the framework of the unified EMEP model*, TNO-Report R 2004/282, Apeldoorn, The Netherlands, 2004

Implementation of the gas phase chemical mechanism CACM and the fine particulate matter module MADRID 2 into the EUROS model

Felix Deutsch[1], Filip Lefebre[1], Jean Vankerkom[1], Stefan Adriaensen[1], Clemens Mensink[1], Frea Blommaert[2], Vera De Saedeleer[2] en Edward Roekens[2]

[1] VITO – Centre for Integrated Environmental Studies, Boeretang 200, B-2400 Mol, Belgium
[2] Flemish Environment Agency (VMM), Kronenburgstraat 45, B-2000 Antwerp, Belgium
e-mail: felix.deutsch@vito.be

Introduction

The EUROS model is an Eulerian air quality model for the simulation of tropospheric ozone over Europe. It was originally developed at RIVM in the Netherlands and was implemented in Belgium in 2001. It is now an operational tool for policy support at the Interregional Cell for the Environment (IRCEL) in Brussels (Delobbe et al., 2002; Mensink et al., 2002).

The base grid of EUROS covers nearly whole Europe with a resolution of 60x60 km. Several subgrids (e.g. around Belgium) with a resolution of down to 7,5x7,5 km can be chosen. EUROS uses ECMWF meteorological data and emission data from EMEP/CORINAIR for the base grid and additional data from a Flemish Emission Inventory for the subgrid in and around Belgium. The vertical structure of the atmosphere is represented in EUROS by four layers: ground layer, mixing layer, reservoir layer and top layer. Ozone chemistry is computed using the CB-IV-mechanism.

The scope of this study is to investigate the possibilities to extend EUROS to model also fine particulate matter. For this purpose an extended literature study covering a range of contemporary aerosol models was carried out. Special attention was paid to their capabilities of modelling secondary aerosol formation in the atmosphere. Chemical gas phase mechanisms (e.g. extensions of existing mechanisms for ozone formation to aerosol modelling), as well as gas phase/solid phase equilibrium models were investigated. Following this literature study, the Caltech Atmospheric Chemistry Mechanism (CACM, Griffin et al., 2002) and the Model of Aerosol Dynamics, Reaction, Ionization and Dissolution 2 (MADRID 2, Zhang et al., 2004) were selected and implemented in EUROS.

CACM is the first mechanism describing the formation of secondary organic aerosol precursors in the atmosphere in a mechanistic way. Hence, this mechanism can be considered inherently superior to the mechanisms existing so far, treating these processes mainly phenomenologically. Additionally, it opens possibilities for future developments as new data becomes available. MADRID 2 contains various modules originating from other aerosol models which showed good performance during literature reviews and additionally some new developments. It treats the formation of secondary aerosols via equilibrium calculations between the gas phase and the aerosol phase. ISORROPIA is used for inorganic compounds, organic compounds are treated via a new developed module (Pun et al., 2001; 2002). Also dynamic processes (e.g. nucleation of particles) are included into MADRID 2.

Methodology

Implementation of the gas phase chemical mechanism CACM into EUROS

The ozone version of EUROS uses the CB-IV-mechanism with 87 reactions and 32 components. The Caltech Atmospheric Chemistry Mechanisms (CACM) comprises in contrast 361 reactions among 122 components. CACM contains besides the complete ozone chemistry also the reactions of various generations of organic compounds during which semi-volatile reaction products are formed which can equilibrate into the solid phase. 42 of these condensable products are treated in CACM, all of them reaction products of anthropogenic and natural organic compounds, e.g. terpenes. Various routines of EUROS (e.g. VOC-split, background concentrations) were adjusted to CACM.

Implementation of the aerosol module MADRID 2 into EUROS

In the Model of Aerosol Dynamics, Reaction, Ionization and Dissolution 2 (MADRID 2) thermodynamic equilibrium calculations are carried out via ISORROPIA (Nenes et al., 1989) for inorganic compounds and via the new developed AEC-SOA-module (Pun et al., 2001; 2002) for organic compounds. Mass transfer between gas phase and solid phase can be taken into account via different approaches, e.g. the CMU Hybrid Model (Capaldo et al., 2000), supposing instantaneous equilibrium for small particles and calculating mass transfer for larger particles. Nucleation of new particles is treated by calculating the relative rates of new particle formation and condensation onto existing particles. Deposition of particles is calculated following a resistance approach.

Secondary organic aerosols are calculated after lumping the 42 condensable compounds from CACM into 5 hydrophilic and 5 hydrophobic surrogate compounds in MADRID 2. The hydrophilic compounds are equilibrated between the gas phase and the "liquid" phase of the aerosol particles according to Henry's law. The necessary activity coefficients are calculated by UNIFAC, which is based on group-contribution theory (Fredenslund et al., 1975; Saxena et al., 1995). The water content of the aerosols is calculated by the ZSR (Zdanovskii-Stokes-Robinson) algorithm. Hydrophobic organic reaction products from CACM are equilibrated between the gas phase and an absorbing organic aerosol phase, consisting of primarily emitted organic aerosols and of other secondary hydrophobic organic compounds. Because both the inorganic and the organic hydrophilic aerosol composition determine the amount of water connected to the aerosol particles and the acidity of the aqueous phase, the inorganic and the organic hydrophilic equilibrium module are called iteratively until constant liquid water content and acidity is reached. Only then the module for the organic hydrophobic compounds is called.

For the implementation EUROS was provided with additional emission data of point and surface sources for ammonia and two size fractions of particles (< 2,5 µm; 2,5 – 10 µm) from the EMEP-database for Europe and from a recent emission inventory for Flanders.

Results and Discussion

The current implementation of CACM and MADRID 2 enables EUROS to calculate mass and chemical composition of aerosols in two size fractions ($PM_{2,5}$ and $PM_{10-2,5}$). The chemical composition is expressed in terms of 7 components: ammonium, nitrate, sulphate, primary inorganic compounds, elementary carbon, primary organic compounds and secondary organic compounds (SOA). The updated EUROS has been tested for several periods in 2003.

Figure 1 shows the modelled daily averaged concentration of $PM_{2,5}$ on August 10th 2003 in the whole EUROS-domain with a resolution of 60x60 km. Figure 2 shows the area of the grid refinement in and around Belgium with a resolution of 15x15 km.

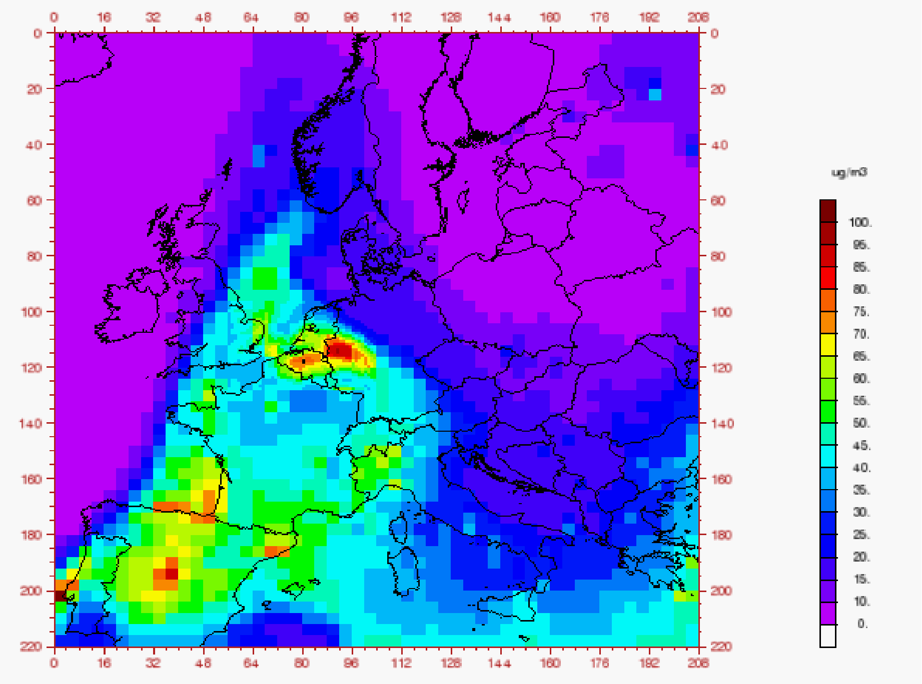

Figure 1: Daily averaged concentration of $PM_{2,5}$ on August 10th 2003 in the EUROS domain.

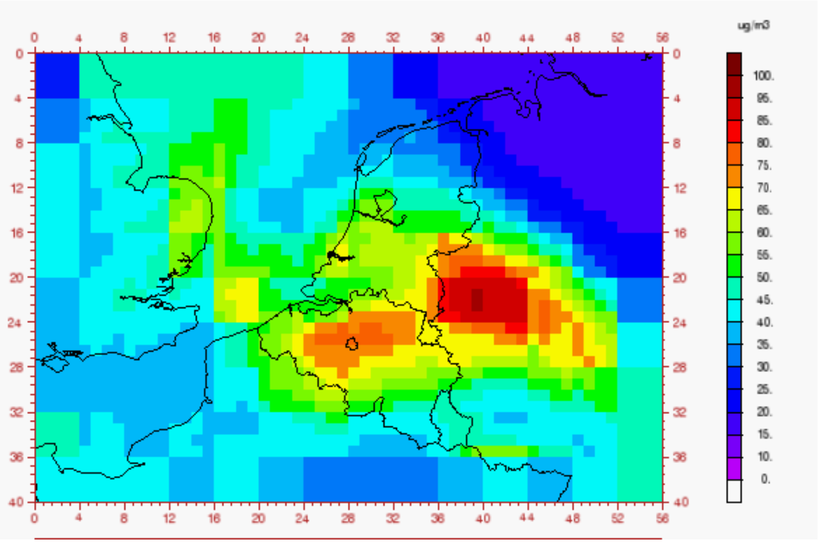

Figure 2: Daily averaged concentration of $PM_{2,5}$ on August 10th 2003 in the area of the grid refinement with a resolution of 15x15 km.

A validation of the model was performed for 4 episodes (each 2 or 3 weeks duration) covering all seasons of the year 2003. The obtained aerosol concentrations were compared to concentrations observed at 5 monitoring stations of the air quality monitoring network of the Flemish Environment Agency (VMM).

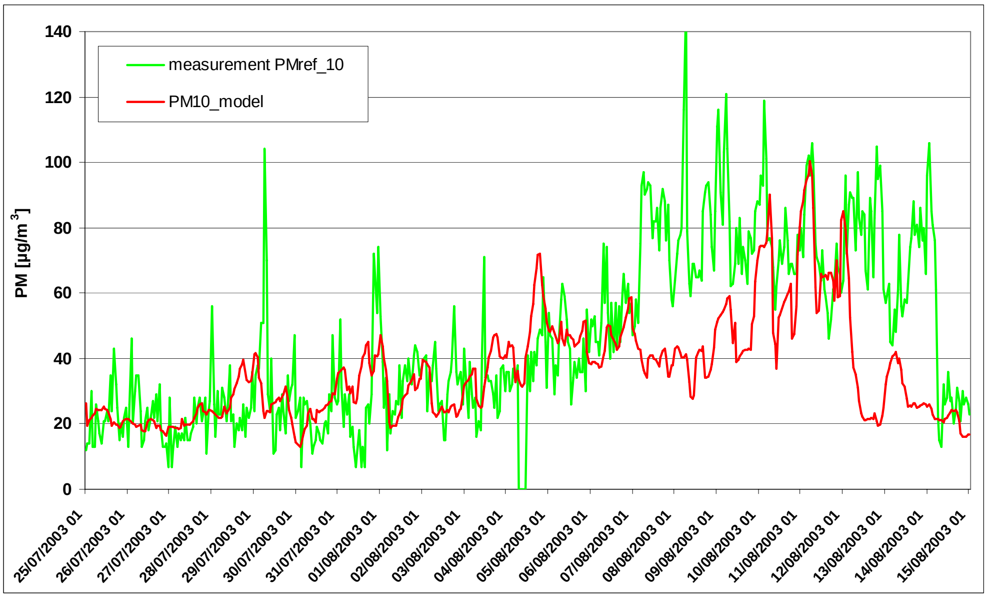

Figure 3: Measured and modelled concentrations of PM_{10} in Antwerp, July 25th-August 15th, 2003.

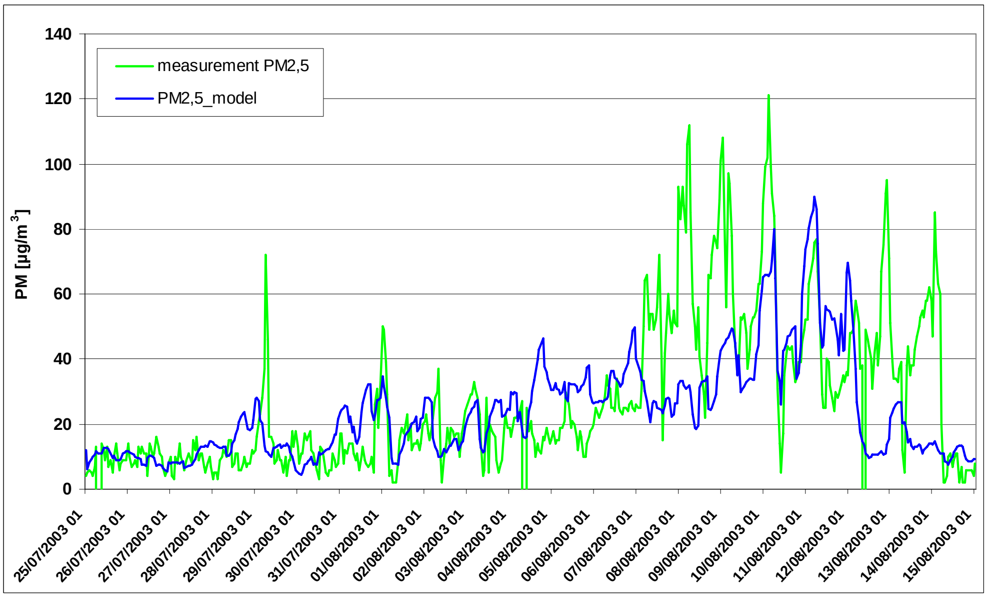

Figure 4: Measured and modelled concentrations of $PM_{2,5}$ in Antwerp, July 25th-August 15th, 2003.

Figure 3 shows as an example PM_{10}-concentrations measured between 25th of July and 15th of August 2003 at a monitoring station in the city centre of Antwerp and PM_{10}-concentrations modelled for the 15x15 km grid cell within which Antwerp is situated. PM_{10}-concentrations have been measured by TEOM and subsequently corrected to account for losses of volatile material ("measurement PMref_10"). Figure 4 shows the measured and modelled $PM_{2,5}$-concentrations for the same time period and monitoring station.

The comparison shows that modelled PM-concentrations are generally consistent with measured concentrations. The trend of the measured values towards higher PM-concentrations during the second part of this episode is reproduced by the model, although on some days quite strong underprediction of PM-mass occurs.

Figure 5 shows the modelled chemical composition of the size fraction $PM_{2,5}$ in Antwerp, also for the time period from July 25th until August 15th, 2003. The main components in the fine fraction were nitrate, sulphate, ammonium and also SOA, thus predominantly secondary components. The primary components were of minor importance in the small particles.

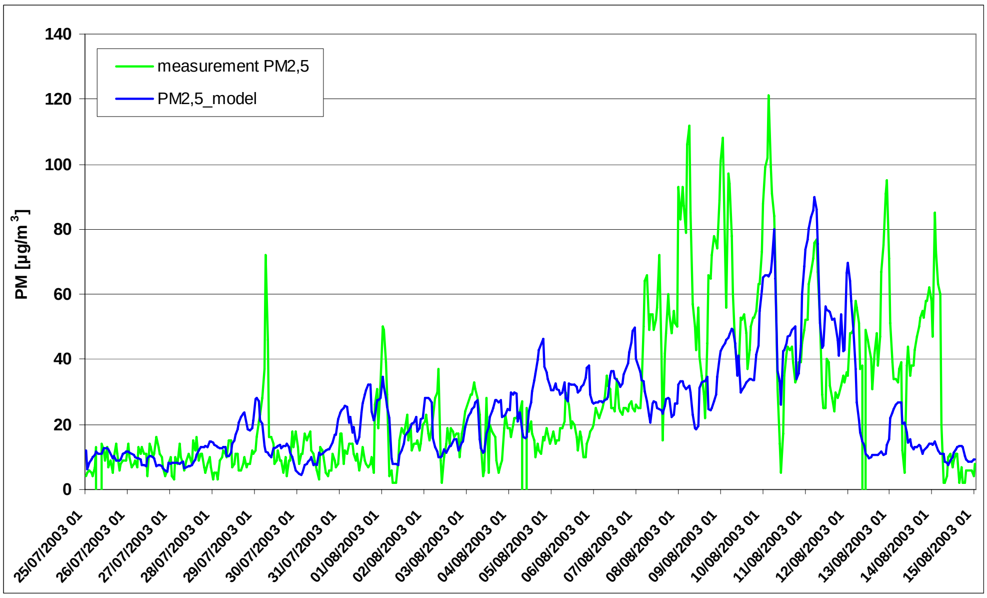

Figure 5: Chemical composition of the size fraction $PM_{2,5}$ in Antwerp in July/August 2003.

Figure 6 shows the chemical composition of the size fraction PM_{10} in Antwerp during the same time period. As anticipated, the primary components of the aerosol are mainly situated on the larger particles.

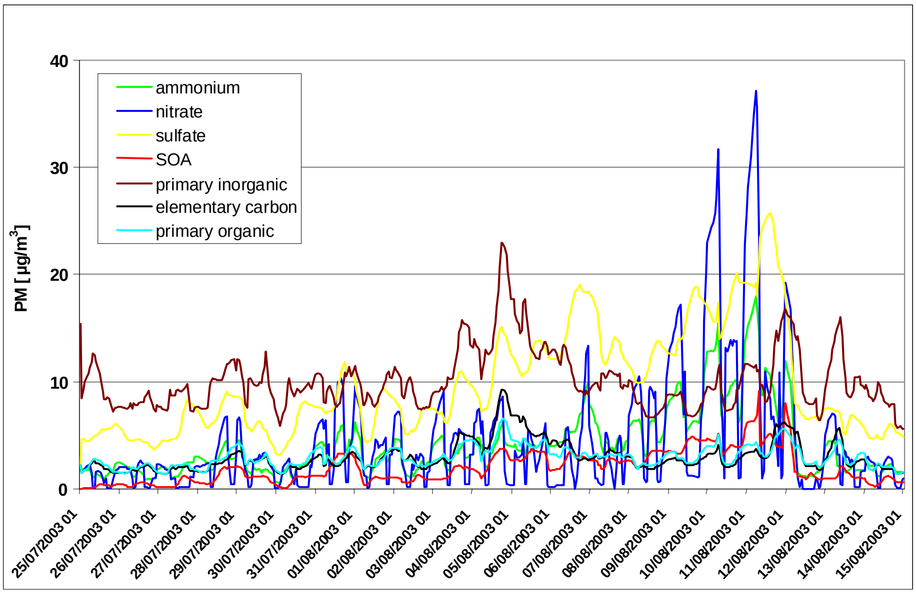

Figure 6: Chemical composition of the size fraction PM_{10} in Antwerp in July/August 2003.

In the size fraction PM_{10} primary inorganic compounds and also elementary carbon show a much higher abundance than in the size fraction $PM_{2,5}$. On average, 54% of all material in the size fraction $PM_{2,5}$ and 11% in the size fraction $PM_{10-2,5}$ were of secondary origin during this episode.

In contrast, during an episode in the autumn, the modelled chemical composition was less dominated by secondary aerosols. Figure 7 shows the chemical composition of the size fraction $PM_{2,5}$ in central Antwerp in the period between October 4th and 19th, 2003.

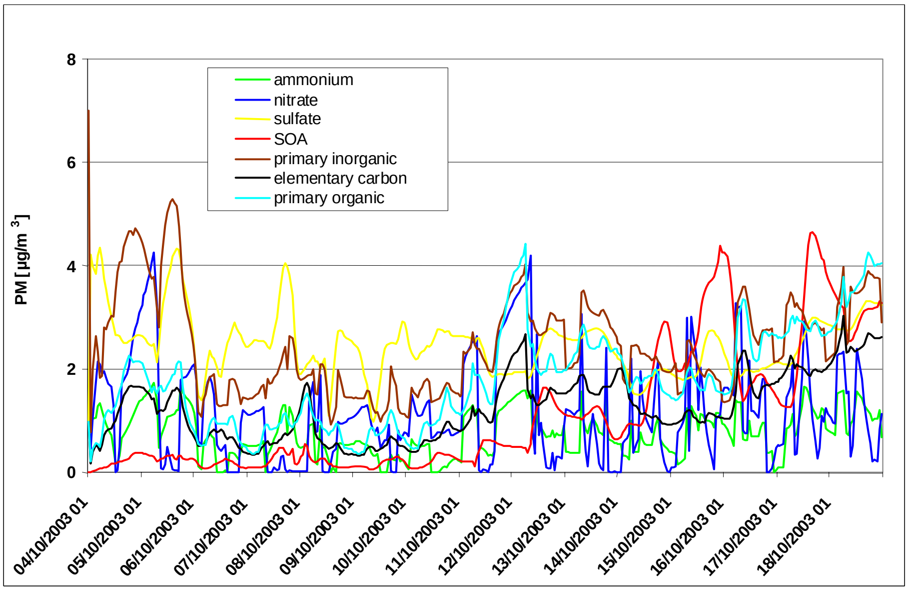

Figure 7: Chemical composition of $PM_{2,5}$ in Antwerp between October 4th and 19th, 2003.

Figure 8 shows the corresponding figure for the chemical composition of the size fraction PM_{10} in October 2003.

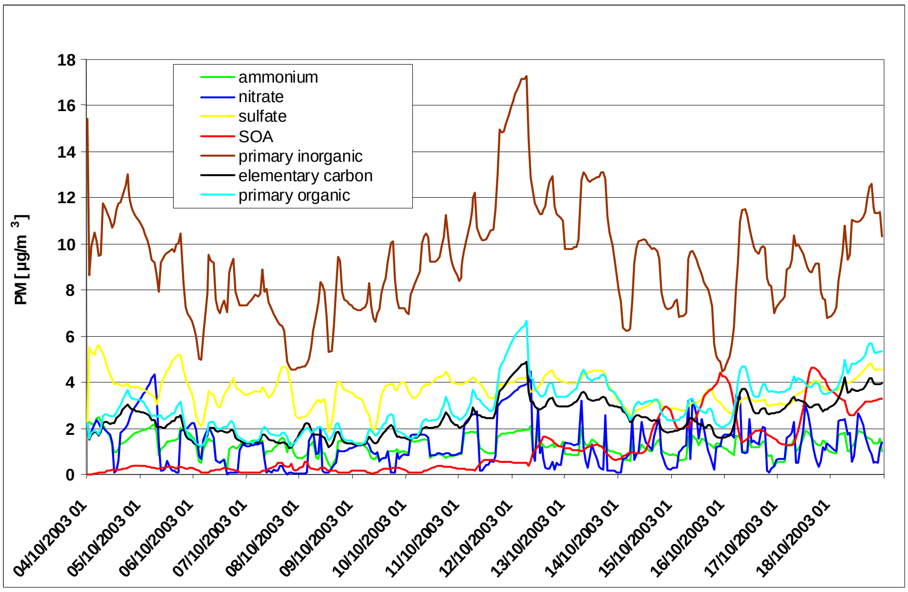

Figure 8: Chemical composition of PM_{10} in Antwerp between October 4th and 19th, 2003.

On average, only 38% of the aerosol mass in the size fraction $PM_{2,5}$ was secondary and again 11% of the mass in the size fraction $PM_{10-2,5}$ was secondary.

Conclusions

The innovative chemical mechanism CACM and the advanced aerosol model MADRID 2 were successfully implemented into the EUROS-model. Hereby the capabilities of EUROS were enlarged in the direction of modelling mass and chemical composition of aerosol particles. Currently, two size fractions and seven chemical components can be modelled.

A comparison showed that modelled PM-concentrations are generally consistent with observed PM-concentrations. Nevertheless, sometimes significant underprediction of PM mass occurred.

The chemical composition of the aerosol showed a strong dependence on the season. High aerosol concentrations during the summer were mainly due to high concentrations of the secondary components nitrate, ammonium and SOA in the size fraction $PM_{2,5}$. During other seasons, secondary components were less abundant in this size fraction, although SOA still contributed significantly to the total aerosol mass. Perhaps the equilibrium between gas phase and aerosol for the SOA-precursors is shifted more towards the solid phase during colder seasons.

The fine particulate matter version of the EUROS-model showed to be suited to determine the most important contributions to aerosol concentrations, including the percentage of secondary aerosols. It can be used to define sources and formation mechanisms of particulate matter and can be an important policy-supporting instrument for drawing up and evaluating reduction scenario's for fine particulate matter.

Literature

Capaldo K.P., Pilinis C. and Pandis S.N. (2000) A computationally efficient hybrid approach for dynamic gas/aerosol transfer in air quality models, *Atmospheric Environment*, **34,** 3617-3627.

Delobbe L., Mensink C., Schayes G., Brasseur O., Passelecq C., Passelecq D., Dumont G. and Demuth C. (2002) BelEUROS: Implementation and extension of the EUROS model for policy support in Belgium, Global Change and Sustainable Development, Federal Science Policy Office, Brussels.

Fredenslund A., Jones R.L. and Prausnitz J.M. (1975) Group-contribution estimation of activity coefficients in nonideal liquid mixtures, *A.I.Ch.R. J.* **21,** 1086-1099.

Griffin R.J., Dabdub D. and Seinfeld J.H. (2002) Secondary organic aerosol 1. Atmospheric chemical mechanism for production of molecular constituents, *J. Geophys. Res.* **107(D17),** 4332, doi:10.1029/2001JD000541.

Mensink C., Delobbe L. and Colles A. (2002) A policy oriented model system for the assessment of long-term effects of emission reductions on ozone, Air Pollution Modelling and its Applications XV, edited by C. Borrego and G. Schayes, Kluwer Academic/Plenum Publishers, pp. 3-11.

Nenes A., Pandis S.N. and Pilinis C. (1998) ISORROPIA: a new thermodynamic equilibrium model for multiphase multicomponent inorganic aerosols, *Aquatic Geochemistry* **4,** 123-152.

Pun B.K., Wu S.-Y. and Seigneur C. (2001) Contribution of biogenic emissions to the formation of ozone and particulate matter: Modeling studies in the Nashville, Tennessee and

Northeast domains, Phase 2 Report for CRC Project A-23, Document Number CP051-01-1, Coordinating Research Council, Inc., Alpharetta, GA, USA.

Pun B.K., Griffin R.J., Seigneur C. and Seinfeld J.H. (2002) Secondary organic aerosol 2. Thermodynamic model for gas/particle partitioning of molecular constituents, *Journal of Geophysical Research*, **107** (D17), 4333, AAC 4-1 – 4-15.

Saxena P., Hildemann L.M., McMurry P.H. and Seinfeld J.H. (1995) Organics Alter Hygroscopic Behavior of Atmospheric Particles, *J. Geophys. Res.* **100,** 18755-18770.

Zhang Y., Pun B., Vijayaraghavan K., Wu S.-Y., Seigneur C., Pandis S.N., Jacobson M.Z., Nenes A. and Seinfeld J.H. (2004) Development and application of the Model of Aerosol Dynamics, Reaction, Ionization, and Dissolution (MADRID), *J. Geophys. Res.* **109,** D01202, doi:10.1029/2003JD003501.

Modeling atmospheric mercury at European scale with the Chemistry Transport Model POLAIR3D

Roustan Yelva [†1], Bocquet Marc,
Musson Genon Luc and Sportisse Bruno
CEREA, Research and Teaching Center in Atmospheric Environment, Joint Laboratory École Nationale des Ponts et Chaussées/Électricité de France R&D. Cité Descartes, Champs sur Marne, F-77455 Marne la Vallée Cedex, France

Abstract

Two mercury chemistry models have been implemented in the Chemistry-Transport Model (CTM) POLAIR3D to perform impact studies at continental scale over Europe. The first one is a simple model allowing to simulate mercury chemical behavior with a scavenging ratio. Four mercury species implied in two reactions and three equilibria are taking into account. The second, conceived on the basis of more complex models, represents nine mercury species interacting in thirteen reactions and twenty-seven equilibria. Simulations for the year 2001 have been performed with the two models and results are compared to the available measurements for air concentrations and wet deposition fluxes. Gaseous elemental mercury (GEM) is relatively well simulated with time averaged air concentrations values included in the range 1.5 to 4.0 ng.m^{-3} for the simple model and in the range 1.5 to 3.4 ng.m^{-3} with the detailed one. On the other hand the deposition fluxes computed by the simple model are negligible and those obtained with the detailed one are more significant but remain underestimated.

Introduction

Mercury is mainly present in the atmosphere under the form of elemental mercury (Hg(0)). Background concentrations are weak, of about 1 ng.m^{-3}. However under the form of methylmercury (Hg(Me)) it is a neurotoxic substance capable to bioaccumulate. Bioaccumulation means an increase of concentration in a biological organism over time compared to the concentration in the environment. For this reason it forms a subject of concern for the different organisations dealing with air quality issues. Among them the United Nations Economic Commission for Europe (UNECE) spotted mercury in the protocol on heavy metals of the Convention on Long Range Transboundary Pollution (CLRTAP).

Atmospheric mercury can be found under multiple forms commonly classified in three categories: elemental mercury (Hg(0)), oxidised mercury (Hg(II)) and particulate mercury

---

[†1] Corresponding author: roustan@cerea.enpc.fr

(HgP), GEM (elemental mercury in gaseous phase) representing by far the main part in mass (95-99 %, Ryaboshapko et al, 2002). Mercury species differ by their chemical and physical properties and consequently have variable behavior. The high saturated vapor pressure and relatively low reactivity and solubility of GEM explain its long life time of about one year (Lindqvist and Rodhe, 1985). Because of their higher solubility oxidised mercury species and particulate ones have much more limited residence time, from hours to days and from days to weeks respectively (Seigneur et al, 2003).

Usually mercury emissions are distributed according to their origins, anthropogenic (chlor-alkali production, waste incinerator), natural (geological mercury, volcanoes) or re-emissions. Re-emissions concern mercury masses that have been previously deposited by atmospheric removal process and which are likely to be re-emitted after transformation in soils or water spreads. Natural emissions and re-emissions basically consist in GEM, but anthropogenic ones are much more diversified and can produce GEM as well as oxidised or particulate mercury. This issue is also considered by Electricité de France (EDF, the french national electricity company) since power plants may represent important sources.

1 Polair3D

Polair3D is a three-dimensional chemistry-transport model developed at ENPC (École Nationale des Ponts et Chaussées) and designed to handle a wide range of applications from passive transport to photochemistry and aerosol modeling (Mallet and Sportisse, 2004). The structure of the code has been thought to benefit from automatic differentiation and to allow the use of several chemistry models (RADM2, RACM, CBM IV, etc...). Two mercury chemistry models have been implemented, after sensitivity analysis and validation the aim is to proceed to impact studies. Inverse modeling could be used later to improve used data set and determine more accurately some key parameters.

1.1 Processes and numerical issues

Classicaly the dispersion of mercury is governed by the following transport equation describing the time and space evolution of concentration c :

$$\frac{\partial c}{\partial t} + \mathrm{div}(\boldsymbol{u}c) - \mathrm{div}(\boldsymbol{K} \cdot \nabla c) + \Lambda\, c = \sigma$$

the processes implied are :

- the advection by wind $\boldsymbol{u}$, $\mathrm{div}(\boldsymbol{u}c)$,
- the turbulent diffusion with $\boldsymbol{K}$ the eddy diffusivity tensor, $\mathrm{div}(\boldsymbol{K} \cdot \nabla c)$,
- the chemistry and wet scavenging are gathered in $\Lambda\, c$,
- the volume emission, σ.

The dry deposition velocity, v_d, and the surfacic emissions, E, are used to determine the ground boundary condition :

$$\mathrm{div}(\boldsymbol{K} \cdot \nabla c) \cdot \boldsymbol{n} = E - v_d\, c$$

with the normal surface vector, inward oriented, $\boldsymbol{n}$. At the top and lateral faces the boundary conditions are:

$$\mathrm{Flux} = \boldsymbol{n} \cdot \boldsymbol{u} c$$

The turbulent diffusion fluxes for these faces are supposed to be negligible in comparison to advection fluxes and set to zero for the numerical resolution.

Different splitting methods are available in POLAIR3D to solve the transport equation. In the case of mercury a simple first order method is applied, begining by advection, then diffusion along x, y and z, and finally chemistry. The splitting allow to resort to different numerical scheme for each one of these steps. A third-order direct space time (DST) with Koren-Sweby flux limiter function scheme is used for advection. Diffusion is spatially discretized in the classical way with a three point scheme and a second-order Rosenbrock method is devoted to the time integration of diffusion and chemistry.

Main pathways for mercury from the atmosphere to biological organisms, especially those of the aquatic food chain, are wet and dry deposition. These two removal processes are crucial within the framework of mercury impact studies since mercury is a threat due to its accumulation.

1.2 Dry deposition

Dry deposition gathers several phenomena which successively control the downward transport of pollutant from the surface boundary layer downto the canopy (Wesely and Hicks, 2000). The dry deposition velocity is defined by:

$$F = v_d\, c(z_r)$$

where F is the flux of pollutant towards the surface and $c(z_r)$ the pollutant concentration at the reference height z_r for which the dry deposition velocity v_d is determined. The expression of v_d as the inverse of the sum of three deposition resistances

$$v_d = \frac{1}{R_a + R_b + R_c}$$

returns to the three main steps in the dry deposition process:

- In the main part of the surface boundary layer, from the reference height to quasi-laminar boundary layer, turbulent diffusion is the dominating process.
- The second part of the downward transport corresponds to the crossing of the quasi-laminar layer where the role of molecular diffusivity, and consequently the nature of the pollutant, becomes considerable.
- The last step refers to the surface mass exchange processes between the air and the canopy.

Currently the parameterizations used in POLAIR3D for the mercury model are inspired from the work of Baer and Nester (Baer and Nester, 1992) with some upgrades to estimate dry deposition velocity over water spread (Hicks and Liss, 1976) and take into account canopy water content (Brook et al, 1999).

1.3 Wet deposition

Wet deposition is the superposition of two phenomena, in-cloud scavenging and below cloud scavenging. Both result in a mass transfer of pollutant from the atmosphere to the surface during precipitation events, but differ in the moment at which materials penetrate the aqueous phase. In the case of in-cloud scavenging, they are removed from gaseous phase by cloud drops and thereafter brought to the surface by rain. The two processes are not always immediately consecutive, pollutants can be carried by suspended cloud drops over long distance before being deposited or even released. Below-cloud scavenging correspond to the mass tranfert of materials from air to rain drops during their fall.

In both case scavenging coefficients are used to estimate the wet deposition flux due to rain. But for in-cloud scavenging the mass present in the cloud drops should be given by the chemistry model. The parameterizations applied in POLAIR3D are those studied by Sportisse for the below-cloud scavenging coefficient (Sportisse and Du Bois, 2002) and proposed by Roselle for the in-cloud scavenging coefficient (Roselle and Binkowski, 1999).

2 Mercury chemistry

Two mercury chemistry models have been implemented in POLAIR3D. The first one has been proposed by Petersen (Petersen et al, 1995), the mercury chemical behavior is represented in the below-cloud scavenging coefficient parameterization. This model is well known as it was one of the first proposed. The second has been developed on the basis of a comparison work of mercury chemistry models (Ryaboshapko et al, 2002). Chemistry kinetic is explicitely treated in both gaseous and aqueous phase.

2.1 Petersen model

The idea behind of this chemistry model consists in considering elemental mercury as a passive tracer in gaseous phase but as a reactive chemical in the aqueous one constituted by rain drops. Ozone is regarded as the only oxidant species in charge of the oxidised mercury formation. Oxidised mercury can be reduced after having formed complex with sulfites ions or being adsorbed by soot particles. Ozone and soot particle concentration fields are forced with climatological values.

Some considerations on orders of magnitude allow to simplify the equations found when we assume the different chemical equilibria reached. A last hypothesis of global equilibrium between the production and the destruction rates of oxidised mercury species lead to express the mercury scavenging ratio as a function of the ozone and soot particles concentrations.

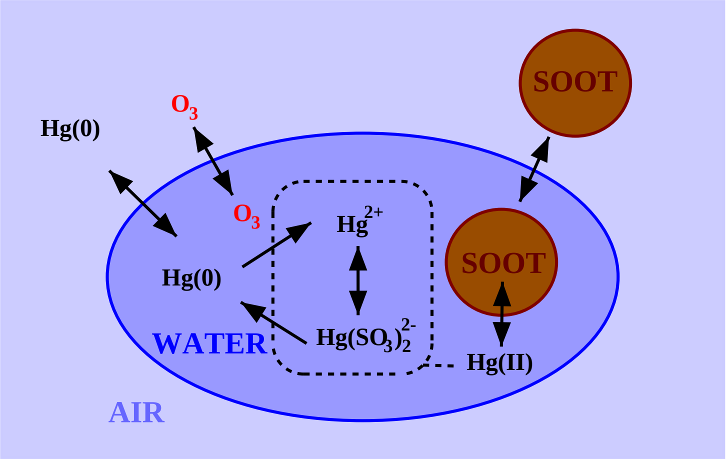

Figure 1: Petersen mercury chemistry model

The main weakness of this chemistry model lies in the fact that oxidised mercury species are not taken into account in the gaseous phase. As GEM is poorly soluble the reaction in aqueous phase with ozone is very limited. Therefore concentrations of Hg(II) and HgP are strongly underestimated.

2.2 Detailed model

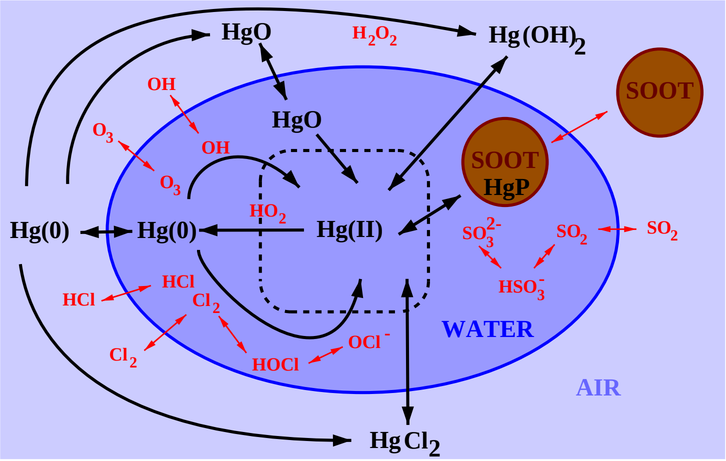

Figure 2: Detailed mercury chemistry model

This model is conceived on the basis of currently developed model (Ryaboshapko et al, 2002). The main difference with the precedent consists in the simulation of oxidation reactions and oxidised species in gaseous phase. These reactions are rather slow in comparison to what happens in aqueous phase, but as oxidised mercury species are easily scavenged it represents a non-negligible process to correctly evaluate deposition fluxes.

Ozone is always globally considered as the main oxidant. However other species can become prevalent locally, as chlorine in the marine boundary layer. In regards of what it is done in the simple model the possible ways of formation and destruction of oxidised species are multiplied.

With this model chemistry kinetics are explicitly simulated even if some quick equilibrium hypothesis are still used. Although the chemistry model is complexified, the linearity property is preserved.

3 Simulations and results

Simulations have been performed with the two models over the year 2001. The spatial domain extends from 12.375°W to 37.125°E in longitude and from 36°N to 72°N in latitude, with a step of 1.125° along both longitude and latitude. Fourteen vertical levels are represented with a top relative height of 5233m.

Meteorological data are provided by the European Centre for Medium-Range Weather Forecasts with a time step of six hours. Emission and observation data are made available by the European Monitoring and Evaluation Program centres.The simulation time step is 900 s, data are linearly interpolated between each data time step.

For our simulations we use the following boundary conditions : 1.75 ng.m^{-3} at west, 1.7 ng.m^{-3} at east, 1.5 ng.m^{-3} at south and 1.42 ng.m^{-3} at north. These values are proposed by the Meteorological Synthesizing Centre - East (MSC-E) in a first approach (`http://www.msceast.org/`). In addition we have chosen a value of 1.6 ng.m^{-3} at the top of the domain. A homogeneous initial concentration of 1.5 ng.m^{-3} is taken in the bulk.

3.1 Simple model

On the figure 3 is represented the GEM annual average concentrations field obtained from the Petersen model. Concentrations values are in the expected order of magnitude, ranging from 1.5 to 4.0 ng.m $^{-3}$ with a spatial average of 1.9 ng.m^{-3}. The most important emissions area are clearly apparent although the scale value is quite restricted and concentration gradient relatively weak. The pollutant mass added in the domain by the sources is superimposed on the background concentrations governed by the boundary conditions.

The comparison of these results with available measurements from the EMEP network (see figure 4) is partly satisfying, but the number of station is insufficient to conclude on the model validation. Moreover the stations are not well spatially distributed, all being in the northern part of the domain.

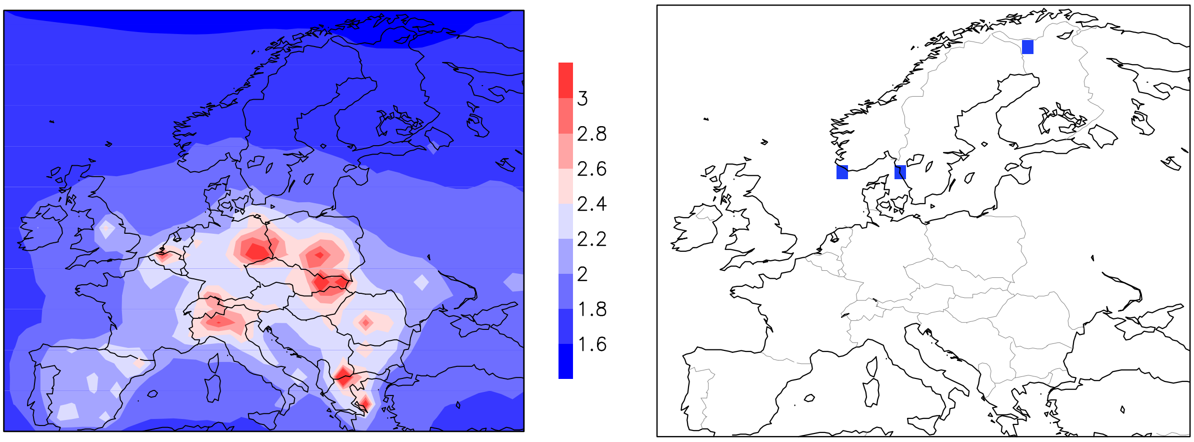

Figure 3: GEM annual average concentration for 2001 in ng.m^{-3} and measurement station localisation.

Since the Petersen mercury chemistry model does not deal with the mercury oxidised species in gaseous phase, the deposition fluxes and especially the wet one are strongly underestimated. The ratio between modeled wet deposition fluxes and measured ones is negligible.

3.2 Detailed model

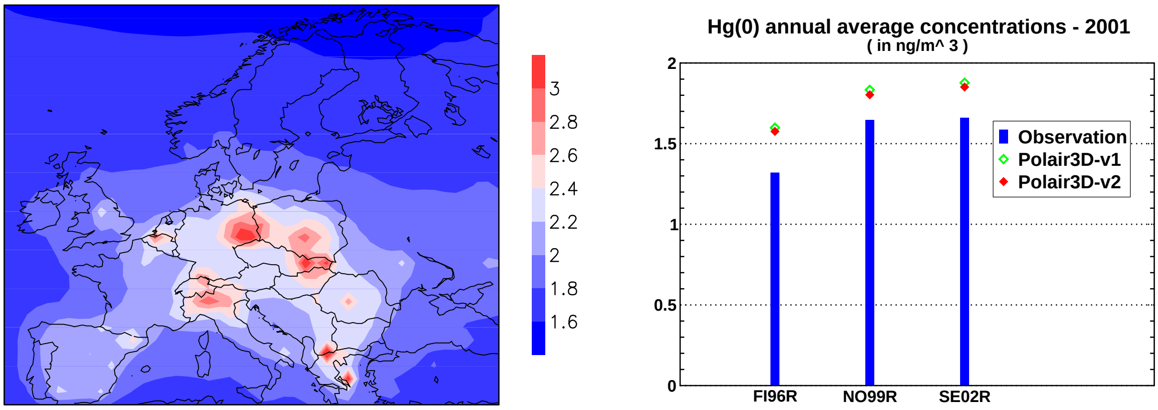

Figure 4: GEM annual average concentration for 2001 in ng.m^{-3} and comparison to measures.

On figure 4 is represented the GEM annual average concentrations field obtained with the detailed model. Concentrations values are quite similar, ranging from 1.5 to 3.4 ng.m $^{-3}$ with a spatial average of 1.9 ng.m^{-3}. Despite slightly better predictions at the stations it is clear that the interest of the detailed model does not lie in a better evaluation of GEM concentration.

A substantial contribution consist in its ability to provide reactive gaseous mercury (RGM = all the gaseous oxidised mercury species) concentration fields (figure 5). RGM annual average concentrations range from 5.1 pg.m^{-3} to 0.73 ng.m^{-3} with a spatial average of 0.016 ng.m^{-3}.

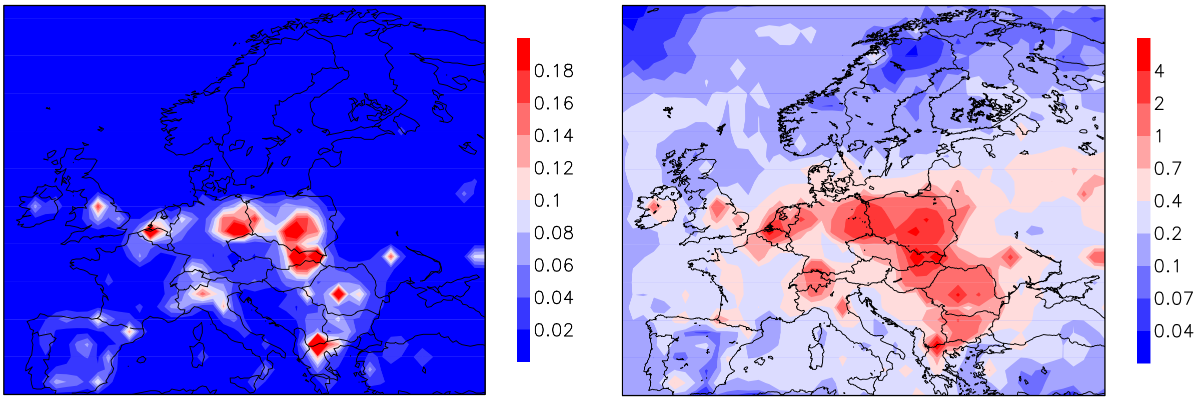

Figure 5: RGM annual average concentration for 2001 in ng.m^{-3} (on the left) and mercury wet deposition flux in g.km^{-2}.y^{-1} (on the right).

Here again the order of magnitude corresponds to the expected values, around one percent of the GEM concentrations. There is a wider range of values with stronger concentration gradients, the emissions area are more emphasized than previously. These qualitative results agree with the different behaviors of GEM and RGM. Oxidised mercury species which are much more soluble than elemental mercury are deposited nearer of mercury sources, the short residence time justifies the weak background concentrations.

The RGM concentrations have to be correctly evaluate in order to get acceptable estimates of the mercury deposition fluxes. Oxidised mercury species represent the main part of the deposited mercury mass. The model results for RGM concentration cannot be directly validated because of the lack of observation site dedicated to these species. However it is possible to assess the wet deposition fluxes since there are stations measuring concentrations in precipitations.

With the detailed model the wet flux values range from 0.03 to 7.4 g.km^{-2}y^{-1} with a spatial average of 0.39 g.km $^{-2}$y^{-1}. Such results constitute a notable progess in comparison to those obtained with the Petersen model which gives a spatial average value of 2.1 10^{-9}g.km^{-2}y^{-1}, but the confrontation with observation data still show a large underestimation of the wet deposition fluxes. The reasons of these discrepansies are not completely determined so far, a probable cause is the difficulty to get reliable information on precipitations and clouds.

3.3 Sensitivity test

Some simple sensitivity test have been performed with the Petersen model. The more impressive results concern the influence of the boundary conditions. A simulation has been made using "clean air" conditions (figure 6). Concentrations values range from 0.023 to 2.4 ng.m^{-3} with a spatial average of 0.26 ng.m^{-3}.

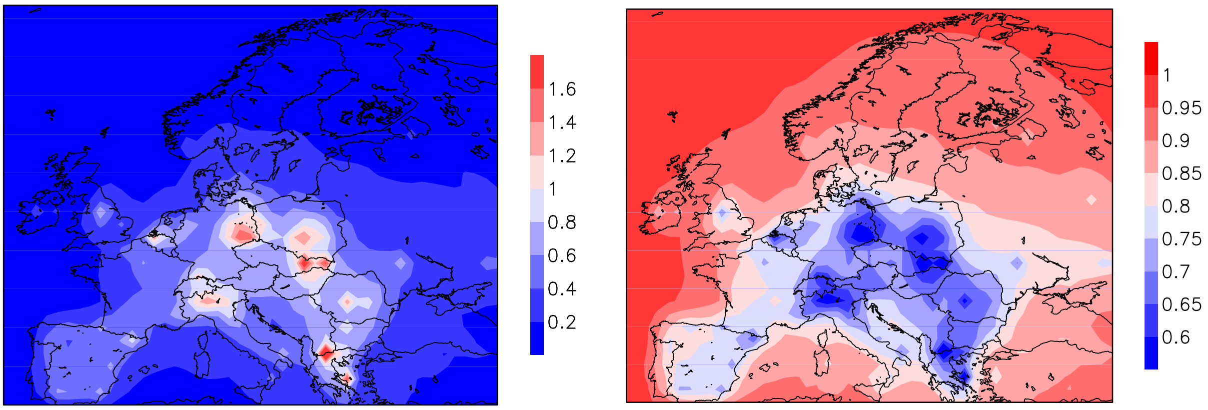

Figure 6: GEM annual average concentration for 2001 in ng.m^{-3} with clean air boundary conditions (on the left) and relative variation compared to the reference result (on the right).

There is no doubt that boundary conditions strongly controll the GEM background concentrations. This is not surprising if one considers the life time of elemental mercury in the atmosphere. Most of the CTM simulating mercury chemistry resort to global or hemispheric model to provide boundary conditions to regional model, but this solution implies that we dispose of the data to perform simulations at this scale. One aim of ongoing work is to use adjoint techniques and inverse modeling in order to improve boundary conditions data set.

Conclusion

Polair3D was extended to simulate the long range transport, chemistry, dry and wet deposition of mercury. Two different mercury chemistry models have been implemented and assessed. The modeled GEM concentrations seem to be in agreement with measurement data for the two models but only the more complex one is able to provide RGM concentration fields and then is likely to estimate correctly wet deposition removal.

We also observe that GEM concentrations are largely dependent on boundary conditions which justifies future work on it. Moreover differences in behavior between GEM and RGM indicate the emission speciation as an other likely crucial parameter for the mercury simulation.

Acknowledgements

The authors would like to thank Ilia Ilyin from MSC-East and Wenche Aas from NILU for kindly providing emission and measurement data collected at EMEP monitoring network. The authors are grateful to European Centre of Medium Range Weather Forecast for the meteorological data. Y. Roustan would like to express his gratitude to ADEME (french Environment and Energy Management Agency) and EDF (Électricité de France) which have supported financially this work.

References

Baer, M. and Nester, K.: Parameterization of trace gas dry deposition velocities for a regional mesoscale diffusion model, Annales Geophysicae, Vol. 10, pp 912-923, 1992

Brook, J.R., Zhang, L., Di-Giovanni, F. and Padro, J.: Description and evaluation of a model of deposition velocities for routine estimates of air pollutant dry deposition over North America. Part I: model development, Atmospheric Environment, Vol. 33, pp 5037-5051, 1999

Hicks, B.B. and Liss, P.S.: Transfer of SO_2 and other reactive gases across the air-sea interface, Tellus, Vol. 28, pp 348-354, 1976

Lindqvist, O. and Rodhe, H.: Atmospheric mercury - a review, Tellus, Vol. 37B, pp 136-309, 1985

Mallet, V. and Sportisse, B.: 3-D chemistry-transport model Polair: numerical issues, validation and automatic-differentiation strategy, Atmospheric Chemistry and Physics Discussions, 4, 1371-1392, 2004

Petersen, G., Iverfeldt, A. and Munthe, J.: Atmospheric mercury species over central and northern Europe. Model calculations and comparison with observations from the nordic air and precipitation network for 1987 and 1988, Atmospheric Environment, Vol. 29, pp 47-67, 1995

Roselle, S.J. and Binkowski, F.S.: Cloud dynamics and chemistry, Science Algorithms of the EPA Models-3 Community Multi-scale Air Quality (CMAQ) Modeling System, EPA Report, EPA/600/R-99/030, 1999

Ryaboshapko, A., Bullock, R., Ebinghaus, R., Ilyin, I., Lohman, K., Munthe, J., Petersen, G., Seigneur, C. and Wängberg, I.: Comparison of mercury chemistry models, Atmospheric Environment, Vol. 36, pp 3881-3898, 2002

Seigneur, C., Karamchandani, P., Vijayaraghavan, K., Lohman, K., Shia, R. and Levin, L.: On the effect of spatial resolution on atmospheric mercury modeling, The Science of the Total Environment, Vol. 304, pp 73-81, 2003

Sportisse, B. and Du Bois, L.: Numerical and theoretical investigation of a simplified model for the parameterization of below-cloud scavenging by falling raindrops, Atmospheric Environment, Vol. 36, pp 5719-5727, 2002

Wesely, M.L. and Hicks, B.B.: A review of the current status of knowledge on dry deposition, Atmospheric Environment, Vol. 34, pp 2261-2281, 2000

National Environmental Research Institute

The National Environmental Research Institute, NERI, is a research institute of the Ministry of the Environment. In Danish, NERI is called Danmarks Miljøundersøgelser (DMU).
NERI's tasks are primarily to conduct research, collect data, and give advice on problems related to the environment and nature.

Addresses:	URL: http://www.dmu.dk
National Environmental Research Institute Frederiksborgvej 399 PO Box 358 DK-4000 Roskilde Denmark Tel: +45 46 30 12 00 Fax: +45 46 30 11 14	*Management* *Personnel and Economy Secretariat* *Monitoring, Advice and Research Secretariat* *Department of Policy Analysis* *Department of Atmospheric Environment* *Department of Marine Ecology* *Department of Environmental Chemistry and Microbiology* *Department of Arctic Environment*
National Environmental Research Institute Vejlsøvej 25 PO Box 314 DK-8600 Silkeborg Denmark Tel: +45 89 20 14 00 Fax: +45 89 20 14 14	*Monitoring, Research and Advice Secretariat* *Department of Marine Ecology* *Department of Terrestrial Ecology* *Department of Freshwater Ecology*
National Environmental Research Institute Grenåvej 12-14, Kalø DK-8410 Rønde Denmark Tel: +45 89 20 17 00 Fax: +45 89 20 15 15	*Department of Wildlife Ecology and Biodiversity*

Publications:
NERI publishes professional reports, technical instructions, and the annual report in Danish.
A R&D projects' catalogue is available in an electronic version on the World Wide Web.
Included in the annual report is a list of the publications from the current year.

Proceedings of the

2nd GLOREAM/EURASAP Workshop

Copenhagen, September 6-8, 2004

Modern developments in modelling and chemical data analysis

Jørgen Brandt and Lise M. Frohn (Eds.)

ISBN 87-7772-886-6

National Environmental Research Institute
Ministry of the Environment · Denmark